AD-A007 913

# SOVIET MATERIAL ON INTERNAL WAVE EFFECTS, NO. 3, APRIL 1975

Stuart G. Hibben, et al

Informatics, Incorporated

Prepared for:

Defense Advanced Research Projects Agency
Navy Foreign Language Service

April 1975

UNCLASSIFIED

SECURITY CLASSIFICATION OF THIS PAGE (When Data Entered)

| REPORT DOCUMENTATION PAGE | READ INSTRUCTIONS BEFORE COMPLETING FORM |
|---|---|
| 1. REPORT NUMBER | 2. GOVT ACCESSION NO. | 3. RECIPIENT'S CATALOG NUMBER: AD-A007 913 |
| 4. TITLE (and Subtitle): Soviet Material on Internal Wave Effects No. 3, April, 1975 | 5. TYPE OF REPORT & PERIOD COVERED: Scientific . . . Interim |
| | 6. PERFORMING ORG. REPORT NUMBER |
| 7. AUTHOR(s): Stuart G. Hibben, John Kourilo, B. L. Shresta, M. Ness | 8. CONTRACT OR GRANT NUMBER(s): N00600-75-C-0018 |
| 9. PERFORMING ORGANIZATION NAME AND ADDRESS: Informatics Inc. 6000 Executive Boulevard Rockville, Maryland 20852 | 10. PROGRAM ELEMENT, PROJECT, TASK AREA & WORK UNIT NUMBERS: DARPA Order No. 2790 Program Code No. L13003 |
| 11. CONTROLLING OFFICE NAME AND ADDRESS: Defense Advance Research Projects Agency/TAO 1400 Wilson Boulevard Arlington, Virginia 22209 | 12. REPORT DATE: April, 1975 |
| | 13. NUMBER OF PAGES: 131 |
| 14. MONITORING AGENCY NAME & ADDRESS (if different from Controlling Office): U. S. Navy Foreign Language Service 4301 Suitland Road, Bldg. 5 Washington, D. C. 20390 | 15. SECURITY CLASS. (of this report): UNCLASSIFIED |
| | 15a. DECLASSIFICATION/DOWNGRADING SCHEDULE |

16. DISTRIBUTION STATEMENT (of this Report)

Approved for public release; distribution unlimited.

17. DISTRIBUTION STATEMENT (of the abstract entered in Block 20, if different from Report)



18. SUPPLEMENTARY NOTES

Scientific . . . Interim

19. KEY WORDS (Continue on reverse side if necessary and identify by block number)

Internal Waves
Capillary Waves
Surface Signature
Turbulent Flow
Ocean Microstructure

20. ABSTRACT (Continue on reverse side if necessary and identify by block number)

This the the third collection of abstracts of recent Soviet articles on generation and detection of internal waves. It is based on items listed in the third Bibliography of Soviet Material on Internal Waves, published January 27, 1975 and covering material received from April through December, 1974.

The abstracts are divided into internal effects, and surface effects comprising active and passive measurement of wave states. An author index is apperded.

DD FORM 1 JAN 73 1473 EDITION OF 1 NOV 65 IS OBSOLETE

PRICES SUBJECT TO CHANGE

UNCLASSIFIED

SECURITY CLASSIFICATION OF THIS PAGE (When Data Entered)

# SOVIET MATERIAL ON INTERNAL WAVE EFFECTS

No. 3, April, 1975

Sponsored by

Defense Advanced
Research Projects Agency

DARPA Order No. 2790



ARPA Order No. 2790
Program Code No. L13003
Name of Contractor:
Informatics Inc.
Effective Date of Contract:
July 1, 1974
Contract Expiration Date:
June 30, 1975
Amount of Contract: $306,023

Contract No. N00600-75-C-0018
Principal Investigator:
Stuart G. Hibben
Tel: (301) 770-3000
Program Manager:
Klaus Liebhold
Tel: (301) 770-3000
Short Title of Work:
"Internal Waves"

This research was supported by the Defense Advanced Research Projects Agency and was monitored by the U. S. Navy Foreign Language Service under Contract No. N00600-75-C-0018. The publication of this report does not constitute approval by any government organization or Informatics Inc. of the inferences, findings, and conclusions contained herein. It is published solely for the exchange and stimulation of ideas.

informatics inc
Systems and Services Company
6000 Executive Boulevard
Rockville, Maryland 20852
(301) 770-3000 Telex 89-521

## INTRODUCTION

This is the third collection of abstracts of recent Soviet articles on generation and detection of internal waves. It is based on items listed in the third Bibliography of Soviet Material on Internal Waves, published January 27, 1975 and covering material received from April through December, 1974.

The abstracts are divided into internal effects, and surface effects comprising active and passive measurement of wave states. An author index is appended.

## TABLE OF CONTENTS

## 1. Internal Effects

Belyayev, V. S., A. S. Monin, and V. T. Paka. Experimental measurements of deep sea turbulence. FAiO, no. 5, 1974, 533-542.

Results of a study of oceanic turbulence are described, as well as the method and turbulimeter employed. The experiments were conducted in the Indian Ocean during the 7th cruise of the R/V Dmitriy Mendeleyev in January-April 1972.

Pulsations in electrical conductivity were measured by a quick-response probe under conditions of standard vertical sounding or tethered "free" fall to a depth of 1200 m. The "sigma" probe used was designed by V. T. Paka (Fig. 1). The electric resistivity of the water

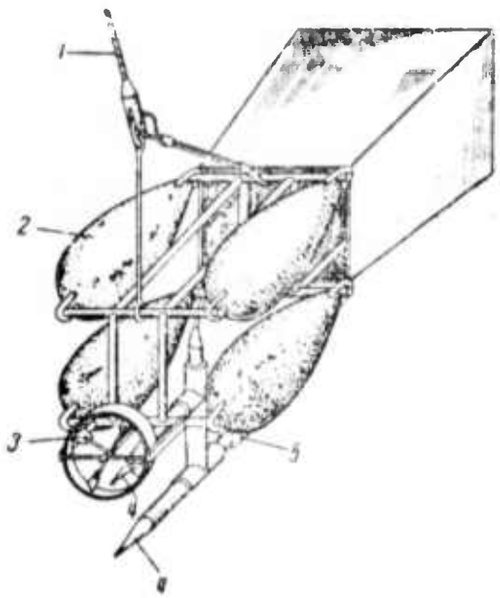


Fig. 1. Sigma Turbulimeter.

1- Electrical cable; 2- weights or frame with a box-like stabilizer; 3- current meter; 4- sensors of electrical conductivity; 5- hydrostatic pressure indicator.

column between the electrodes of the sensor (4) is connected to a high-frequency oscillatory circuit, modulating the signal amplitude. Amplitude modulation is linear over the range 0.02-0.06 ohm$^{-1}$ cm$^{-1}$. Noise level at the output is equivalent to a temperature fluctuation of $10^{-4}$ °C. The relative speed of the instrument package is measured by a current meter (3).

The average electrical conductivity $\bar{\sigma}$, relative probe speed V, and electrical conductivity fluctuations $\sigma'$ measured between the lower boundary of the thermocline (~250 m) and a depth of 800 m are shown in Fig. 2. The figure indicates that large fluctuations of electrical conductivity

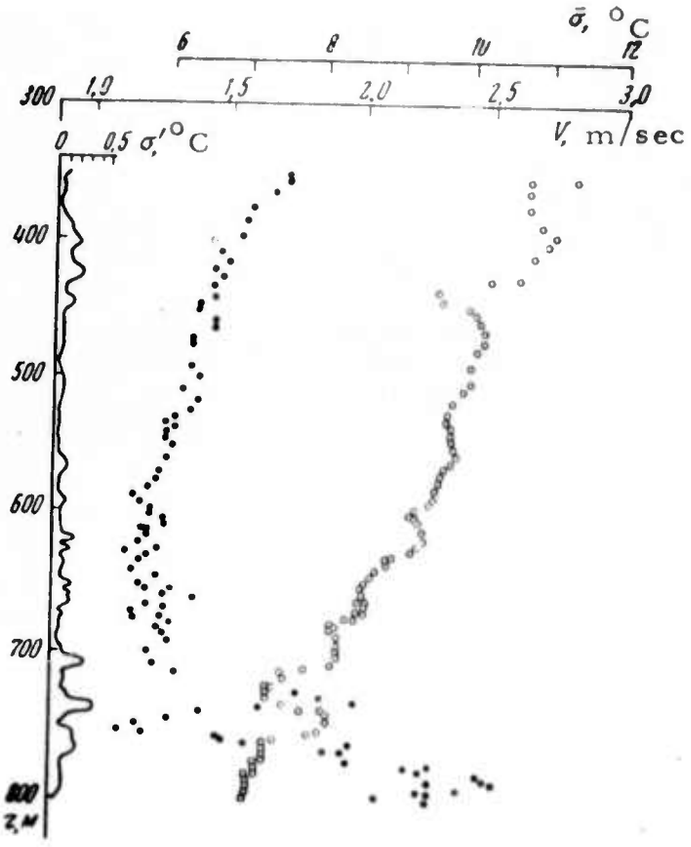


Fig. 2. Vertical distribution of $\bar{\sigma}$ (open circles), V (solid circles); and $\sigma'$ (solid line).

are associated with large vertical gradients of the average electrical conductivity and with the relative speed of the probe.

The vertical distribution of average electrical conductivity, obtained by vertical sounding to a depth of 1250 m, (at $10^{\circ}59N$; $55^{\circ}40E$) is shown in Fig. 3. Conductivity fluctuations were observed during

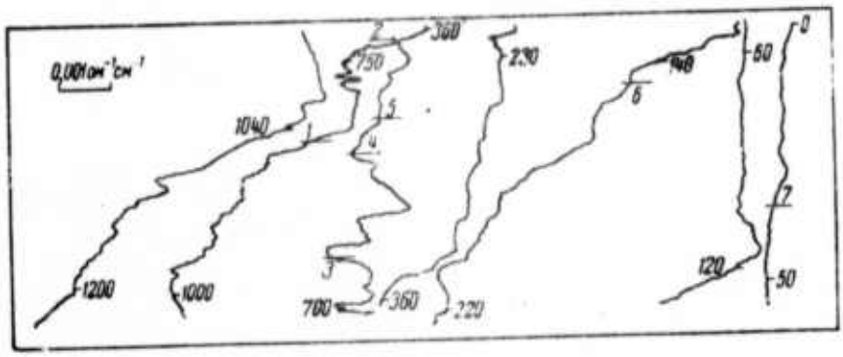


Fig. 3. Record of average electrical conductivity during probe descent.

9 minute intervals at seven levels (indicated by single numbers in Fig. 3). Variations of the average electrical conductivity, mean square fluctuations of electrical conductivity, and depth of the probe during 9 minute-intervals are shown in Fig. 4.

Spectral densities $E^{(\sigma)}(k)$ of fluctuations $\sigma'$ observed during 9 minutes intervals are shown in Fig. 5.

Energy spectra $k\,E^{(\sigma)}(k)$ of fluctuations $\sigma'$ increase with a drop in k more quickly in the high frequency range, and slower in the low frequency range. At smaller depths, they tend to have maxima at the frequency of ship roll.

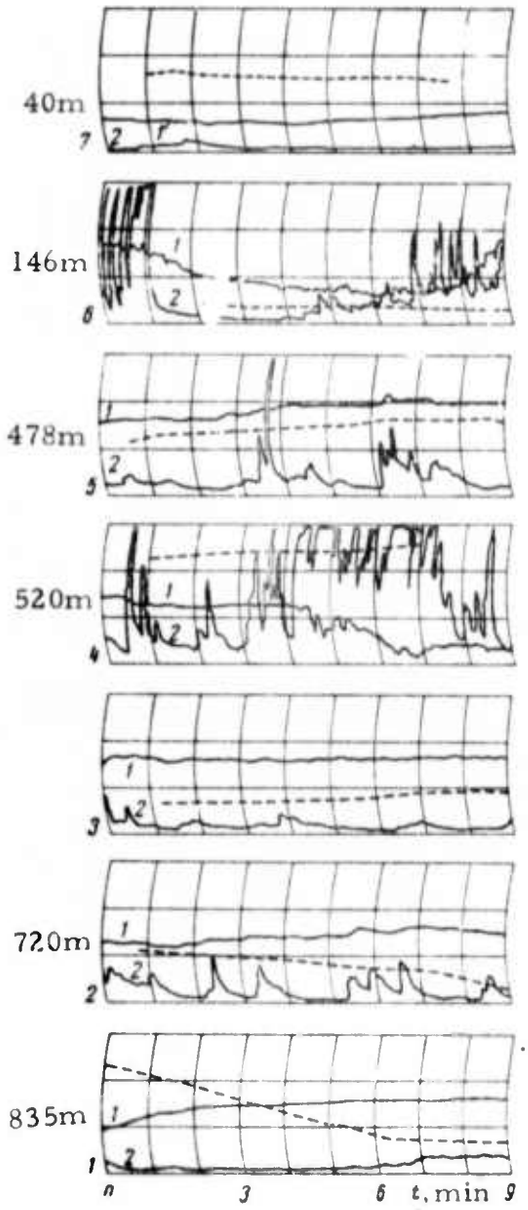


Fig. 4. Variations of $\bar{\sigma}(1)$, $(\bar{\sigma}')^2$ (2), and probe depth (dashed line) during observations of electrical conductivity fluctuations.

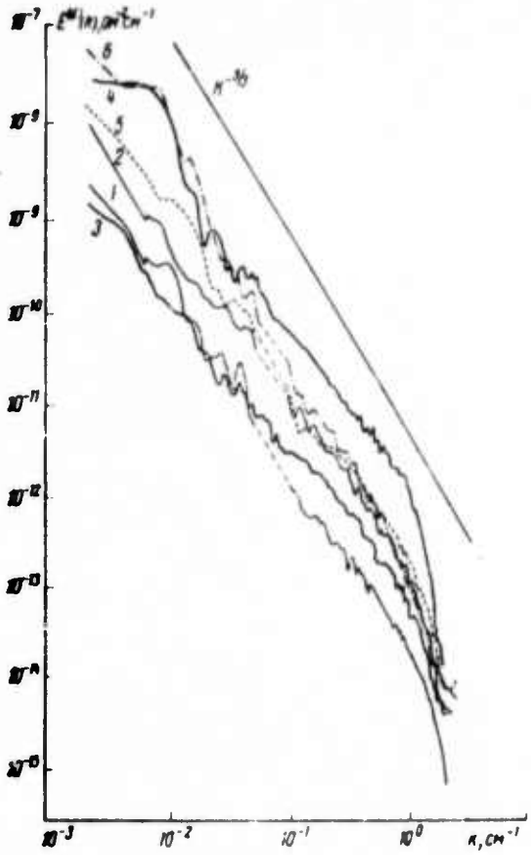

Fig. 5. Spectral densities of electrical conductivity fluctuations (1- 835m; 2- 720m; 4- 520m; 5- 478m; 6- 146m)

Dissipation spectra $k^2 E^{(\sigma)}(k)$ of fluctuations are shown in Fig. 6. At all levels except 146m, they display maxima at $10^{-1} cm^{-1} < k < 2\ cm^{-1}$.

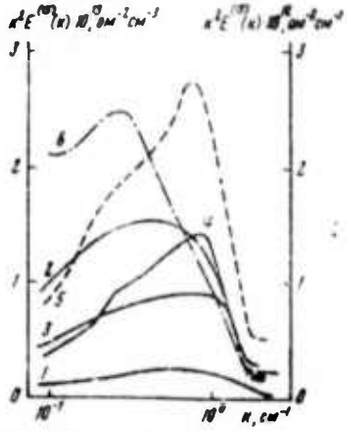

Fig. 6. Smoothed dissipation spectra of electrical conductivity fluctuations. (1- 835m; 2- 720m; 4- 520m; 5- 478m; 6- 146m).

At smaller depths, $k^2 E^{(\sigma)}(k)$ curves also have pronounced maxima at the frequency of ship roll.

Turbulence intermittence was observed at all measured levels (see Fig. 4). It was proposed to use the running structural function $D(\tau_n)$ of fluctuation $\sigma'$ as a criterion for turbulence intermittence (Fig. 7).

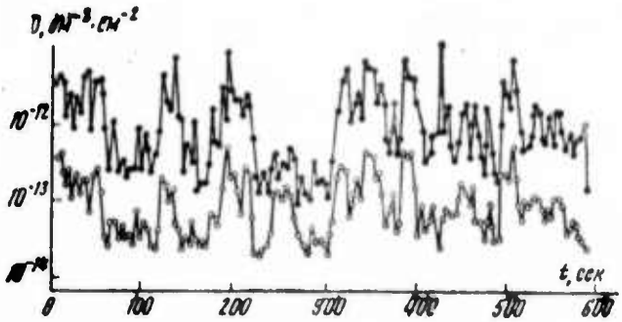


Fig. 7. Running structural function of electrical conductivity fluctuations at 720 m for 1 cm shift (open circle) and 30 cm (solid circles).

The periodicity displayed in the variations of $D(\tau_n)$ ($\sim$80 sec periods) is thought to be associated with the passage of internal wave packets. Turbulence intermittence was manifested in the histograms of $\sigma'$ values as well (Fig. 8).

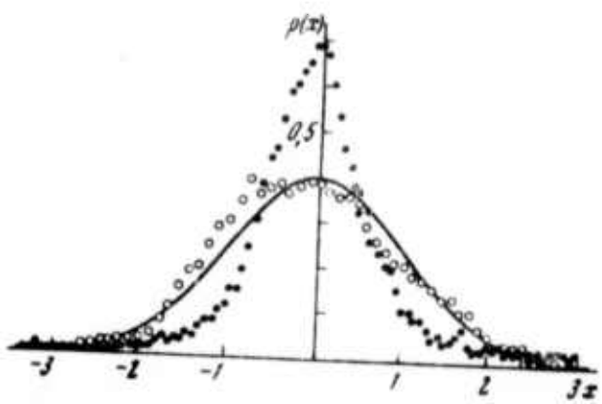


Fig. 8. Histograms of electrical conductivity fluctuations at a depth of 720 m with time separation of 5 min.

Belyayev, V. S., R. V. Ozmidov, and M. L. Pyzhevich. Empirical laws for one-dimensional spectral density distributions of velocity and electrical conductivity pulsations in the ocean. Okeanologiya, no. 5, 1974, 802-805.

This covers the same exercise of the foregoing paper, reviewing measurements of pulsations in flow velocity and electrical conductivity performed in the Atlantic Ocean during the 9th cruise of the R/V Academician Kurchatov and in the Indian Ocean during the 7th cruise of the R/V Dmitriy Mendeleyev. Experiments were conducted both in the region of equatorial currents and in a relatively quiet region, both under instrument towing and vertical sounding conditions. The vertical structures of temperature and salinity in the uppermost oceanic layer differed in the two areas of experiments. The data on oceanic turbulence were analyzed without accounting for background hydrometeorological conditions.

Spectral densites $E_1(k)$ of pulsations of the longitudinal velocity component u' at depths of 20-213 m for $k = 4.6 \times 10^{-2} - 5.9 \times 10^{0}$ $cm^{-1}$ are shown in Fig. 1 for both the Kurchatov and Mendeleyev; spectral densities of pulsations of electrical conductivity $\sigma'$ at depths of 23-217 m for $k = 6.9 \times 10^{-2} - 6.1$ $cm^{-1}$ are shown in Fig. 2 for the Mendeleyev.

Histograms and empirical integral functions of $\lg E_1(k)$ distribution for u' and $\sigma'$ are shown in Fig. 3, a and b respectively.

Statistical parameters of $\lg E_1(k)$ distributions are given in the table.

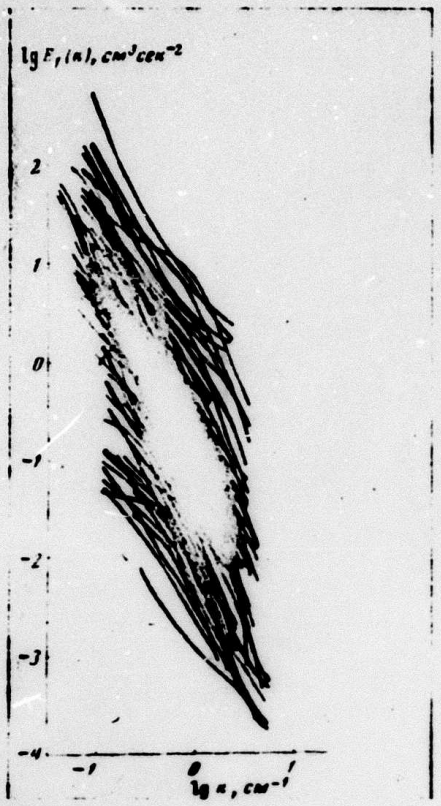


Fig. 1. Family of smoothed $E_1(k)$ curves of velocity pulsations in the ocean.

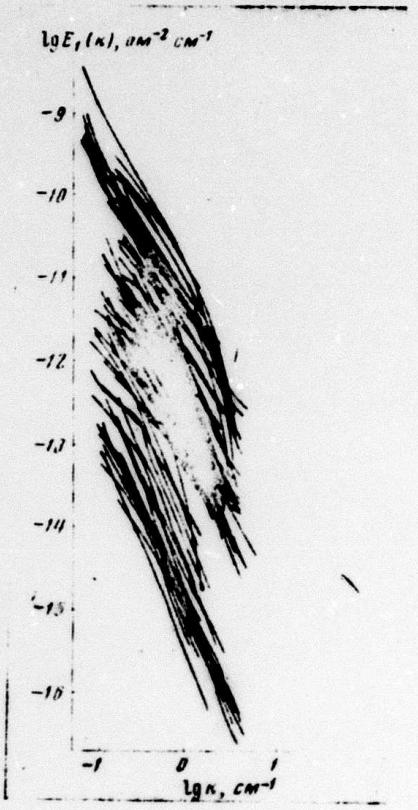


Fig. 2. Family of smoothed $E_1(k)$ curves of electrical conductivity pulsations in the ocean.

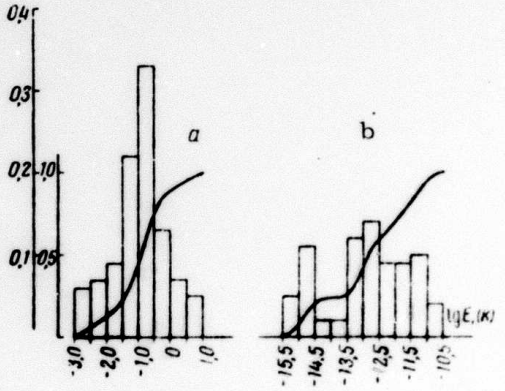


Fig. 3. Histograms and en pirical integral function of $\lg E_1(k)$ distribution for current velocity pulsations (a) and electrical conductivity pulsations (b) in the ocean at $k = 1\ cm^{-1}$. (left vertical scale corresponds to histograms)

Parameters of $\lg E_1(k)$ distributions for current velocity pulsations and electrical conductivity pulsations

| | $m_1$ | D | S | A | E | D(A) | D(E) |
|---|---|---|---|---|---|---|---|
| u' | -0.94 | 0.64 | 0.80 | -0.09 | 0.01 | 0.06 | 0.20 |
| $\sigma'$ | -12.87 | 1.72 | 1.31 | -0.35 | -0.92 | 0.07 | 0.25 |

The probability that $\lg E_1(k)$ has a normal distribution, evaluated using Kolmogorov's criterion, was found to be 70% for current velocity pulsations, but only 7% for electrical conductivity pulsations.

Bezuglov, V. A., G. Ya. Vasilevskis, and Yu. A. Shcherbina. Effect of flow deformation on turbulent diffusion of dye. IN: Tr. 18-y Nauch. konf. Mosk. fiz.-tekhn. in-t, 1972. Ser. Aeromekhanika. Protsessy upr. Dolgoprudnyy, 1973, 25-30. (RZhMekh, 4/74, #4B1047). (Translation)

Results are presented of an experimental study on the effect of turbulent flow deformation, in a pipe with the Venturi-type nozzle, upon the relative rms value of pulsations of passive dye concentration near the axis of pipe, $c'/\langle c\rangle = \left[\langle (c/\langle c\rangle - 1)^2\rangle\right]^{1/2}$, and upon the density of probability distribution of these pulsations. It is shown that in a smooth pipe, the ratio $c'/\langle c\rangle$ near the axis can be represented with sufficient accuracy by a parabolic function. Behind the nozzle, this ratio is "compressed" proportionally to the ratio between the pipe diameter and nozzle section, while at the axis the ratio $c'/\langle c\rangle$ is somewhat decreased. The latter is explained as being caused by an intermittence decrease owing to flow deformation.

Belyayev, V. S., A. S. Monin, R. V. Osmidov, and V. I. Pata. Experimental study of small-scale turbulence in the ocean. FAO, no. 9, 1974, 959-975.

This article details the methods and instrumentation used in complex measurements made since 1969 during four expeditions organized by the Shirshov Institute of Oceanography. The 2nd, 5th, and 7th cruises of the R/V Dmitriy Mendeleyev and the 9th cruise of the R/V Akademik Kurchatov were conducted in the framework of a broad program of research on small-scale fluctuations of hydrophysical fields in ocean test areas.

The data collected in two test areas (Fig. 1) on the 7th cruise

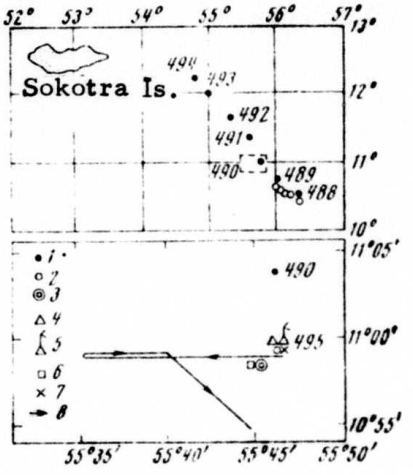


Fig. 1. Test area and type of measurements:

1- hydrological series, bathythermogram, probing with the AIST-STD meter and acoustic ocean current meter; 2- probing with same meters as in 1; 3- multiple probings with AIST; 4- buoy station using moorings with current meters and photothermographs; 5- radio buoy for thermistor chain; 6- measurement with a sigma deep-sea probe; 7- bathythermogram; and 8- towing tacks with turbulimeters. The dashed rectangle is shown in the lower figure to a large scale.

of the Dmitriy Mendeleyev (Indian Ocean in 1972) are presented as an attempt to correlate small-scale fluctuations of hydrophysical fields with background hydrological conditions. Apparently, differences in shape and absolute value of statistical characteristics of small-scale oceanic turbulence measured in the two test ares (Fig. 2 and 3) can be

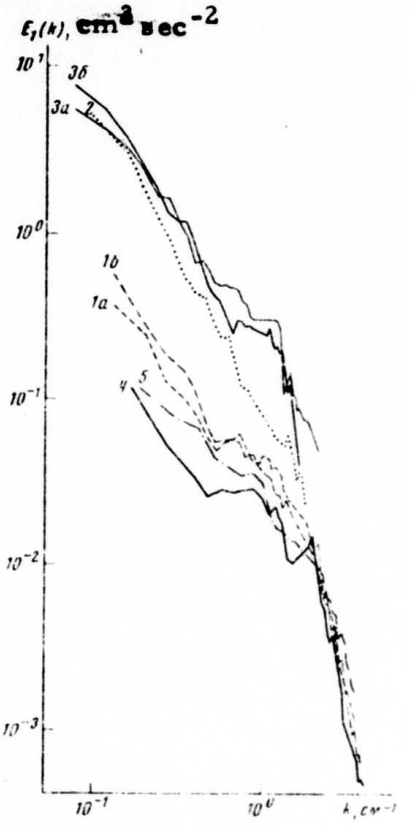


Fig. 2. Spectral density of current velocity fluctuations in test area A. Observation depth (m): 1a, 1b- 100; 2- 105; 3a, 3b- 115; 4- 120; and 5- 187.

correlated with the difference in averaged background hydrological factors including large-scale fluctuations in the same two areas (Fig. 4 and 5).

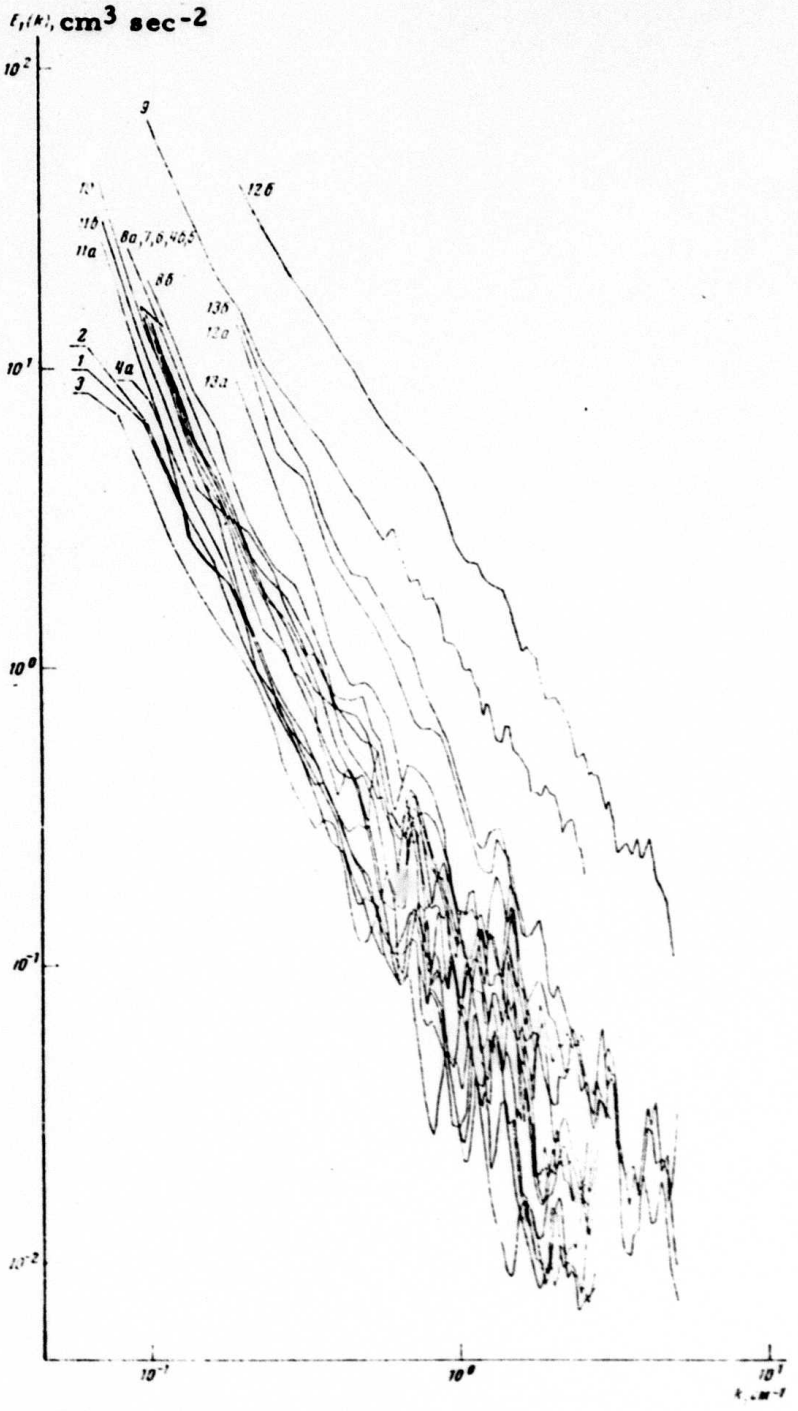


**Fig. 3. Spectral density of current velocity fluctuations in test area B. Observation depth (m): 1- 20; 2- 37; 3- 55; 4a and 4b- 77; 5- 94; 6- 103; 7- 127; 8a and 8b- 138; 9- 157; 10- 160; 11a and 11b- 168; 12a and 12b- 195; 13a and 13b- 213.**

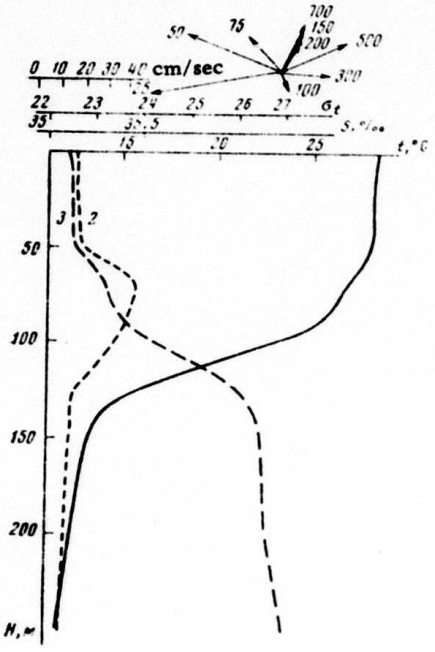


Fig. 4

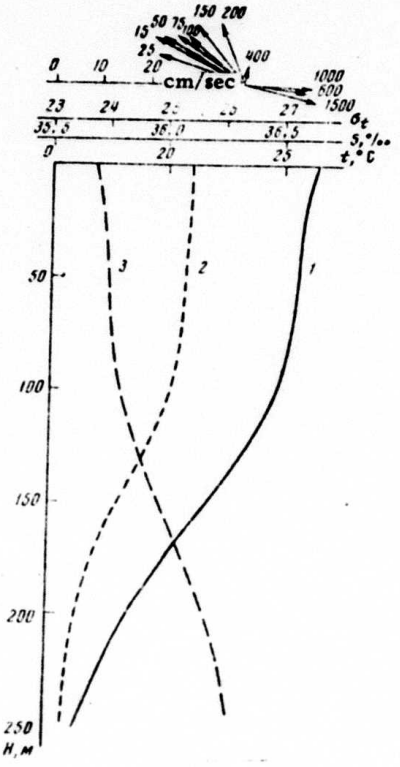


Fig. 5

**Fig. 4 and 5. Vertical temperature (1), salinity (2), and density (3) profiles and vertical distribution of current vectors in test areas A (Fig. 4) and B (Fig. 5) from standard hydrological data and buoy station data.**

However, the difference noted between a pair of spectral curves obtained at the same (Fig. 3, curves 12a and 12b) or nearly the same (Fig. 2, curves 3 and 4) depth levels in a given test area cannot be explained on the basis of averaged background conditions, including large scale fluctuations. Furthermore the mesoscale background data measured with special instruments (e. g., Fig. 6 and 7) are difficult to correlate with the turbulimetric data because of the noncorrespondence of these two sets of data in space and time.

Similarity of the respective vertical profiles in Fig. 6 and 7 reflects a layered vertical structure of the hydrophysical fields. Thus, small-scale oceanic turbulence is determined by local background conditions in a quasihomogeneous layer. This dependence is illustrated by the experimental data in Fig. 8 which were obtained at the same levels as

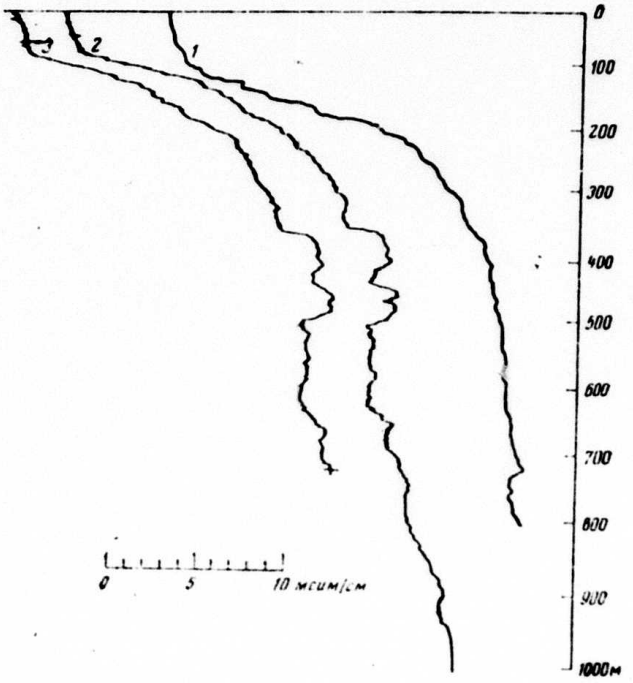


Fig. 6. Vertical profile of electrical conductivity (in relative units) from measurements with the OKB CT probe (curves 2 and 3) and AIST meter (curve 1) at station 497, 18 March 1972, 5:10 PM (2) and 5:40 PM (3) and at st. 495, 16 March 1972, 5:04 PM (1).

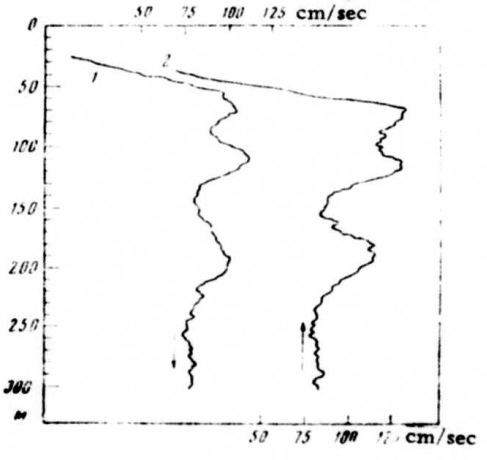


Fig. 7. Current modulus vertical profiles, obtained on board a drift vessel in descent and rise of TO IOAN acoustic meter (arrows indicate meter direction; velocity scales are shifted); st. 506, Mar 23, 1972, 2:14 PM (1) and 2:40 AM (2).

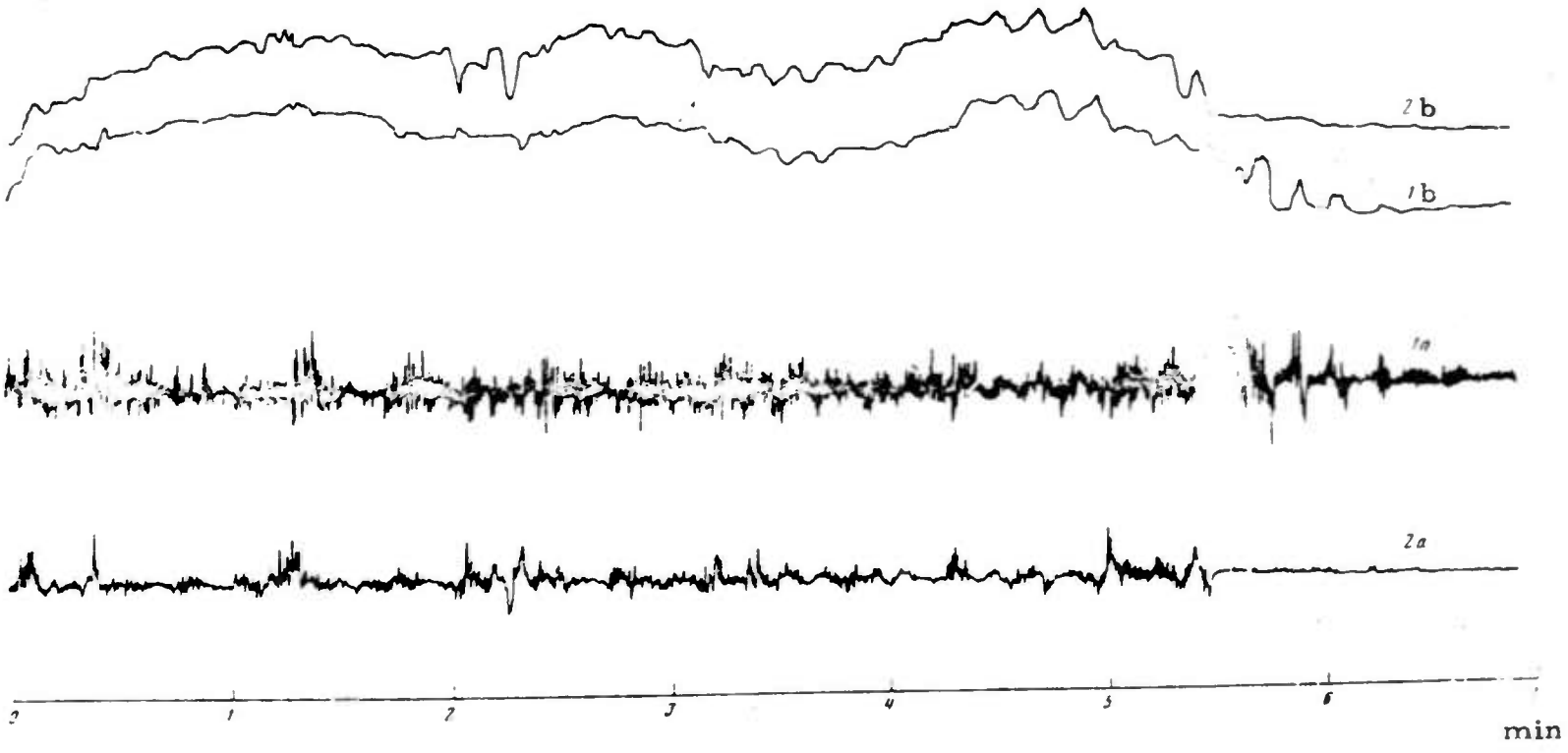


Fig. 8. Oscilloscope traces of average (1b and 2b) and oscillating (1a and 1b) components of electrical conductivity from synchronous measurements at two depth levels with 70 cm vertical spacing.

turbulimetric data. Variability of small-scale fluctuations of hydrophysical fields in the ocean, even at short horizontal spacings along a measuring tack is shown in Fig. 9.

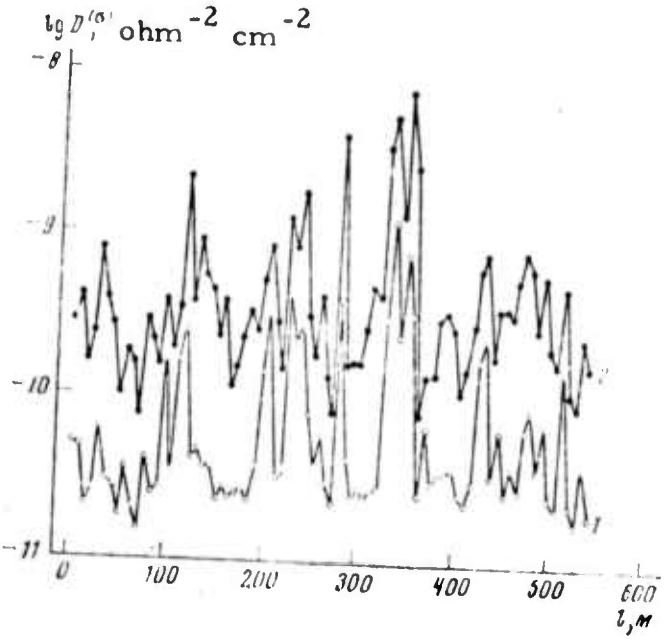


Fig. 9. Slide structural function of electrical conductivity fluctuations for 2.7 cm (1) and 85 cm (2) spatial shifts along horizontal cross-section, from data of towed turbulimeters.

The authors show that the measured spectra of current velocity fluctuations in test area A (Fig. 2) can be described adequately, at least in their intermediate frequency range, by the universal curve used by H. L. Grant et al. (J. Fluid Mech, v. 12, no. 2, 1962) to describe a locally isotropic turbulence. The shape of the spectral curves in Fig. 2 is typical of that of the current velocity spectra at relatively small Reynolds numbers ($10^4$ to $4 \times 10^4$).

The measured spectra in test area B (Fig. 3) are approximated by the theoretical curve of the Monin model of a stratified fluid. Using this approximation the average dissipation rate of turbulent energy and equalization rate of temperature inhomogeneity were determined to be about $10^{-2}$ $cm^2/sec^3$ and $10^{-3}$ to $10^{-4}$ $deg^2/sec$, respectively. The turbulence scale was of the order of step dimensions in the fine density field structure in the ocean.

In summary, small-scale turbulence in a stratified ocean is governed by factors variable in both space and time, which explains the diversity of spectral shapes in fluctuation fields.

Belyayev, V. S., A. S. Monin, and R. V. Ozmidov. A thousand spectra of ocean turbulence. DAN SSSR, v. 217, no. 5, 1974, 1053-1056.

Results of processing the experimental horizontal velocity u, temperature T, and electrical conductivity $\sigma$ data of the upper 200 m oceanic layer are presented in Fig. 1 in the form of spectral density curves $E_1(k)$ of small-scale fluctuations of the cited variables. The data were recorded at different depths in three and seven test areas during the 9th cruise of the R/V Akademik Kurchatov (Atlantic Ocean, 1971) and the 7th cruise of the R/V Dmitriy Mendeleyev (Indian Ocean, 1972), respectively.

The signal recordings from various sensors towed by the cruising ships were used to calculate the spectra. Each spectrum in Fig. 1 is the average of 5 to 10 spectra, so that about 1000 individual spectra are summarized in this figure. Explanation of the letter indexes in Fig. 1 is given in Table 1. Fig. 1 shows 1) a great variety of turbulence modes in the upper ocean layer, 2) a uniform turbulence at all depth levels in some test

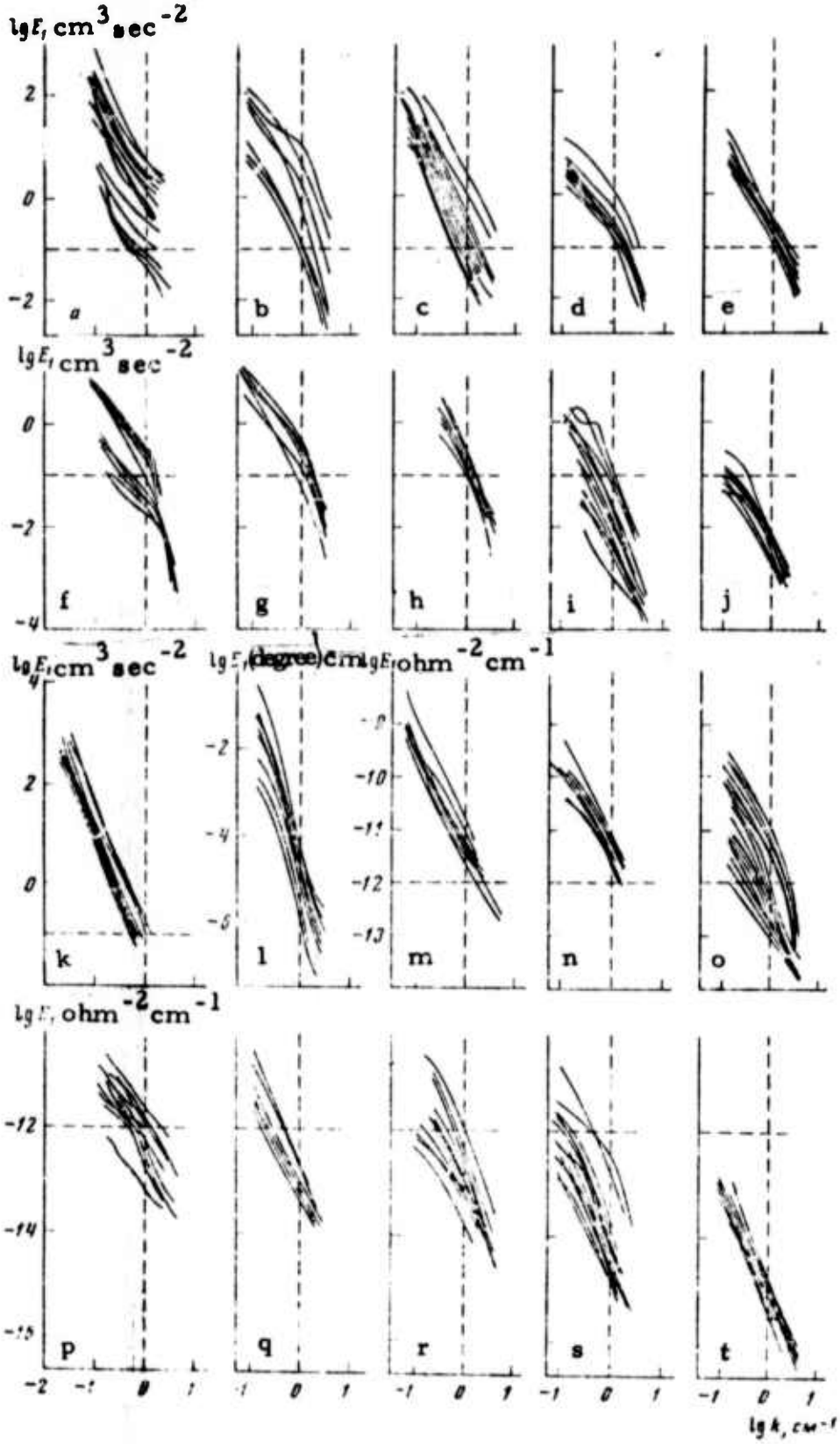


Fig. 1. Families of spectral density curves. Some curves are omitted to avoid overcrowding.

| a | b | c | d | e | f | g | h | i | j | k | l | m | n | o | p | q | r | s | t |
|---|---|---|---|---|---|---|---|---|---|---|---|---|---|---|---|---|---|---|---|
| 7.3.μ | 9.5.μ | 7.7.μ | 9.6.μ | 7.8.μ | 7.5.μ | 9.7.μ | 7.8(2).μ | 7.4.μ | 7.2.μ | 7.6(1).μ | 9.6.T | 7.8.σ | 7.6(1).σ | 7.6(2).σ | 7.7.σ | 7.2.σ | 7.4.σ | 7.3.σ | 7.5.σ |
| 127 | 70 | 195 | 30 | 55 | 115 | 52 | 107 | 67 | 120 | 90 | 40 | 141 | 54 | 149 | 157 | 77 | 67 | 70 | 187 |
| 70 | 87 | 157 | 40 | 95 | 115 | 36 | 75 | 120 | 120 | 80 | 50 | 145 | 68 | 149 | 195 | 120 | 65 | 35 | 150 |
| 70 | 60 | 213 | 60 | 170 | 115 | 140 | 75 | 49 | 138 | 104 | 60 | 170 | 60 | 45 | 94 | 120 | 60 | 35 | 120 |
| 72 | 80 | 195 | 50 | 161 | 115 | 90 | 106 | 103 | 77 | 128 | 60 | 110 | 14 | 23 | 160 | 120 | 80 | 70 | 105 |
| 72 | 30 | 213 | 60 | 110 | 115 | 110 | 149 | 60 | 77 | 142 | 50 | 170 | 10 | 217 | 195 | 77 | 70 | 72 | 90 |
| 35 | 50 | 168 | 77 | 141 | 105 | 73 | 23 | 120 | 181 | 150 | 40 | 175 | 69 | 132 | 213 | 77 | 60 | 52 | 115 |
| 118 | 40 | 138 | 40 | 170 | 100 | | 185 | 60 | 181 | 176 | 77 | 16 | 89 | 23 | 138 | | 75 | 72 | 55 |
| 35 | | 94 | 50 | | 100 | | 125 | 75 | 138 | 163 | 30 | 95 | | 75 | 168 | | 120 | 70 | 129 |
| 35 | | 103 | | | 100 | | 125 | 65 | | 136 | | 55 | | 75 | 141 | | 49 | 91 | 80 |
| 35 | | 138 | | | 187 | | 23 | 80 | | 142 | | | | 106 | 174 | | 103 | 118 | 100 |
| 103 | | 121 | | | 120 | | | 60 | | | | | | 71 | 138 | | 120 | 127 | |
| 30 | | 77 | | | | | | 70 | | | | | | 71 | | | | 103 | |
| 52 | | 160 | | | | | | | | | | | | 125 | | | | | |
| 91 | | 168 | | | | | | | | | | | | 125 | | | | | |
| 70 | | 141 | | | | | | | | | | | | 71 | | | | | |
| | | 77 | | | | | | | | | | | | 106 | | | | | |
| | | 20 | | | | | | | | | | | | 146 | | | | | |
| | | 55 | | | | | | | | | | | | 71 | | | | | |
| | | 33 | | | | | | | | | | | | | | | | | |

**Table 1. Explanation of Fig. 1 letter indexes. The second line index contains cruise number, test area number, and signal type, in that order. Column figures are depths in m. in the same order as the upper left ends of spectra in Fig. 1.**

areas, with turbulence nonmonotonically variable with depth in other test areas, i.e., alternating thin layers of weak and strong turbulence; and 3) changing shape of turbulence spectra.

Turbulence modes are correlated with the average hydrological conditions in the test areas and thickness of the upper homogeneous oceanic layer. A trend is revealed towards a weakening of velocity fluctuations with an increase in the average vertical gradient of water density. The slope of nearly all spectral density curves in log-log coordinates is steeper than 5/3, and increases with increase in wave number k from $10^{-1}$ to $10^{1}$ $cm^{-1}$. This conclusion was drawn also from the existence of peaks of dissipation spectra $k^2E_1(k)$ (not shown). In many cases, the energy spectra $kE_1(k)$ indicate small Reynolds numbers of turbulence, the absence of an inertial region, and nonuniversality of small-scale spectral regions.

Kofanov, Ye. S., N. K. Shelkovnikov, A. A. Pivovarov, and Yu. I. Gorbatov. Method and measuring system for study of the structure of small-scale sea turbulence. VMU, no. 2, 1974, 171-177.

A description is given of a system for measuring temperature pulsations in the ocean simultaneously at four points in three mutually perpendicular directions. The article includes a short description of a method for determining geometry and dynamics of temperature inhomogeneities, based on the measurements of temperature pulsations at several spaced points, as well as some sample calculations.

The block diagram of the measuring system is given in Fig. 1.

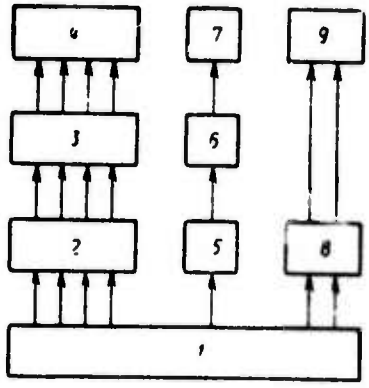


Fig. 1.

1- set of sensors (thermocouples); 2- four-channel amplifier; 3- control unit; 4- recording unit; 5- measuring bridge; 6- balance unit; 7- automatic recording potentiometer; 8- two-channel amplifier for tachometer of current meter; 9- count-rate recorder.

A complete schematic of a recording channel is also included.

The measuring system includes specially designed high-sensitivity current meters and platinum resistance thermometers. Its characteristics are as follows: drift - ~0.1 sec; sensitivity of recording channel - ~0.002° C/mm; sensitivity of galvanometer - $10^{-5}$ A (MM) m[sic]; accuracy of temperature gradient measurements - 0.02° C/m in the temperature range of 5-26° C.

The bottom mount for submerged part of the measuring system is illustrated in Fig. 2. The rods with sensors are secured on ball

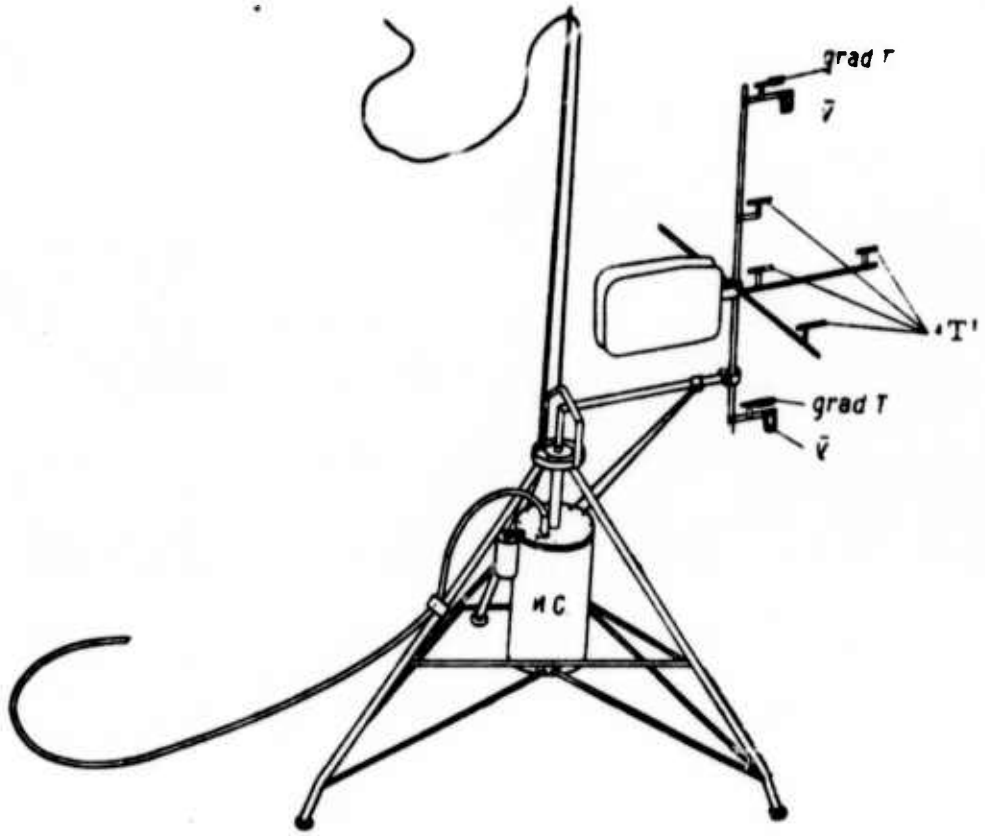


Fig. 2. Sketch of bottom system.

bearings and can be oriented in the flow direction. The mast is positioned vertically for heeling angles not exceeding 30°.

Sabinin, K. D., and A. N. Serikov. Some results of measurements of space-time characteristics of short-period internal waves in the tropical Atlantic. FAiO, no. 10, 1974, 1062-1074.

Temperature fluctuations measured during two days in 1970 from the R/V Sergey Vavilov in the Atlantic are analyzed using Fourier transforms, and the spectral distribution of internal wave parameters is discussed. Measurements were made from the drift vessel by means of three thermistor chains spaced in a layer 90 to 125 m deep, each carrying four temperature sensors and one depth gauge. Calculations of spectral distribution were made for each consecutive 40 min.period with a 10 min. differential between starts of each period.

The internal wave parameters of wave number k, frequency f, and height h were calculated for more or less well-defined trains of relatively regular (narrow band) waves within each recording period. The selected data presented in Table 1 and figures 1, 2, and ? show that the wave

| Wave train (period numbers) | Train duration | Wave parameters: Period, min. | Length, km. | Height, m. | Orientation, deg. | Mode |
|---|---|---|---|---|---|---|
| | **8/31/1970** | | | | | |
| I (15—19) | 00 ч. 02 м. — 01 ч. 26 м. | 17÷35,5 | 0.36÷1,11 | 8÷15 | 314÷27 | II |
| II (30—41) | 02 40 — 05 18 | 13÷23 | 0,57÷0,80 | 11÷20 | 331÷335 | I |
| III (46—53) | 05 29 — 07 24 | 15÷25 | 0.44÷0,85 | 9÷19 | 347÷1 | I |
| IV (90—94) | 13 10 — 14 33 | 13÷24 | 0,50÷1,20 | 9÷12 | 32÷71 | I—II |
| V (94—102) | 13 52 — 15 38 | 15÷23 | 1,30÷2.40 | 12÷19 | 356÷24 | I |
| VI (133—137) | 20 28 — 21 48 | 25÷32 | 1,18÷4.70 | 13÷15 | 343÷100 | I |
| VII (141—146) | 21 47 — 23 17 | 21÷31 | 0.50÷1,60 | 9÷11 | 26÷67 | II—III |
| | **9/1/1970** | | | | | |
| VIII (196—205) | 6 52 — 9 01 | 17÷33 | 1.10÷2.00 | 8÷13 | 292÷38 | I |
| IX (197—205) | 7 02 — 9 01 | 15÷25 | 0.66÷1.20 | 8÷14 | 24÷53 | I |
| X (209—212) | 9 01 — 10 10 | 20÷26 | 0.70÷1,50 | 11÷15 | 19÷65 | I |

Table 1. Principal data on wave trains.

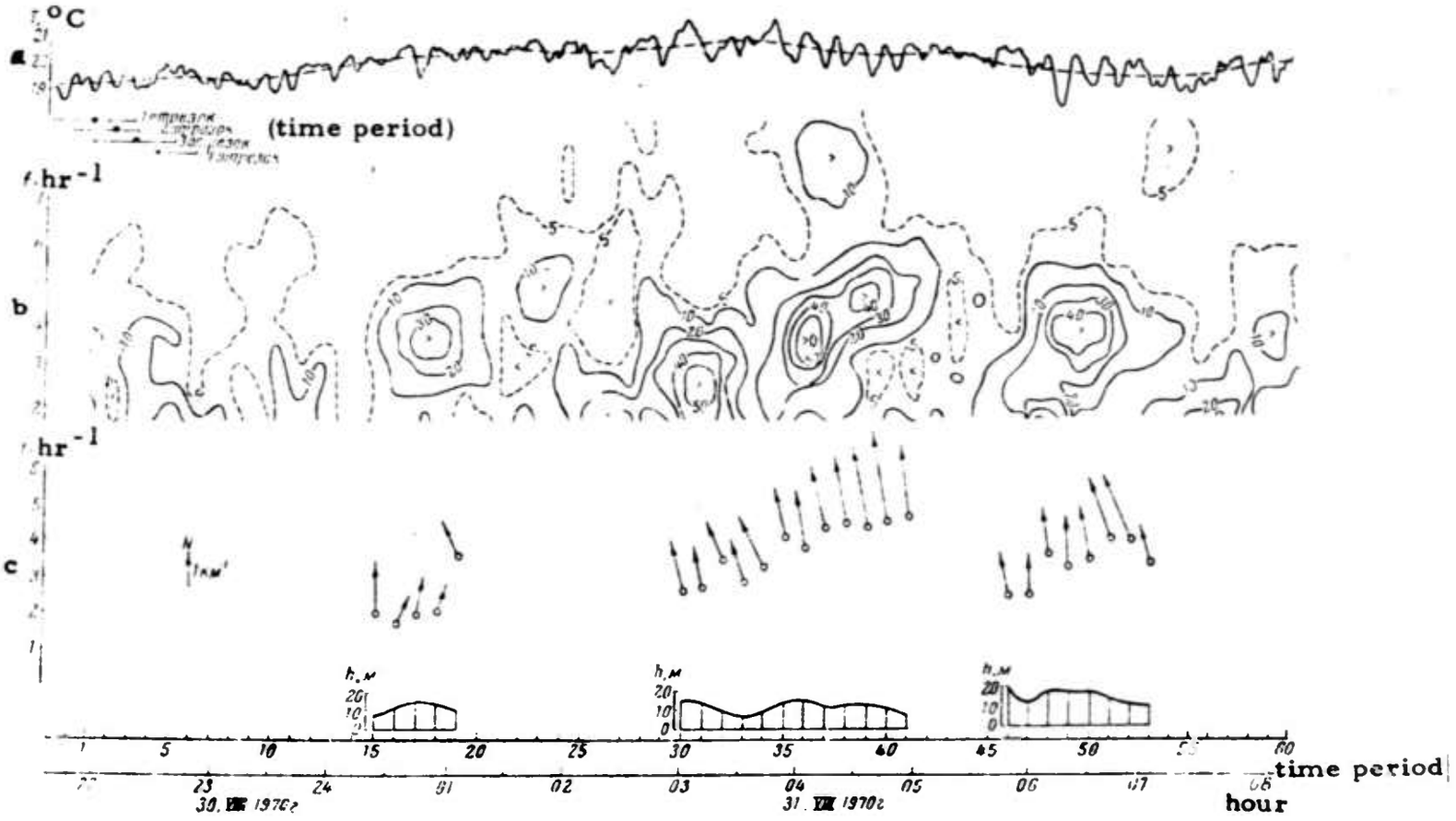


Fig. 1a- temperature fluctuations recording, b- periodogram, c- wave numbers (arrows), frequency (ordinate of arrow origin), and wave height in the trains I, II, and III (lower curves).

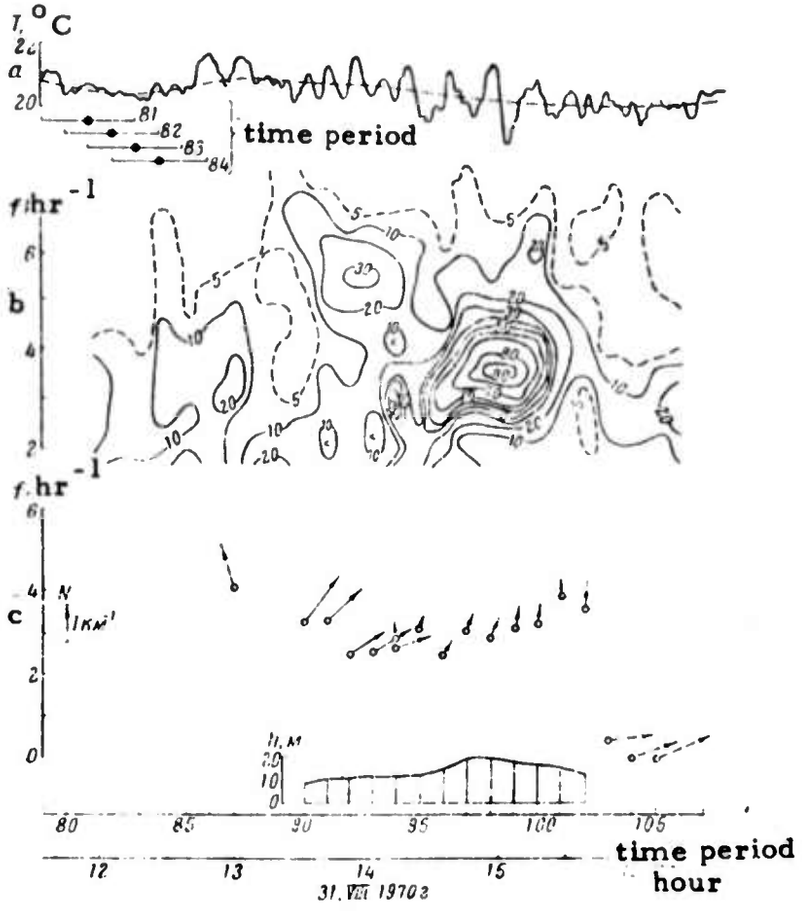


Fig. 2. a- temperature fluctuation recording, b- periodogram, c- wave parameters of trains IV and V.

parameters within each wave train are not constant. An error analysis was made to determine whether the parameter fluctuations are due to measurement errors. Calculations of $< k >$, $< f >$ and the error probability limits show that for most wave trains k and f variations in time exceed the limits of probable deviations from mean $< k >$ and $< f >$ values, attributable to errors of measurement. This finding is illustrated for wave train II by position of the cross, which represents $< k >$, $< f >$, and limits of measurement errors (Fig. 4). A close examination of the data in Table 1 and Fig. 1 to 4 reveals that most of the energy of the observed internal waves is concentrated in separate trains of short-period (13 to 35 min.), 360 m to 4.7 km long waves, which occupy 1/3 of the total recording time. Each wave

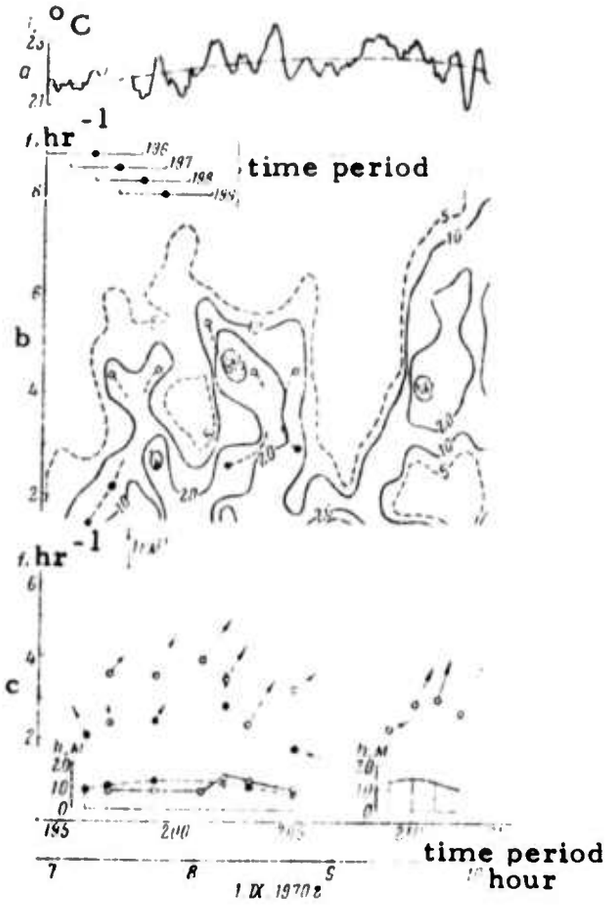


Fig. 3. a- temperature fluctuations recording, b- periodogram, c- wave parameters of the trains VIII, IX, and X (same notation as in Fig. 1).

train continues for 1 to 3 hr. Sometimes, as in train II, the waves, attain h = 20 m. The north, northwest, or northeast directions of wave propagation are predominant. As Table 1 and Fig. 4 show, most of the k, f points of the observed wave trains belong to curves such as the dashed curve in Fig. 4a, which are close to the calculated dispersion curves of the lowest (I and II) wave modes. A fairly clear pattern of k and f values increasing in time and space emerges from examination of data for wave train II. This pattern supports the hypothesis of a locally fluctuating source of wave train II.

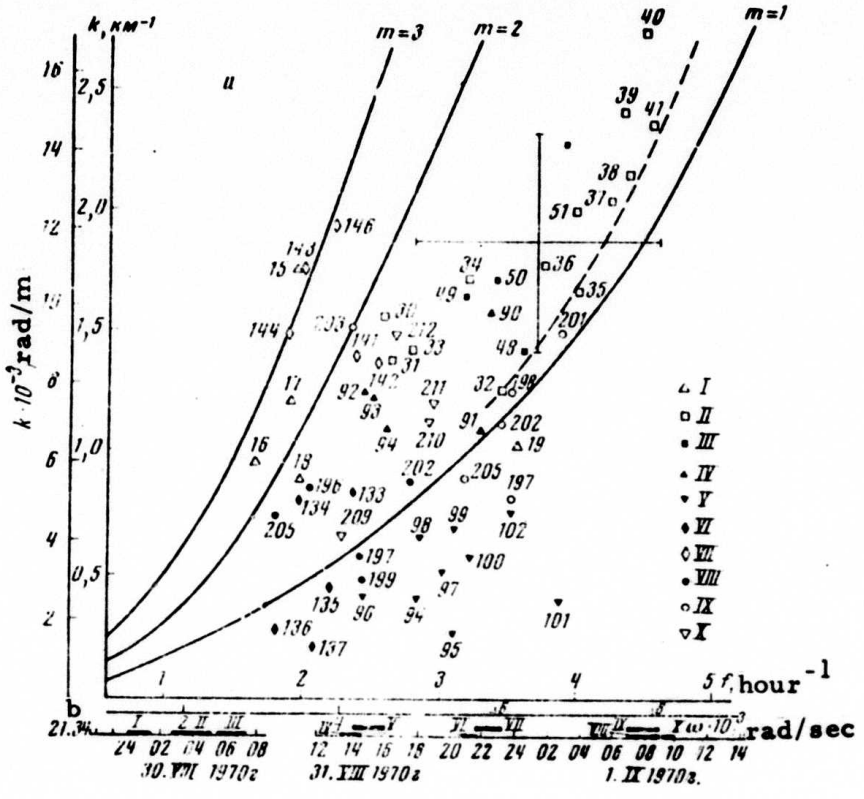


Fig. 4. a- dispersion ratio $k_m$ (f) for modes m = 1 to 3 of internal waves and k, f points of different time periods; b- wave train position on time scale, Roman numerals are train numbers.

The simultaneous existence is also noted of wave trains VIII and IX, having approximately the same direction and amplitude, but with k an f values differing by a factor of two. A strong deviation of most k, f points of train V from the dispersion curve of mode I waves is attributed to the partly standing nature of the waves which are oriented in a direction normal to the drift direction of the vessel.

The standing wave ratio calculated by two independent methods supports the existence of a system of two waves propagating in opposition to each other. An analysis of directions of all measured waves led to the conclusion that the short-period internal wave field is anisotropic, although

the existence of western-oriented waves cannot be ruled out. Newly detected characteristics of short period internal waves include frequency fluctuations in time and space, predominance of one direction of wave trains, and the possibility of generation of waves with a standing wave ratio different from zero. The observed phenomena agree with the resonance hypothesis of wave generation.

Leonov, A. I., and Yu. Z. Miropol'skiy. Nonlinear theory of propagation of stationary internal gravity waves. MZhiG, no. 5, 1974, 189-190.

This is the summary of a paper presented on June 6, 1974 at the General Seminar of the Institute of the Problems of Mechanics of the Academy of Sciences. A new nonlinear equation is reported, which describes stationary plane internal waves as a function of a single external parameter-the distributed Vaisalaa-Brunt frequency. The equation is derived on the assumption that fluid stratification is the sole source of vorticity.

In an approximation of weak nonlinearity, solutions to the cited equation are analyzed by the Poincare method for the cases of long internal waves in shallow water and a narrow pycnocline. It is shown that long waves in shallow water are stable against longitudinal disturbance but unstable against transverse disturbance. Nonlinear partial differential equations are set up using the approximation of geometric optics for the amplitude and phase of short internal waves. These equations coincide with adiabatic approximation of the L'yuk-Uizem (?) theory. Particular formulas are derived for linear or weakly nonlinear stratification. The equations of the amplitude and phase characteristics are solved in explicit form for limiting waves (solitons). The parameters of nonlinear internal waves are evaluated for the Vaisalaa-Brunt frequency distributions typical of the ocean.

Leonov, A. I., and Yu. Z. Miropol'skiy. Stationary internal gravity waves with finite amplitude. DAN SSSR, v. 218, no. 6, 1974, 1287-1290.

It is shown that nonlinear stationary internal waves in a steadily stratified fluid can be described by the fundamental hydrodynamic equation as a function of only one external parameter, namely the Vaisalaa-Brunt frequency $N^{-2}$. In contrast with the Long equation, the derived equation does not contain unknown random functions.

The cited equation with given boundary conditions is solved in the approximation of weak dispersion and weak nonlinearity. In the case of long waves, i.e., $\epsilon = H^2/\lambda \leq 1$ (H is the fluid depth, $\lambda$ is wavelength), there exists a solution of the form

$$F_1(\zeta, \eta) = W(\eta)U(\zeta), \tag{1}$$

where $\zeta = \theta\lambda^{-1}$ and $\eta = zH^{-1}$ are dimensionless variables, $\theta = x - vt$, x and z are horizontal and vertical coordinates, and V is the wave propagation rate. The function $W(\eta)$ is determined by solving the boundary value problem. The function $U(\zeta)$ is determined from the equation

$$\partial^3 U/\partial\zeta^3 + \gamma U^2 + \beta_1 \alpha U = 0, \tag{2}$$

where

$$\gamma = -\beta_0 \int_{-1}^{0} \Omega' W^3 d\eta + \mu\left[\frac{1}{2}\int_{-1}^{0} \Omega (W')^2 W\, d\eta + \int_{-1}^{0} \Omega' W' W^2\, d\eta\right], \quad \alpha = \int_{-1}^{0} \Omega W^2\, d\eta, \tag{3}$$

$\beta = \beta_0 + \epsilon\beta_1 + \epsilon^2\beta_2 + \ldots$ is the eigenvalue of the nonlinear boundary value problem, $\Omega(\eta - F) = N^2(\eta - F)(N_0^2)^{-1}$ is a dimensionless parameter, $(0 \leq \Omega \leq 1)$, $F = \psi(Hv)^{-1}$ is a dimensionless variable and $\psi$ is the wave flow function. Equation (2) coincides with the Korteweg-de Vries equation. Solution of (2) describes, depending on the ratio of integration constants, either a solitary wave (soliton)

$$U(\zeta) = -2a \operatorname{ch}^{-2}(\sqrt{a\gamma/6}\zeta) + b, \tag{4}$$

or a cnoidal wave

$$U(\zeta) = \frac{2a}{s^2} \operatorname{dn}^2\left(\sqrt{\frac{a\gamma}{3}}\frac{\zeta}{s}, s\right) + b, \tag{5}$$

where a is the wave amplitude, b is an additive constant, and dn(x, s) is a Jacobian elliptic function with modulus s ($0 < s < 1$). There can exist, at $\gamma < 0$, solitary internal waves of the trough type as shown in Fig. 1a (curve 1).

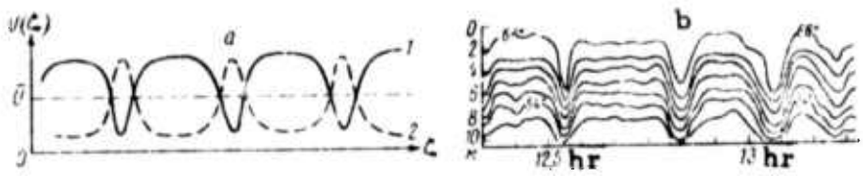


Fig. 1. a- Periodic wave close to solitons sequence: curve 1 - $\gamma < 0$; 2 - $\gamma > 0$; 1b- internal waves in shallow water. Isotherms in °F, from the literature.

Solution (5) and that for the frequency $\omega$ correspond to each normal mode internal wave. The parameter $\gamma$ of nonlinear internal waves is calculated for two typical $N^2$ distributions in the ocean. In the case of $N^2 = N_o^2 = \text{const}$, where $N_o^2$ is the maximum $N^2$ value, $\Omega = 1$ and the nonturbulent density distribution $\rho_o$ (H) is exponential. It is shown that $\gamma_n < 0$ for each odd mode and $\gamma_n = 0$ for even modes. It follows that a general solution would be a set of nonlinear waves close to negative solitons and simusoidal waves. Hence, with $N^2$ const and the predominant first mode in shallow water, propagation of a group of negative solitons would be observed (Fig. 1b). The second typical case is represented by a stratified model

$$\rho_0 = \begin{cases} \rho_1 = \text{const} & \text{при } 0 > \eta > -l, \\ \rho_2 = \text{const} & \text{при } -l > \eta > -1, \end{cases} \tag{6}$$

where $l$ is the depth of discontinuity. Then, $\Omega = \delta(\eta + l)$. Calculation of

$\gamma$ shows that a solution in this case hardly differs from the Boussinesq approximation. If the upper layer is thinner than the lower, the solitons are positive ($\gamma > 0$); in the opposite case, the solitons are negative ($\gamma < 0$). At $\ell = 1/2[1 + \mu/8] + O(\mu^2)$, where $\mu$ is the characteristic of deviation from Boussinesq approximation, $\gamma = 0$ and the waves are sinusoidal.

Miropol'skiy, Yu. Z. Propagation of internal waves in an ocean with horizontal inhomogeneities in the density field. FAiO, no. 5, 1974, 519-532.

The author notes that most studies of internal wave behavior in the ocean concentrate on variation of parameters as a function of depth, while neglecting the horizontal direction. The latter should be accounted for, however, in view of the typically long horizontal propagation range of internal waves.

The study accordingly examines free internal waves propagating in a mean-density ocean as a function of Vaisalaa-Brunt frequency N and density $\rho$ in both x and z coordinates. The problem is solved by a method analogous to geometrical optics. The possibility for standing internal waves in an unbounded ocean is shown. Analysis of internal wave growth shows that they tend to approach local N frequency; also, wave amplitude increases with reduction in pycnocline depth. The study demonstrates the possibility of turbulence being generated by internal waves propagating in an ocean with horizontal density variability.

Borisenko, Yu. D., and Yu. Z. Miropol'skiy. Effect of nonlinearity on statistical distributions of internal waves in the ocean. Okeanologiya, no. 5, 1974, 788-796.

Statistical distributions of internal waves in the ocean are analyzed on the basis of the Longuet-Higgins theory. Expressions for the first two moments of distribution are derived from nonlinear equations based on the theory of internal waves. Theoretical results are compared to experimental data obtained from observations on isotherm fluctuations at two stations in the Atlantic Ocean.

Empirical distributions of probability density for isotherm fluctuations are given in Fig. 1.

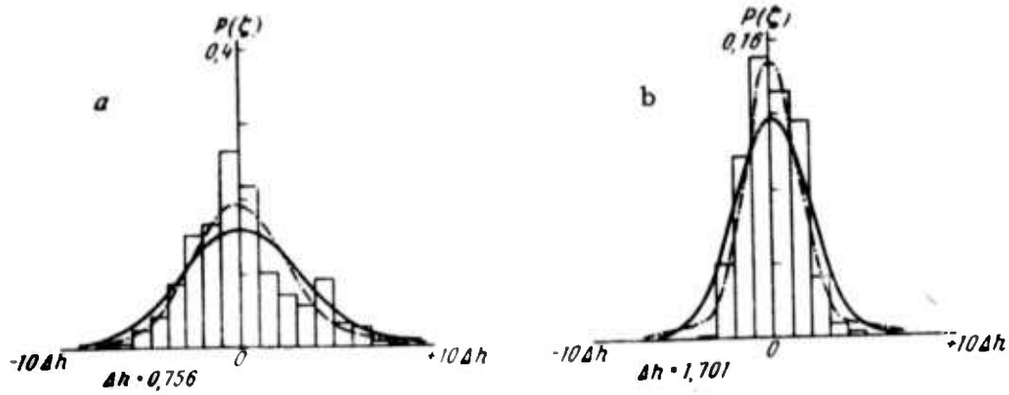


Fig. 1. Histograms of distribution density P (ζ).

a - station 1, isotherm 15° C; b - station 2, isotherm 17.5° C. Dashed line - distribution density calculated by the Longuet-Higgins formula.

Spectral functions of isotherm fluctuations within the $1.96 \times 10^{-2}$ $min^{-1}$ - $6.27 \times 10^{-1}$ $min^{-1}$ frequency range, calculated using data obtained in the Atlantic Ocean (Miropol'skiy, 1973), are shown in Fig. 2.

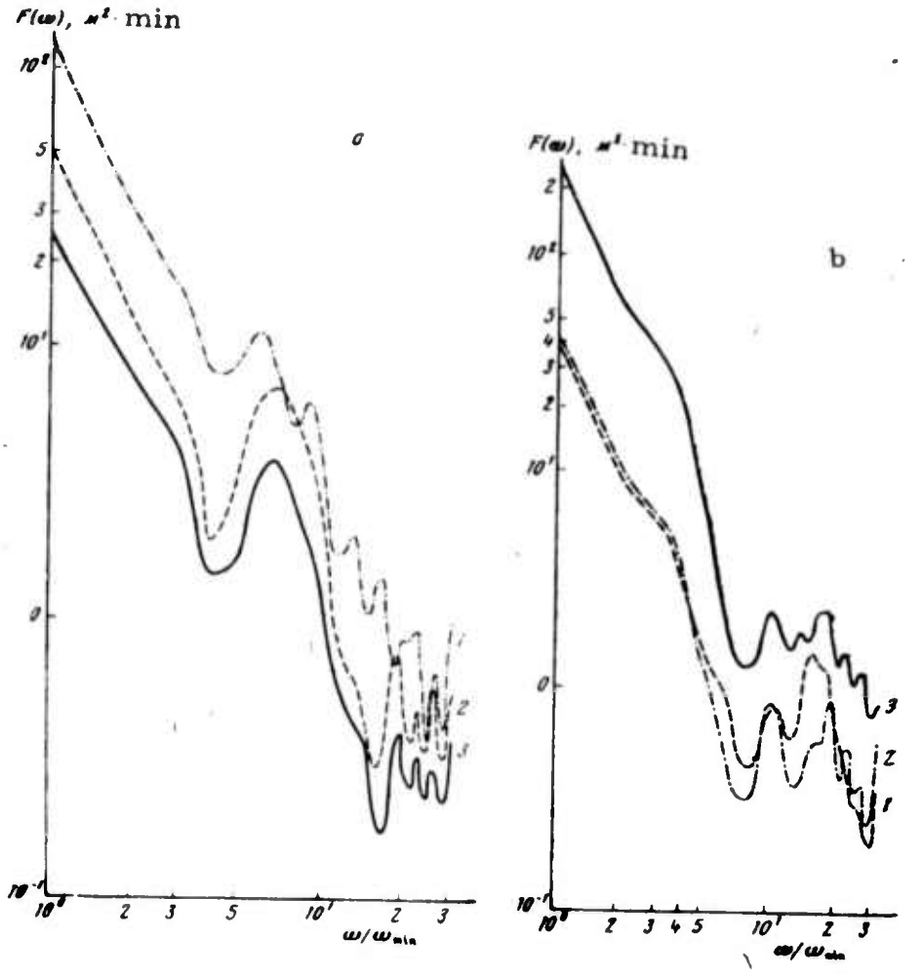


Fig. 2. Spectral functions $F(\omega)$ for various isotherms.

a- Station 1: 1-15°, 2-21°, 3-22.5°;
b- Station 2: 1-16°, 2-17.5°, 3-18°.

Empirical and theoretical values of dispersion $\mu$ and coefficient of skewness S for various isotherms are listed in the following table.

The authors conclude that the coefficient of skewness is a positive quantity in the case of a weak nonlinearity and prevalence of the first mode in internal waves.

| Isotherm, °C | | $\mu_э$, м² | $\mu$, м² | $S_э$ | $S$ |
|---|---|---|---|---|---|
| Station 1 | 22,5 | 0,97 | 1,03 | 0,369 | 0,367 |
| | 21— | 1,56 | 1,78 | 0,969 | 0,527 |
| | 19,5 | 2,68 | 2,95 | 1,010 | 0,687 |
| | 18 | 4,60 | 4,83 | 0,682 | 0,701 |
| | 16,5 | 6,63 | 6,71 | 0,400 | 0,522 |
| | 15 | 6,35 | 6,81 | 0,197 | 0,289 |
| Station 2 | 18 | 14,36 | 14,31 | 0,104 | 0,059 |
| | 17,5 | 11,57 | 11,74 | 0,044 | 0,013 |
| | 17 | 11,19 | 11,33 | −0,0048 | 0,217 |
| | 16 | 12,90 | 13,03 | 0,049 | 0,019 |
| | 15 | 32,07 | 32,33 | 0,042 | 0,077 |

Table 1

Garnich, N. G., and Yu. Z. Miropol'skiy. Some characteristics of the fine thermal structure of the ocean. Okeanologiya, no. 4, 1974, 595-601.

Vertical sounding of the temperature field to a depth of 600 meters was conducted in the central part of the Timor Sea, during the 7th cruise of the R/V Dmitriy Mendeleyev in 1972. Series of measurements at 2 hour intervals were made using the AIST salinity-temperature probe.

The vertical distribution of the average temperature in the tested area is shown in Fig. 1, a. Typical vertical distributions of temperature as detected by the AIST probe are shown in Fig. 1, b.

Spectral functions were calculated for temperature profiles described by the relation

$$T_i(z) = \bar{T}_i(z) + \theta_i(z), \qquad (1)$$

In order to avoid effects of statistical inhomogeneity of the random component $\theta_i(2)$, each $\theta_i$ series was divided into n homogeneous depth intervals of length $\ell$ and new series were calculated by

$$\theta_n = \sum_{i=1}^{I} \theta_{i,s} \qquad (2)$$

The length of new series was $L = I\ell$ where I = 7 is number of subintervals.

Spectral functions calculated for n = 7 depth intervals are shown in Fig. 1.

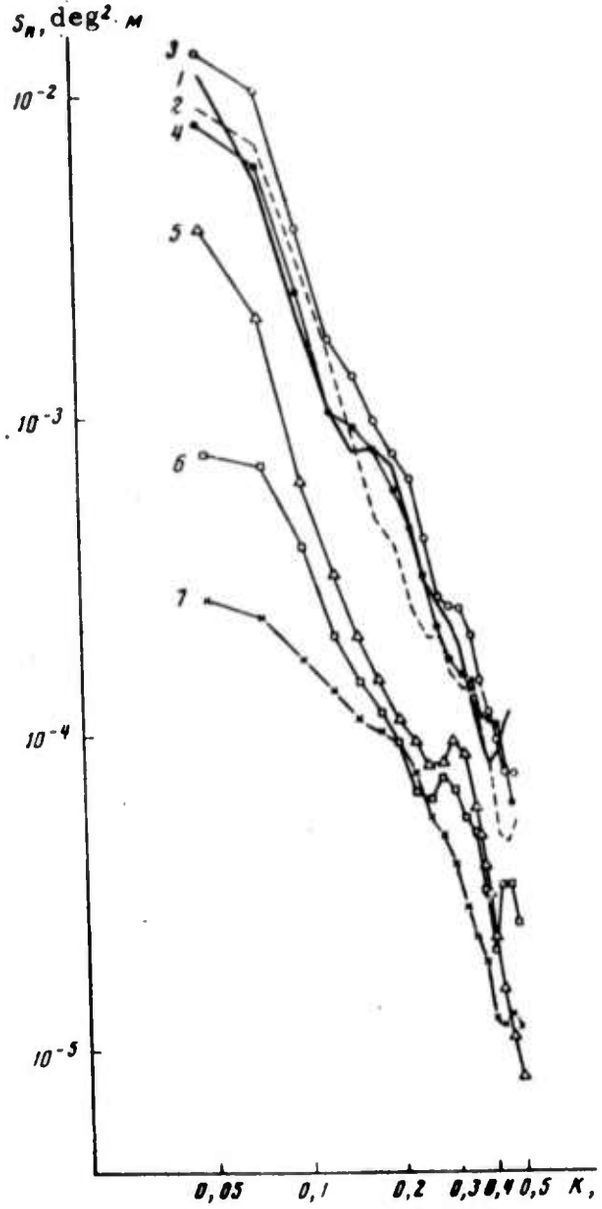


Fig. 1. Spectral functions $S_n(\kappa)$ for depth intervals
n = 1 - 50-120 m; 2 - 100-170; 3 - 150-200; 4 - 200-270; 5 - 300-370; 6 - 400-470; 7 - 500-570.

Spectral functions $S_n(k)$ shown in Fig. 1 are seen to be similar to each other, and decrease monotonically as $k^{-3}$.

Depth dependences for the vertical gradient of the average temperature $(d\bar{T}/dz)_n$, standard deviation $\sigma_n$ $(d\bar{T}/dz_n)^{-1}$ are shown in Fig. 2.

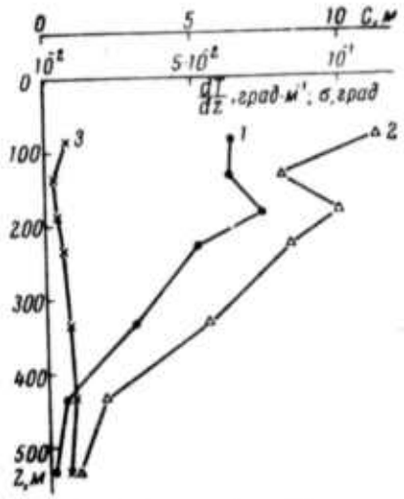


Fig. 2. Depth dependences for $(d\bar{T}/dz)_n$ (1), $\sigma_n$ (2), and $C_n$ (3).

The fact that the standard deviations are proportional to the vertical gradients of the average temperature, i.e., C = const (see Fig. 2) suggests that the depth dependence for $S_n(k)$ may be determined by the depth dependence for $(d\bar{T}/dz)_n$. In that case the following relation may be assumed:

$$S_n(k) \sim k^{-\beta}. \tag{3}$$

The spectral functions normalized by $(dT/dz)n^2$ are shown in Fig. 3.

As can be seen in Fig. 3, equation (3) is satisfied only for small wave numbers, i. e., large scale inhomogeneities, $\lambda > 10$ m. The average value of $\beta$ is $7 \times 10^{-4}$. The results shown in Fig. 4 confirm that conclusion.

Hence the relation C = const is satisfied only for small wave numbers, i. e., large-scale vertical inhomogeneities in the temperature field. An explanation offered for this result is that vertical

microstructure in the ocean is generated by different mechanisms: by breaking of high-amplitude internal waves at small $\lambda$, by layer convection, and by "salt fingers" at small $\lambda$. More refined experiments are needed to resolve this question.

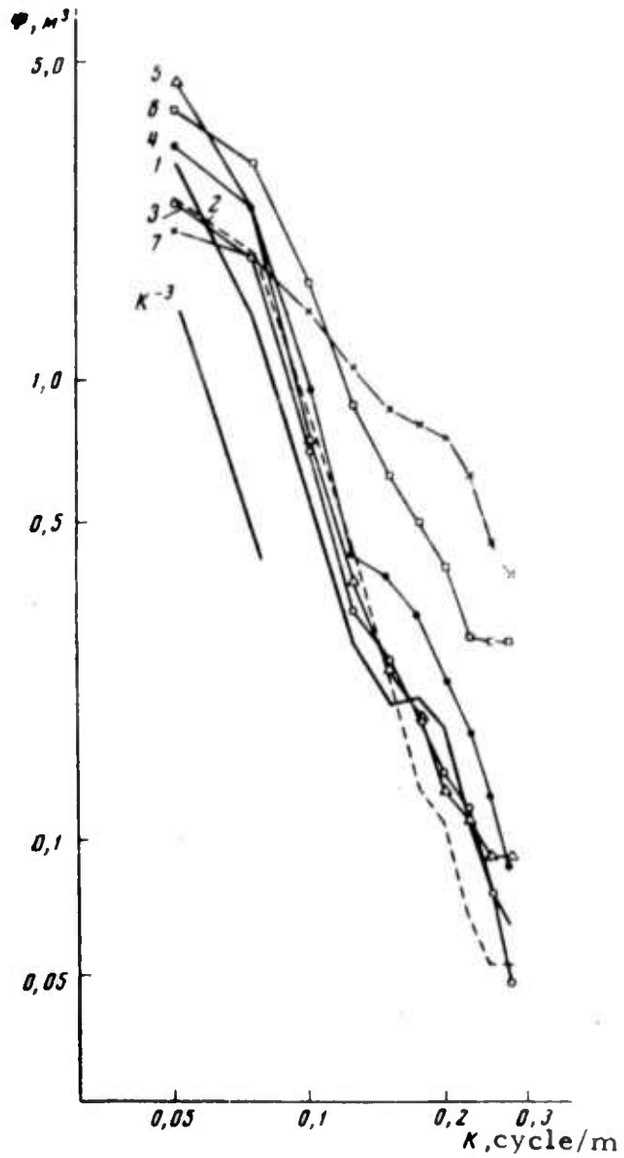


Fig. 3. Normalized spectral functions $\psi_n(k)$ for n depth intervals.

n = 1- 50-120 m; 2- 100-170; 3- 150-200; 4- 200-270; 5- 300-370; 6- 500-570.

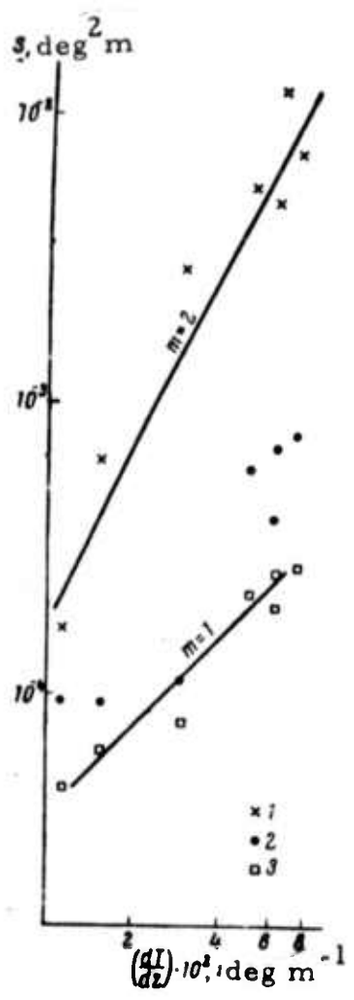


Fig. 4. Dependence of $S_n$ on $(d\bar{T}/dz)_n$ at different k.

1- k = 0.025; 2- k = 0.2; 3- k = 0.275.

Desnyanskiy, V. N., and Ye. A. Novikov. Modeling of cascade processes in turbulent currents. PMM, v. 38, 1974, 507-513.

Modeling of cascade processes of energy transmission, vorticity, and nonuniformity of admixture concentration using the spectrum of turbulent motion is of special interest in the study of turbulent flows. Cascade processes control the internal structure of flows and mechanisms of turbulent dissipation. It has been possible in recent years to obtain computer modelling of a two-dimensional spatial-periodical flow at modest viscosity, and to obtain the portion in the energy spectrum $E(k) \sim k^{-3}$ (Batchelor, 1969; Lilly, 1969, 1971; Gavrilin et al., 1972) which corresponds to the cascade process of vorticity transmission (Batchelor, 1969; Kraichman, 1967). The authors are aware of only one work on numerical modeling of three-dimensional periodical flows (Orszag and Patterson, 1972), in which the Reynolds numbers are however still too small to trace the cascade process of energy transmission and to obtain the portion of spectrum with the -5/3 power law. In addition to improving numerical experiments with a large number of degrees of freedom, it is also of interest to develop methods for reducing the number of degrees of freedom in a way that would not prevent realization of cascade processes. Such a method is suggested in the present work.

Model equations for collective degrees of freedom - Fourier amplitudes of velocity field, summed over an octave of wave numbers (wave number modulus changes by a factor of two within an octave), are derived from the hydrodynamics equation. The stationary solutions of these equations which give similarity laws in corresponding inertial intervals ($k^{-5/3}$ in three-dimensional, or $k^{-3}$ in two-dimensional turbulence) are analyzed. Nonstationary problems of formation of cascade processes have been numerically analyzed by Desnyanskiy and Novikov (1974).

Bogdanov, Yu. A., V. A. Burkov, V. M. Pavlov, and Ye. A. Plakhin. Some inhomogeneities of water stratification in the Gulf Stream area. Okeanologiya, no. 5, 1973, 755-759.

Results of integrated observations of fine structure in the Gulf Stream waters are reported and discussed. The observations were made in February 1972 during a cruise of the R/V Dmitri Mendeleyev. They included measurements of the absolute attenuation coefficient $\epsilon$ and transparency $\theta = 10^{-\epsilon}$ of water samples; vertical distribution of $\epsilon$ and temperature T; and composition and content of suspended particles in the same water samples. The SGN-M spectral turbidity meter, the FPR vertical profiling transparency meter coupled with a bathythermograph, and the AIST-STD recording meter were used to measure absolute $\epsilon$, $\epsilon(z)$ and T(z), respectively.

The cited optical and hydrologic parameters were measured at three ship stations: no. 351 at latitude 28°46' N and longitude 78°48' W; 352 at 28°44' N and 79°26' W, and 354 at 28°44' N and 79°50' W. The vertical profiles of the measured parameters are shown for all three stations. Homogeneity of the upper 100 m oceanic layer is deduced from the profiles at the station 351. The profile of suspended particle concentration shows a sharp increase in concentration at 10 m, and a decrease to a minimum at 100 m. The profiles at stations 352 (Fig. 1) and 354 (Fig. 2) are especially revealing, insofar as these stations were located near mid-Gulf Stream. They indicate optical stratification of waters, which is supported fully by the quantitative distribution of suspended particles. In the 200 to 300 m layer at station 352, the particles are rich in coarse carbonate material. At the same station, the T(z) profile plotted from AIST recordings exhibits three steps within the 0 to 200 m layer having small T gradients. The centers of these steps coincide with observed optical anomalies.

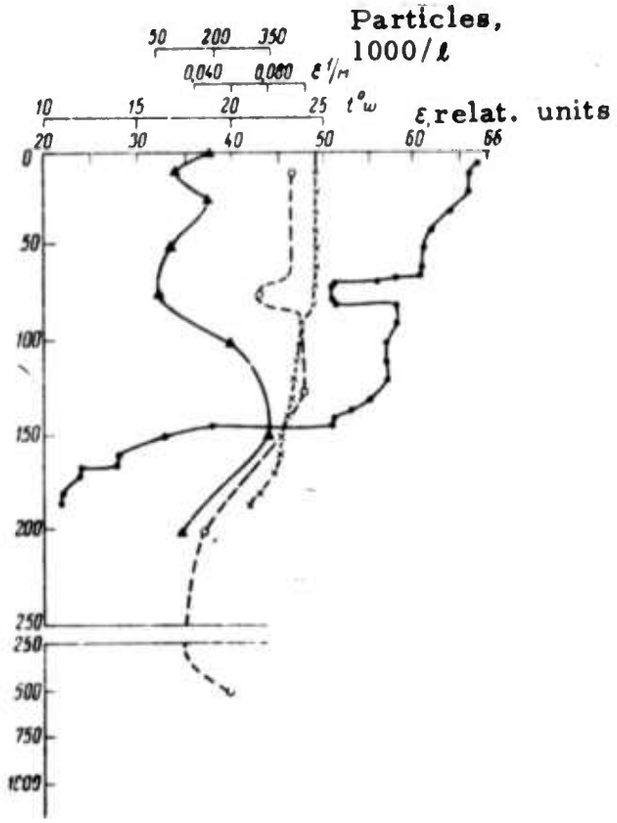


Fig. 1

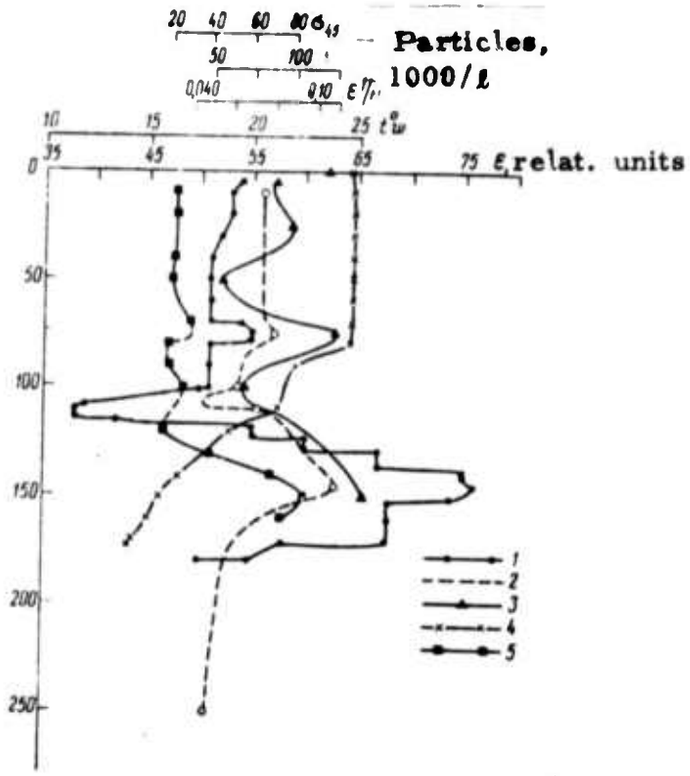


Fig. 2

Fig. 1 and 2. Vertical profiles of optical and hydrologic parameters at stations 352 and 354: 1- $\epsilon$ given by FPR meter; 2- $\epsilon$ given by SGN-M meter; 3- suspended particle concentration; 4- water T from bathythermograph data; 5- light scattering coefficient $\sigma_{45}$ at 45°, in relative units.

At station 354, the optical structure of the upper 200 m layer (Fig. 2) appears to be very complex. The turbid (to 78% transparency) layer, 60 m thick, centered around 145 m depth, is correlated with T discontinuity. Transparency at the 250 m level increases to 89%.

A summary of the cited data led to the conclusion that the 50 to 75 m upper layer is occupied by Gulf Stream waters, and may be in turn subdivided into several layers of decreased transparency and increased suspended particle content. Such a clear stratification of waters may be attributed to the hydrologic structure of the area. The depth of a sharp peak of suspended particle concentration within the 0 to 50 m layer coincides with that of minimum salinity and the steps of the T(z) profile. The low salinity indicates a possible influx of coastal waters.

Stiro, D. B. Study of vertical turbulent diffusion in the Baltic Sea. IN: Sb. Fiz. atmosfery, Vil'nyus, no. 1, 1973, 163-166. (RZhGeofiz, 4/74, no. 4V42). (Translation)

The coefficient of vertical eddy diffusion was calculated from an equation which describes tracer distribution (Ozmidov, Popov, 1965) using published data on $Sr^{90}$ concentration. The coefficient K varies from 0.6 to 0.9 $cm^2$/sec. The calculated data are compared with results of other authors. The $Sr^{90}$ concentrations on the surface and at 200 m depth in the Baltic Sea in 1960 and 1961 were calculated.

Bogdanova, A. K. The structure of the turbulent velocity field in the Bosporus area of the Black Sea. IN: Sb. Materialy Vses. simpoz. po izuchennosti Chern i Sredizemn. morey, ispol'z. i okhrane ikh resursov, Sevastopol', 1973, Ch. I, Kiyev, Izd-vo Nauk dumka, 1973, 59-63. (RZhGeofiz, 4/74, no. 4V49). (Translation)

Current velocity measurements by means of a BPV-2 meter have been carried out for 2.5 days in calm weather at 10, 25, 50, and 85 m. levels at one point, at 91 and 91.5 m levels at another point in the Bosporus area of the Black Sea. Using the current velocity observation series (at 10 min. discrete time), mean square root deviations, turbulence intensity, and coefficient of horizontal turbulent transport are calculated with different averaging periods. The coefficients of vertical turbulent transport are calculated from the equations of turbulent kinetic energy. Also, correlation functions, spectral density, and energy spectra are calculated. Analysis of the cited parameters indicated that, in the upper layer of Black Sea waters,

small-scale eddies play the major role in eddy thermal diffusion. Importance of intermediate-scale eddies increases in the Black Sea-to-Mediterannean transition layer. The 12 h. eddy is predominant in the bottom current of Mediterannean waters. Concurrently with the decrease in vertical diffusion momentum in the layer (85 m) of a sharp density jump, an increase in horizontal transport is noted. In that case, energy increases on account of the large-scale spectral region of turbulent eddies.

Gagoshidze, Sh. N. The transformation of stationary internal and surface waves in the presence of a stationary current and depth variability. IN: Trudy. Zakavkaz. n.-i. gidrometeorol. in-t, no. 31(37), 1973, 26-38. (RZhGeofiz, 4/74, no. 4V219). (Translation)

The problem of wave parameter transformation under conditions of variability in depth and in stationary current velocity is analyzed, on the basis of a linear theory of plane waves propagating on the surface of contact discontinuity and the free surface of two ideal flows with different densities.

Fundamental correlations of the amplitude and wavelength transformation coefficients for both interface and free surfaces are derived from the energy balance equation and the condition of periods equality in deep and shallow waters. Simplified design correlations of the cited coefficients are derived for certain specific ranges of depths and stationary current velocities.

Abramov, A. A., B. A. Tareyev, and V. I. Ul'yanova. Long waves and baroclinic instability on the inclined surface of an interface. IN: Vnutrenniye volny v okeane. SO AN SSSR, Novosibirsk, 1972, 244-256.

Results are given of a numerical analysis of frontal waves instability at a discontinuity surface in a stratified flow. The analysis covers the range of long waves and baroclinic instability, i.e., the $3 \leq \alpha \leq 12$ range of Richardson numbers and $0 \leq \beta \leq 1$ range of Rossby numbers $\beta = kU/f$, where U is the characteristic velocity and f is the Coriolis force. Thus the analysis previously made by Orlanski (Jour. Atmosph. Sci., v. 25, no. 2, 1968) is extended to cover the range of higher Ri numbers, and then to determine applicability rangesof the Kotsohin and the quasigeostrophic Phillips models of instability on the inclined surface of an interface.

Solution of a set of differential equations for the amplitude of small pressure disturbances on the inclined interface (Fig. 1) reduces

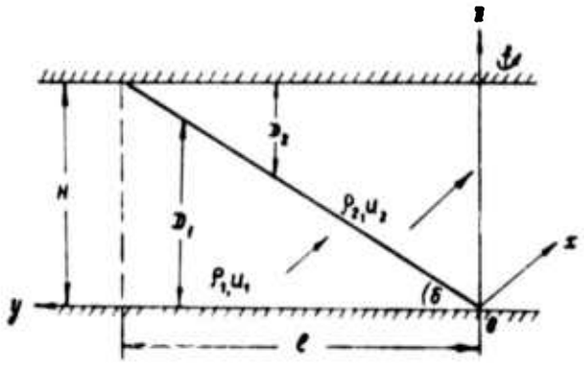


Fig. 1. Geometry of stratified flow.

to the problem of determining the eigen value of the instability increment $\tau$ as a function of $\alpha$ and $\beta$. In the most general case, $\tau = \tau_r + \tau_i$ is a complex number. The complex $\tau$ values are calculated for baroclinic instability of

the vortex gradient and internal gravity waves. In the case of the vortex gradient waves, $\tau_i$ and $\tau_r$ are calculated by integration of the set of differential equations using the method of successive calculations described by the authors in IFAiO, no. 2, 1972, 139. The $\tau_i$ and $\tau_r$ values are plotted versus $\alpha$ at $\beta = 0$ to 0.4. The contour map of $\tau_i$ eigenvalues (Fig. 2) shows that, within the Kotschin instability region (above the

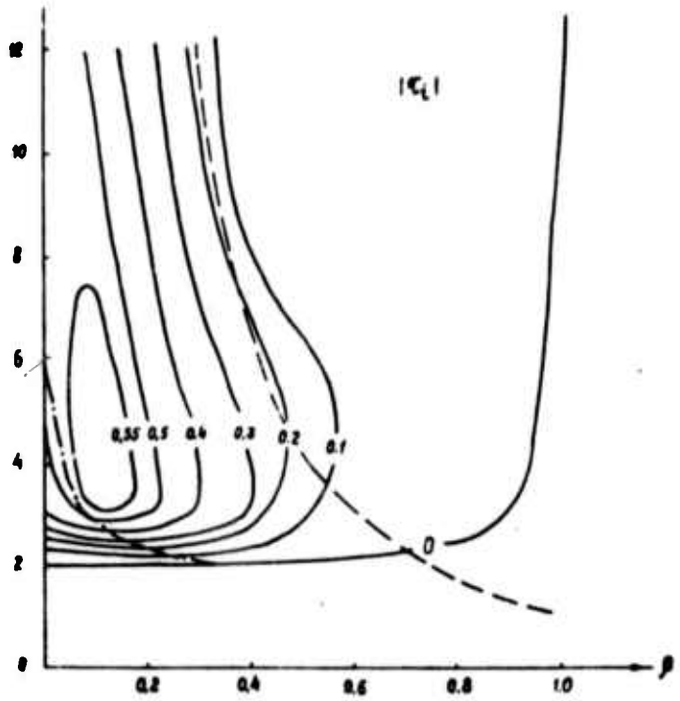


Fig. 2. Contour map of $\tau_i$ within the Kotschin instability region: the region of solely imaginary $\tau$ is to the left of the dot-dash line; the dashed line is the neutral line of the Phillips geostrophic model in the absence of beta-effect.

$\tau_r = \tau_i = 0$ curve) at $\alpha > 6$ $\tau$ becomes complex and a second $\tau$ eigenvalue appears, which is always smaller than the fundamental eigenvalue. At high $\alpha$ and small $\beta$, $\tau_r = 0$ in the Phillips model. Approximation of $\tau_r$ in the Phillips model becomes satisfactory only at very high $\alpha$ values, e.g., $\alpha = 100$ and $\beta = 0.02$.

In the case of internal gravity waves, numerical analysis shows that $\tau$ eigenvalues are real ($\tau_i = 0$) and are outside the boundaries of the unit circle in the $\tau$ - plane. The approximation $\tau = (\alpha - 1) + \beta^{-2}$ shows that, within the analyzed $\alpha$ and $\beta$ ranges, the Kelvin-Helmholz instability of gravity waves is absent. This is illustrated by the table of selected $\tau$ eigenvalues and the corresponding $\tau_r = \tau_r(\beta)$ plots (Fig. 3).

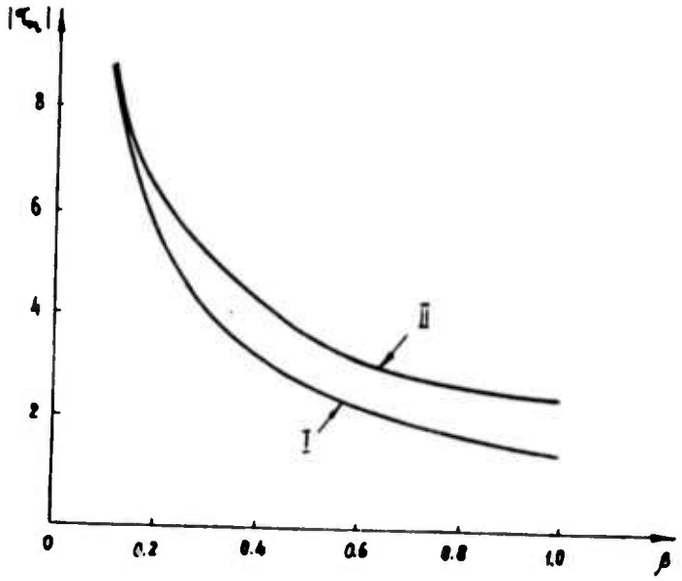


Fig. 3. Dimensionless phase velocity $\tau_r$ versus Rossby number $\beta$ (proportional to wave number) for internal gravity waves. Curve I - $\alpha = 4$, curve II - $\alpha = 9$.

The cited data thus confirm the insignificance of the beta-effect on behavior of internal gravity waves.

Yefimov, V. V., and V. M. Kushnir.
Analysis of the high-frequency portion of an ocean wave spectrum. Okeanologiya, no. 1, 1974, 30-36.

Results are described of the statistical processing of natural recordings of ocean waves. The functional mode of the HF portion of wave spectra obeys the expression $\omega^{-p}$, where $4 < p < 6$. For determining the probable value of exponent p in the case of wind waves, recordings of the surface waves were used, which were obtained in the storm test area of the Marine Hydrophysical Institute in the Black Sea.

Surface waves were measured by capacitive string wavemeters, attached to a fixed pole at 300 m from the coast at a depth of 15 m. Signals from the sensors were transmitted to the coast by cables, where they were converted to digital code and recorded on magnetic tapes. Values of discreteness in measurements were varied as a function of the statistical structure of the measured process, such that the ordinal number is maintained at a fixed level, at which the spectral density decreases from maximum at $\omega = \omega_o$ to a quantization value, determined by noise. Observation series treated were as long as $10^4$ numbers. Intervals of discreteness in different cases were varied from 0.06 to 0.5 sec.

In the present work, frequency spectra of surface waves are calculated and their behaviors analyzed. Table 1 shows the calculated results of the most likely exponent of the function, which is close to the behavior of the HF portion of the spectrum. It is seen that the exponent p' for different series of measurements lies in the range of 4 to 5; the average value of p' is 4.36. It is noted that the difference between the obtained average value of p' = 4.36 and the usually accepted value p' = 5 is not great. However, this may indicate the fact that during shaping of the HF portion of the sea wave spectrum, it is necessary to consider some other physical mechanism, which is different from that used in the expression based on the hypothesis

Table 1

| Wave frequency, $f_o$ Hz | Ave. wind velocity, $\bar{u}$ m/sec. | Exponent p' | Criterion $\epsilon/D$ | F-distribution quantiles at $\alpha = 0.05$ | Frequency range for analysis, $1.3 f_o - f_{max}$, Hz |
|---|---|---|---|---|---|
| 0,183 | 7—8 | 4,2 | 1,08 | 1,3 | 0,238—1 |
| 0,183 | 9—11 | 4,4 | 1,25 | 1,3 | 0,238—1 |
| 0,266 | 7—11 | 5,3 | 1,2 | 1,4 | 0,346—0,835 |
| 0,234 | 7—9 | 4,5 | 1,42 | 1,32 | 0,302—0,92 |
| 0,29 | 5—7 | 4,2 | 1,5 | 1,45 | 0,37 —0,8 |
| 0,316 | 3—4 | 4,4 | 1,56 | 1,37 | 0,41 —1,23 |
| 0,286 | 5—7 | 4,4 | 1,4 | 1,45 | 0,37 —0,84 |
| 0,167 | 9—11 | 5,3 | 1,15 | 1,25 | 0,216—0,84 |
| 0,15 | 8—12 | 4,0 | 1,17 | 1,35 | 0,195—0,85 |
| 0,266 | 9—10 | 4,2 | 1,0 | 1,40 | 0,238—1 |
| 0.268 | 4 | 4,5 | 1,45 | 1,40 | 0,346—0,82 |
| 0.218 | 5—7 | 4,2 | 1,72 | 1,45 | 0,28 —0,65 |
| 0,183 | 6,5 | 4,4 | 1,2 | 1,3 | 0,238—1 |
| 0,322 | 4—6 | 4,1 | 1,35 | 1,5 | 0,416—3,2 |
| 0,322 | 4—6 | 4,8 | 1,08 | 1,5 | 0,416—3,2 |
| 0,322 | 4—6 | 5,0 | 1,43 | 1,5 | 0,416—3,2 |
| 0,322 | 4—6 | 4,0 | 1,05 | 1,5 | 0,416—3,2 |
| 0,322 | 4—6 | 4,2 | 1,23 | 1,5 | 0,416—3,2 |
| 0,322 | 4—6 | 4,4 | 1,30 | 1,5 | 0,416—3,2 |
| 0,21 | 7—9 | 4,2 | 1,06 | 1,3 | 0,27 —1,75 |
| 0,18 | 7—9 | 4,2 | 1,20 | 1,3 | 0,238—1 |
| 0,30 | 9,5 | 4,0 | 1,15 | 1,45 | 0,39 —0,8 |
| 0,266 | 9,5 | 3,9 | 1,58 | 1,50 | 0,346—0,7 |
| 0,266 | 9,5 | 3,8 | 1,82 | 1,6 | 0,346—0,68 |

of Phillips, namely

$$S(\omega) = \beta g^2 \omega^{-5}, \qquad (1)$$

where $S(\omega)$ - spectral density; $\beta$ - dimensionless constant; q - acceleration of gravity; $\omega$ - angular frequency.

Ivanov, Yu. A., and Ye. G. Morozov.
Deformation of internal waves by a flow with horizontal velocity shift. Okeanologiya, no. 3, 1974, 457-461.

A mathematical model is discussed for deformation of internal gravity waves by a flow with horizontal velocity shift. A numerical

analysis was carried out for negative values of $k_x x - \omega t = \pi/2$ in a flow with horizontal velocity shift is given in Fig. 1.

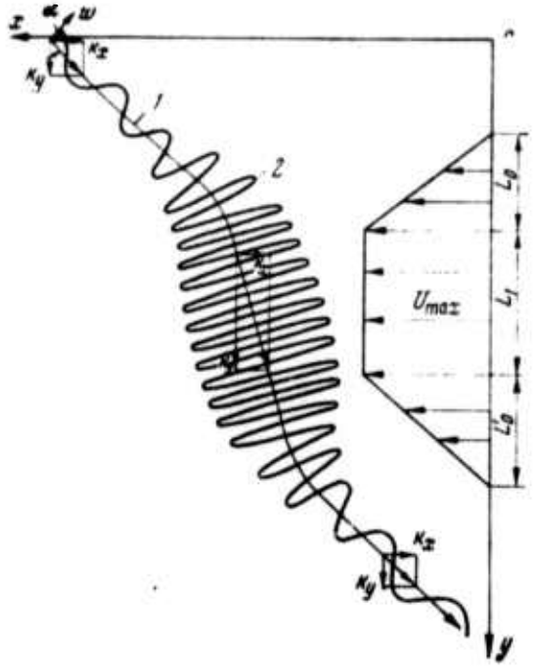


Fig. 1. Qualitative picture of the distribution of the average flow velocity U and deformation of internal waves.

1 - wave propagation direction; 2 - variation of w along the ray.

Variation of the amplitude of internal waves in a flow with horizontal velocity shift is illustrated in Fig. 2 and 3.

Numerical analysis shows that a large horizontal velocity shift induces significant deformation of internal waves over a wide frequency range. As the horizontal velocity shift decreases the frequency range narrows toward the high frequencies. However, deformation of internal waves does not depend on $L_0$ (see Fig. 1). Furthermore, calculated values

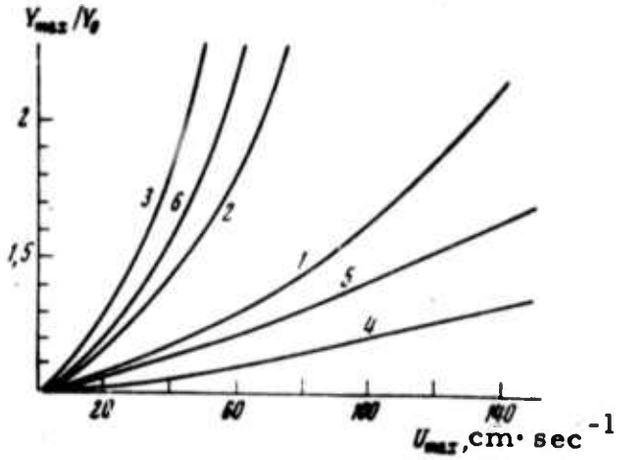


Fig. 2. Dependences of the ratio between the maximum and initial amplitude of internal waves on the maximum velocity shift for different modes and frequencies:

1 - $\omega = 0.20 \times 10^{-2}$ sec$^{-1}$, n = 1; 2 - $0.20 \times 10^{-2}$ sec$^{-1}$, n = 2; 3 - $0.20 \times 10^{-2}$ sec$^{-1}$, n = 3; 4 - $0.6 \times 10^{-3}$ sec$^{-1}$, n = 1; 5 - $0.17 \times 10^{-2}$ sec$^{-1}$, n = 1; 6 - $0.25 \times 10^{-2}$ sec$^{-1}$, n = 1.

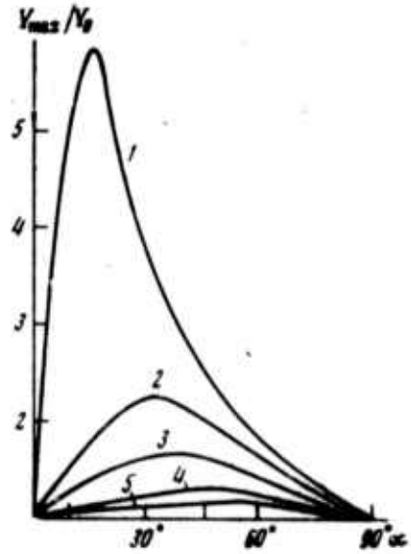


Fig. 3. Dependences of the ratio between the maximum and initial amplitude of the first mode on the initial incident angle $\alpha$ at $U_{max} = 100$ cm x sec$^{-1}$ and different frequencies:

1 - $0.24 \times 10^{-2}$; 2 - $0.22 \times 10^{-2}$; 3 - $0.20 \times 10^{-2}$; 4 - $0.14 \times 10^{-2}$; 5 - $0.6 \times 10^{-3}$.

of wave numbers at the beginning and end of the $L_0$ interval agree very well with values obtained using the Jones formula (1974) approximated for the present problem.

Chistyakov, A. I. The use of depth-stable bodies with towed oceanographic measurement systems. IN: Sb. Issled. okeanich. turbulentnosti, Moskva, Izd-vo Nauka, 1973, 139-142.

A mathematical model of a filtration process is developed for the effects of wave-induced ship motion on oceanographic measurements made with towed systems. Filtration is accomplished most simply and efficiently by using a passive intermediate depth-stable fish attached to the faired towing line, as described by Ozmidov (Report no. 2 of this series, Oct. 1974, p. 4). The filtering effect of the depth-stable fish is evaluated in terms of three main factors: the length of towing line from the stern to the depth-stable fish ($X_1$), the position of diving planes of the depth-stable fish ($X_2$), and the position of the fish suspension point coordinate on the horizontal axis in relation to the fish's center of gravity ($X_3$). A factorial experiment is described to establish the effect of the cited factors on the filtration process. The experiment was set up with the towed system assembled from devices widely used for oceanographic studies. A hydrodynamic body of airplane-like design was used as the depth-stable fish. The upper and lower limits of factor variations were: 45 and 30 m, -12 and +19 deg, and 1.2 and 1.1 m for $X_1$, $X_2$ and $X_3$, respectively. The angle of deflection of the tow line varied from 18 to 30 deg. The experiment made it possible to obtain the regression function $y = f(X_1, X_2, X_3)$, where y is the process output. The regression coefficients $b_i$ taken as the measure of $X_n$ effects on the process were calculated. The significance of $b_i$ for a 95% confidence coefficient was given as $b_i > 0.123$. Standard dispersion $\sigma^2$ of angular displacements of the instrument packages was evaluated by statistical treatment of experimental data. Results of the experiment are summarized in Table 1. The following conclusions are drawn from the analysis of the factorial experiment.

It is concluded that a significant improvement in the motion dynamics of oceanographic instrument packages is made possible by

| Experiment No. | Factors | | | Output $y = 1/\sigma^2$ 1/grad$^2$ | Matrix row | $b_i$ |
|---|---|---|---|---|---|---|
| | $x_1$ | $x_2$ | $x_3$ | | | |
| 1 | − | − | − | 0,132 | $x_0$ | 2,06 |
| 2 | + | − | − | 0,188 | $X_1$ | 0,216 |
| 3 | − | + | − | 0,350 | $X_2$ | 0,375 |
| 4 | + | + | − | 0,286 | $X_1X_2$ | 0,00875 |
| 5 | − | − | + | 2,8 | $X_3$ | 1,82 |
| 6 | + | − | + | 3,63 | $X_1X_3$ | 0,371 |
| 7 | − | + | + | 4,05 | $X_2X_3$ | 0,298 |
| 8 | + | + | + | 5,07 | $X_1X_2X_3$ | 0,0387 |

Table 1. Results of factorial experiment.

the use of an intermediate depth-stable body. The most significant factor of filtration is $X_3$. To increase the effect of filtration of interference from tow ship motion, the suspension point of the depth-stable body must be in the forward-most possible position. The $X_1$ and $X_2$ factors are mutually independent. The $X_3$ factor interacts positively with either $X_1$ or $X_2$, thus, the higher is $X_3$, i. e., the more forward the suspension point, the greater is the filtration effect from the increase in $X_1$ or $X_2$ (upward deviation of the diving planes).

Fel'zenbaum, A. I. A method for calculation of flow velocity, temperature and salinity fields in the ocean. DAN SSSR, v. 217, no. 1, 1974, 79-82.

A method is proposed for calculation of flow velocity, temperature and salinity fields in the ocean as functions of near-surface atmospheric processes. The method is based on a generalization of multiparametric models of temperature and salinity, and integral equations of turbulent temperature conductivity and salt diffusion for a multilayered ocean.

The multilayer ocean model consists of a stratosphere for which temperature and salinity are specified, and a troposphere in which these parameters are to be determined. The troposphere consists of a quasi-isothermic layer and seasonal and main thermoclines. The thickness of the quasi-isothermic layer is a function of horizontal coordinates and time, while the thickness of other layers are unvariable and specified. After some simplification, all calculations are done in the framework of a plane problem.

The equations derived are applicable to the ocean in general, including equatorial zones. If nonlinear accelerations were to be taken into account, however, the cited planar model would not suffice.

Mogilko, V. A., and Yu. A. Shcherbina. A new characteristic of the structure of turbulent pulsations. Tr. 18-y Nauch. konf. Mosk. fiz.-tekhn. in-t, 1972. Ser. Aeromekhanika. Protsessy upr. Dolgoprudnyy, 1973, 31-36. (RZhMekh, 4/74, #4B1039). (Translations).

A new characteristic was proposed for describing the scale of irregularities in a turbulent flow, named the S-function. This function is introduced as the distribution of probabilities of intervals between two successive zeros of the equation $c(t) = c_i$ ($c_i$ is an arbitrary number; $c(t)$ = concentration of passive tracer, and is assumed to be a stationary random function). Apparatus is described for measuring the S-function, and results are given of measurements in a submerged axially symmetric jet. It was established that the S-function is described by a log normal distribution of probabilities within a wide range of c values.

Karabasheva, E. Z., N. G. Kozhelupova, Yu. Z. Miropol'skiy, V. T. Paka, and B. N. Filyushkin. Some data on the spatial structure of internal wave fields in the ocean. Okeanologiya, no. 3, 1974, 462-467.

Measurements of spatial variations in ocean temperature, performed during the 2nd cruise of the R/V Dmitriy Mendeleyev in 1969 are described. The experiments were conducted in a test area in the North Atlantic along four pairs of tacks (see Fig. 1, a), using towed thermistor chains. Control experiments were conducted by using a hydrological buoy with a BPV current meter and photothermograph, and a radio buoy with an 8-thermistor chain set at depths of 40-180 m.

The area of measurements was found to be characterized by a distinctive seasonal thermocline at depths of 30-90 m, as illustrated in Fig. 1, b.

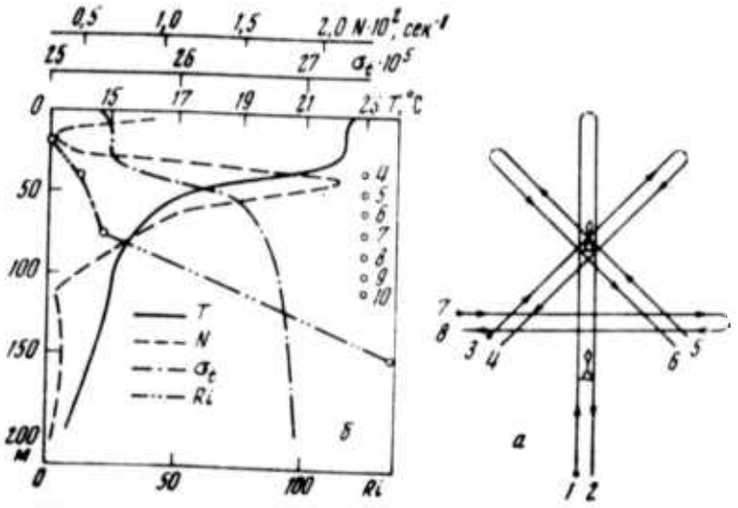


Fig. 1. Layout of tacks (a) and vertical distributions of temperature T(°C), conditional density $\sigma_t$, Vaisalaa frequency N, and Richardson number $R_i$ in the test area.

One-dimensional spectra of spatial temperature pulsations along individual tacks are shown in Fig. 2. They follow fairly well the

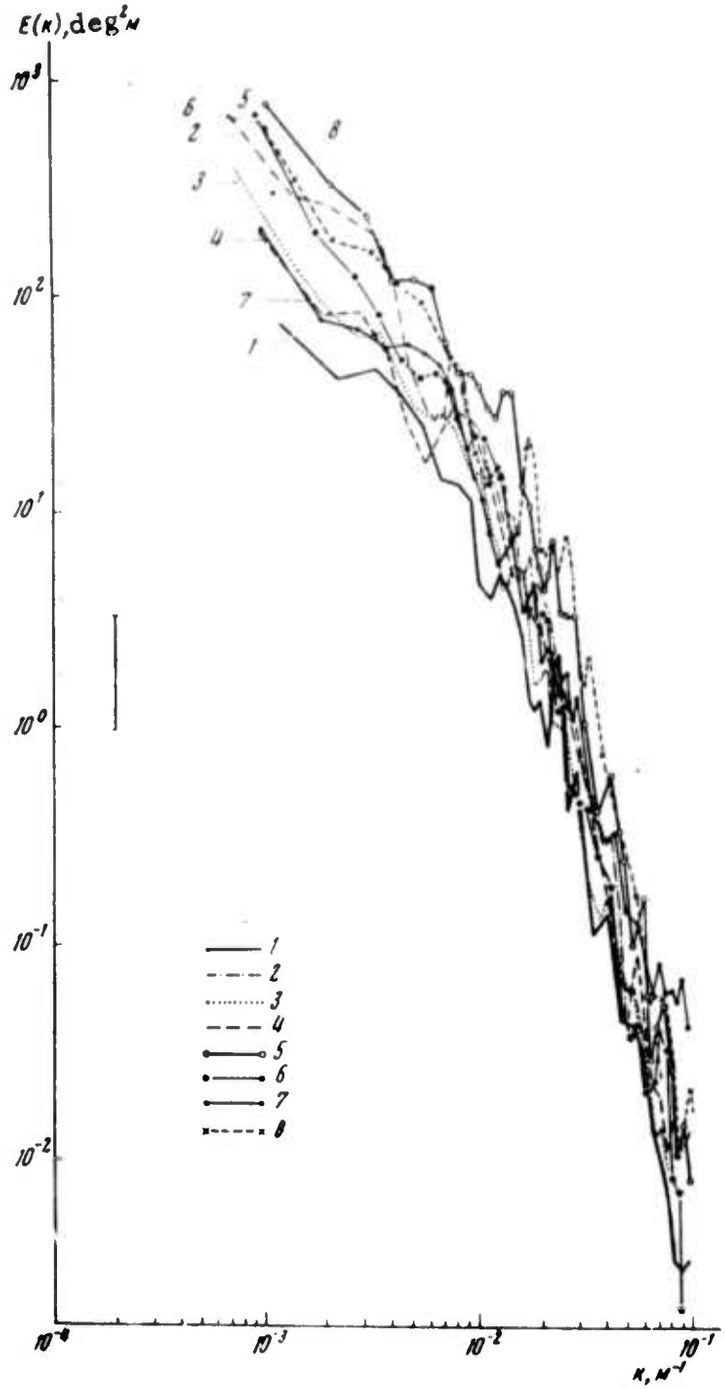


Fig. 2. Spectra of temperature pulsations along tacks 1-8 (sensor 5).

inverse power law $S \sim k^{-n}$ where $3 \leq n \leq 4$. The results shown in Fig. 2 suggest an isotropic temperature field at $k \geq 2 \times 10^{-2}$ $m^{-1}$, and an anisotropic one at $k \leq 2 \times 10^{-2}$ $m^{-1}$.

Two dimensional correlation functions for temperature pulsations are shown in Fig. 3. These were calculated by a method developed by Laykhtman et al., (1973) for four outgoing and return tacks with angles of $\pi/4$ between them.

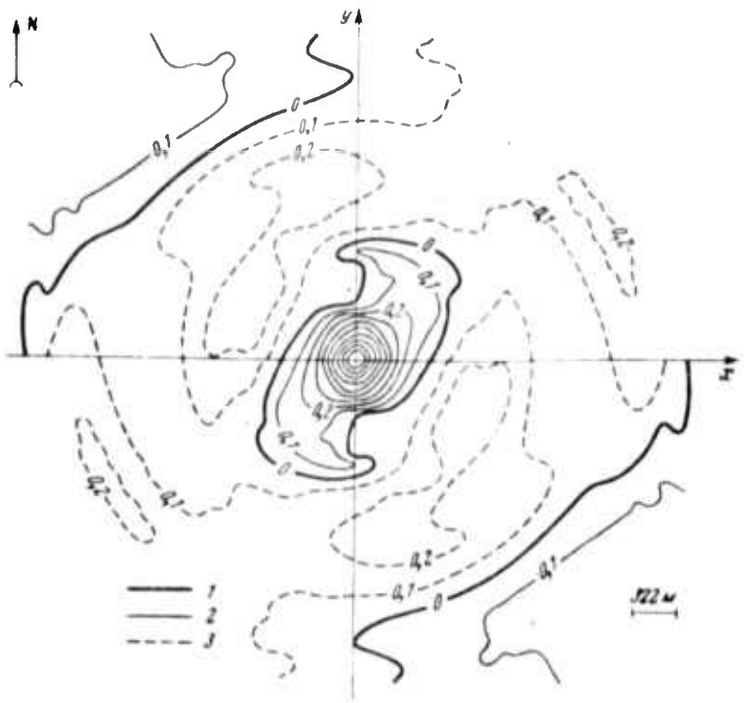


Fig. 3. Two-dimensional spatial correlation function for temperature pulsations at a depth of 60 m.

1 - zero values of correlation function; 2 - positive; 3 - negative.

As Fig. 3 shows, the internal wave field is isotropic over small intervals ($\sim$ 300 m) but anisotropic over large intervals. It is also somewhat directional in a NE-SW line.

Babiy, M. V., and L. V. Cherkesov. The effect of an underwater obstacle on long wave deformation. IN: Sb. Mor. gidrofiz. issled., no. 2(61), 1973, Sevastopol', 5-14. (RZhGeofiz, 1/74, no. 1V83). (Translation)

The title problem is examined in the framework of the linear theory of long waves in a homogeneous rotating liquid of variable depth. The Coriolis coefficient is assumed to be constant. A two dimensional periodical flow is postulated. The free surface is described by the expression $\zeta(x, t) = \zeta(x) \exp(-i\sigma t)$. The effect of localized variations of depth on wave profile is analyzed for the cases of wave crest and trough at a constant ocean depth, and for several constant-depth regions interconnected with regions of linearly variable depth. A solution is derived for each region. The level and speed of current at the boundaries are assumed to be continuous. Variations in reflected and refracted wave profiles are calculated for different depths and obstacle dimensions.

Geshev, P. I. Characteristics of the coefficient of turbulent exchange in a viscous sublayer. ZhPMTF, no. 2, 1974, 61-66.

Nonstationary equations are examined for longitudinal (flow direction) pulsations in velocity and concentration within the bounds of a viscous sublayer. Evaluations based on experimental data permit one to neglect certain terms in these equations in the case of turbulent exchange. In the resulting approximation expressions are obtained for coefficients of turbulent viscosity and diffusion. The variation in behavior of these coefficients is discussed for the case of large Schmidt (Prandtl) numbers. The behavior of turbulent Schmidt number in the viscous sublayer is analyzed.

Sekerzh-Zen'kovich, Ya. I. Steady state, finite amplitude capillary gravity waves generated by periodic pressure on the surface of a fluid flowing over a wavy bottom. DAN SSSR, v. 215, no. 1, 1974, 68-71.

A rigorous solution is obtained to the problem of an ideal incompressible fluid subjected to periodic surface pressure, expressed by an infinite trigonometric series, and acting over a periodic wavy bottom, also expressed as a trigonometric series. The particular case is examined in which the arc length of the bottom surface wave coincides with the length of a developed free linear wave, corresponding to a viscous flow for the case of a plane horizontal bottom and a constant pressure over the surface. Some approximate solutions are discussed. This work is an extension of an earlier paper by the author on an analogous problem, except that the surface pressure was constant rather than periodic.

Samodurov, A. S. Internal waves in a medium with a Vaisalaa-Brunt frequency dependent on the horizontal coordinate. FAiO, no. 3, 1974, 306-310.

Behavior of internal waves in an ocean region, where wave frequency $\omega$ approaches the Vaisalaa-Brunt frequency N(x, z), is analyzed for the particular case of N = N(x), where x is the horizontal coordinate in Cartesian coordinates. The problem of determining small deviations u and w of the waves' velocity components from the average stationary state is reduced to solving the expression for the flow function

$$\psi = \varphi(x, z)e^{i\omega t} \qquad (1)$$

Then the deviations u and w can be determined from

$$u = \partial\varphi/\partial z, \qquad w = -\partial\varphi/\partial x \tag{2}$$

The function $\varphi$ in (1) is determined for an infinite ocean with a linear vertical density profile $\rho(z)$ using a Boussinesq approximation, i.e., assuming $\rho_o$ constant. Typically, the linear $\rho$ distribution in the ocean is maintained by a geostrophic current perpendicular to the x-z plane.

Under the cited conditions, the governing set of equations of motion for an incompressible stratified liquid reduces to a single equation for the function $\varphi$ in the orthogonal system of coordinates r and q. These are defined in terms of $\omega$, N, x, z, H, and L, wher H and L are the vertical and horizontal distances, respectively, corresponding to the maximum ($\sim 10^{-3}$) relative $\rho$ variation in the ocean.

The main conclusion from the analysis is that the amplitude and length of internal waves increase and decrease, respectively, toward decreasing N(x) and, ultimately, break down in the vicinity of $N(x) = \omega$ with the resulting generation of turbulence in a stratified layer. During measurements, local increase in amplitude of internal waves in the vicinity of a breaking point is visualized as a wave train.

Karyakin, Yu. Ye., and V. G. Sharov. A finite difference method for calculating the turbulent boundary layer of an incompressible liquid. I-FZh, no. 2, 1974, 298-304.

Numerical computation of a turbulent boundary layer is made using an implicit finite difference method to solve the equations of the layer motion, both in the presence and absence of injection on a streamline surface. The equations of motion are presented in the form of a single differential equation in Leese variables $\xi$ and $\eta$. Two numerical grids are used for the approximation. Both approximation methods produced finite-difference

equations of the type

$$a_i F_{i-1,j+1} + b_i F_{i,j+1} + c_i F_{i+1,j+1} = g_i, \quad i = 1, 2, \ldots, N-1. \tag{1}$$

where $F = \partial f / \partial \eta$ is the unknown grid function; $a_i$, $b_i$, $c_i$, and $g_i$ are variable factors; and N is the number of nodal points across the boundary layer. Equation (1) is solved by iteration with successive calculations of f in each layer at $\xi$ = const. A certain point $x = x_t$ was used as the starting point in computation; this point is assumed to be the transition from laminar to a developed turbulent boundary layer.

Calculations for the main region of flow are in good agreement with experimental data. The theoretical data calculated on the basis of the local similarity hypothesis are acceptable only for flows with a negative pressure gradient. In the presence of injection into boundary layer, the finite-difference method adequately describes the deformation in velocity profile, even at fairly high injection parameter values.

Pavel'yev, A. A. Development of grid turbulence in a flow with a fixed velocity gradient. MZhiG, no. 1, 1974, 38-47.

A mathematical model is developed to calculate a boundary layer flow, a pipe flow, a mixed flow, or any other turbulent shear flow. To simplify the analysis a homogeneous grid turbulence in a flow with constant velocity gradient $\partial u_1 / \partial X_2$ is assumed. Two mathematical models of such a flow are developed from the Napier-Stokes equations. One model of five partial differential equations can be used to calculate a flow at any arbitrary Reynolds number, Re; the other model of three such equations describes the flow at a large Re. The five equations of the first model give the mean fluctuating velocity components $< u_2^2 >$ and $< u_3^2 >$ along two axes, the mean Reynolds stress $< u_1 u_2 >$, the turbulent energy E, and the turbulence

length scale L. The equations for $< u_1 u_2 >$, E, and L represent the second model.

Solutions for the derived equations were obtained by computer. Calculated results have compared favorably with available experimental data.

Gledzer, Ye. B. Solution of functional equations in a theory of turbulence. MZhiG, no. 1, 1974, 21-28.

The author analyzes equations defining turbulent flow of a viscous incompressible fluid. Small scale turbulence is described by a Guassian field of external forces with Gaussian mean value equal to zero. Using this model, a set of functional equations is solved for the characteristic functional $\Phi[z]$ of the spatial-temporal Fourier transform of turbulent velocity field, u (x, t).

Next a closed set of functional equations is derived to determine the functional $\psi_{ij}[z]$ of the true tensor $\psi_{ij}$ of velocity field reaction to an infinitesimal external force. Both functionals $\Phi[z]$ and $\psi_{ij}[z]$ are expressed through the true spectral tensor $B_{ij}$ of velocity field and the true tensor $\psi_{ij}$ of the cited reaction. An approximate solution of the functional equation for $\Phi[z]$ is obtained in the form of a Gram-Charlier series in which Gaussian characteristic functional with $B_{ij}$ is the zero approximation. A method of graphical repesentation of functions and operators is used to determine $\psi_{ij}[z]$ and $\Phi[z]$.

The approximate solution obtained indicates an upper frequency bound in large-scale fluctuations of a velocity field.

Dotsenko, S. V. Teoreticheskiye osnovy izmereniya fizicheskikh poley okeana (Theoretical fundamentals of measuring physical fields of the ocean). Leningrad, Izd-vo Gidrometeoizdat, 1974, 152 p.

The author, who publishes frequently on oceanographic instrumentation, deals in this monograph with the theory of measurement of various physical fields of the ocean and with the corresponding measuring instruments. The monograph summarizes both Soviet and non-Soviet publications on theoretical aspects of some specific instruments or methods used in hydrophysical studies. Dotsenko's original studies make up a significant part of the published sources cited.

Chapter 1 discusses problems of hydrophysical measurements, including classification and mathematical descriptions of the operation of linear measuring instruments, capable of averaging in space and time. A mathematical description is also given of the instrument range function and multidimensional determinate and random fields.

In Chapter 2 the equation relating output signal of a moving instrument to the magnitude of its measured field is derived and anlyzed. Hydrophysical field measurement by vertical probing is the subject of the third chapter. Distortions of measured characteristics, caused by the instrument moving at a constant speed or rolling with the vessel are studied here.

The fourth chapter concerns measurement of statistical characteristics of isotropic or locally isotropic hydrophysical fields by an instrument towed or drifting at a constant speed. Typical spectra of an output signal are shown, and the concept of equivalent spectral characteristic is introduced. Field measurement with sensors of different configurations and different orientation with respect to direction of instrument motion is analyzed.

In Chapter 5, distortions of the spectra caused by the vessel rolling during measurement of random field components are studied, and tolerance limits of the instrument to roll or pitch are evaluated.

The sixth chapter treats measurement of random field components, using instruments with a multielement sensor array. Spectral characteristics of such instruments are examined in relation to different methods of connecting the elements, and the effect of spectral characteristics of the elements is evaluated. A method for designing such an instrument with preselected spectral characteristics is given.

In the final chapter methods of calculating spread functions of various sensors designed for measuring physical fields are described, and directions are indicated for experimental determination of spread functions. Most study results have been reduced to directly applicable formulas. Graphs and tables applicable to all practical cases are offered because of difficult application of certain formulas.

There are 11 appendices (calculations and tables) and 93 references, about 80% of them Soviet.

Davidan, I. N., T. A. Pasechnik, and V. A. Rozhkov. Determining the components of a wave energy balance equation in a spectral form, and some results of model calculations of probability characteristics of wave conditions. Trudy GOIN, no. 122, 1974, 59-78. (RZhMekh, 10/24, no. 10B602). (Translation)

A wave energy balance equation is presented, and a discussion given on the right-hand components of this equation. Based on generalized experimental data individual component values are calculated. Some cases of a partial analytic solution to the balance equation are given, together with the algorithm for its numerical solution. Results are discussed of modelling actual wave situations.

Kononkova, G. Ye., L. V. Boborchaya, T. I. Kavasheva, T. P. Petrovskaya, K. V. Pokazeyev, and V. A. Razumov. Effect of turbulent flow on wind waves. Vod. resursy, no. 1, 1974, 179-182. (RZhGeofiz, 8/74, no. 8V70)

An experiment was performed in an aerohydrodynamic channel to evaluate the effect of turbulent flow on wave formation, specifically on its energy and spectrum. Wind range was 8.3 - 14.5 m/sec. Turbulence was generated by injecting a horizontal jet at a depth of 10 to 20 cm, with $Re = 3 \times 10^4$. The range of mean wave periods was 0.32 - 0.45 sec, mean wave height was 2.4 to 4.5 cm. Wind and turbulent jet directions were the same. Waves were registered with a wire wave gage, while turbulent flow velocity was recorded by motion pictures of floating neutral particles in the stream. Calculations are made for dispersion, autocorrelation function and wave spectrum on the water surface. The drop in wave energy caused by turbulent flow is analyzed; the degree of suppression is evaluated as a function of dispersion, both with and without turbulent flow. Energy loss occurs mainly at the high-frequency spectral ranges, and is apparently caused by energy transfer from the surface to the turbulent layer.

Shekhvatov, B. V., and E. V. Suvilov. A temperature recording current meter with a magnetic recorder. Okeanologiya, no. 5, 1973, 883-886.

The type TsITT improved self-contained recording meter for simultaneous measuring of speed and direction of currents and water temperature is described in detail. The improvements include a digital data recording system which provides direct data input to a computer with a large-capacity magnetic storage. The meter was designed at the Academy's

Shirshov Oceanographic Institute, for measurements from aboard ship, buoy stations, piers, etc.

The measured parameters are converted into variable resistances, measured by the method of ordered weighing on a bridge. The data are recorded on magnetic tape using a progressive binary code. A general view and a block-diagram (Fig. 1) of the meter show its main components. The components are enclosed in a cylindrical casing designed

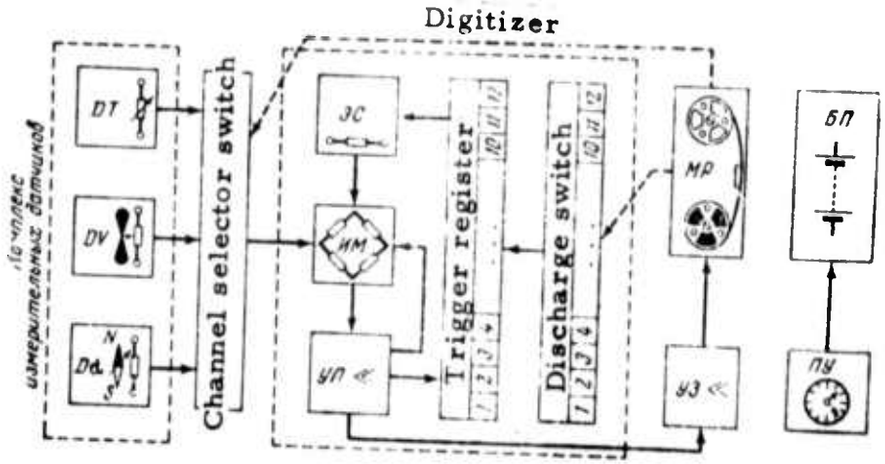


Fig. 1. Temperature and current recording meter. DT-temperature sensor; DV-current velocity sensor; Dα-current (direction) indicator; ЭС-standard resistance, БП-power supply; MP-magnetic recorder; УЗ-write amplifier; ПУ-timer.

to withstand 200 atm hydrostatic pressure. All electromechanical systems are combined into a single unit which is fastened to the upper lid of the instrument. The temperature sensor, a solid-state thermistor, is mounted on the outer face of the lid. The current velocity sensor assembly and its magnetic coupling with the potentiometer are mounted on the bottom lid; this sensor rotates on a vertical axis. The current-direction indicator is a self-correcting potentiometric compass. Start-stop operation of the magnetic recorder is optimized by its synchronization with the discharge switch and tape drive mechanism of the magnetic recorder. In this way, a constant on-off time of pulse signals is assured, regardless of speed variations of the tape-drive mechanism and in the absence of stabilization

of rotational velocity. The write amplifier combines a coded pulse shaper and amplifier of the magnetic recorder output.

Specifications of the TsITT are as follows:

| | |
|---|---|
| Current speed measurement range - 2.5 to 150 cm. sec$^{-1}$ | |
| Speed measurement accuracy to 10 cm. sec$^{-1}$ | $\pm$10% |
| Speed measurement accuracy from 10 to 150 cm. sec$^{-1}$ | $\pm$3% |
| Direction measurement accuracy | $\pm5^{\circ}$ |
| Temperature measurement range | 1 to 30° C |
| Temperature measurement accuracy | $\pm$0.02° C |
| Duration of a three parameter measurement cycle | 18 sec |
| Intervals between measurement cycles | 5, 15, and 30 min. |
| Capacity of magnetic recorder | 10,000 cycles |
| Supply voltage | 12 v |
| Battery capacity | 3 a-hr |
| Maximum immersion depth | 1.5 km |
| Duration of self-contained operation | 6 months |
| Dimensions of instrument less stabilizers -length, diam., | 840 mm<br>220 mm |
| Instrument weight in air | 60 kg |

Akhmedov, T. Kh., and A. I. Kvasov. Possibilities for applying laser optical methods for image analysis in the study of turbulent flows. IN: Sb. Probl. gidroenerg. i vod. kh-va. Vyp. 11, Alma-Ata, Nauka, 1974, 150-157. (RZhMekh, 8/74, #8B958) (Translation)

A discussion is given of a directional optical filtering system for two-dimensional images. The design makes it possible to separate out lines with a preselected direction from a negative which is characterized by a variable amplitude transmission coefficient. The possibility was discussed for applying this design in analysis of the velocity field of visualized turbulent flow during the diffusion of an aerated water jet in a rigid diffusion funnel.

Chistyakov, A. I. Automatic control of towed systems for oceanographic measurements. IN: Sb. Issled. okeanich turbulentnosti, Moskva, Izd-vo Nauka, 1973, 143-148.

The dynamics of a towed system with an automatically depth-stabilized towed body are analyzed by a method of experimental programming. The purpose of the analysis was to develop a mathematical model for automatic stabilization of the depth-stable body's longitudinal motion. Such a model would be helpful in synthesizing a control system for a towed system with an active depth-stable body.

The output of the automatic stabilization process is formulated in terms of four main factors,

$$y(X_1, X_2, X_3, X_4) = \frac{1}{\sigma^2}, \qquad (1)$$

where $\sigma^2$ is the standard deviation of angular displacements of the instrument package; $X_1$, $X_2$, $X_3$, and $X_4$ are factors which represent the effects of the signals from the sensors for trim $\theta$ and angular velocity $\dot{\theta}$ of the depth-stable body, and the sensors for depth variations $H_k$ and trim $\theta_k$ or angular velocity $\dot{\theta}_k$ of the instrument package, respectively. The factorial experiment was set up to reveal the effects of each sensor signal and the interaction between the signals on automatic stabilization of the instrument package. The automatic control system consisted of elements of the AP-5 and AP-61 automatic pilots.

The experimental program and the calculated regression coefficients $b_i$ in the regression function (1) are tabulated. Statistical analysis shows that $|\theta b_i|$ values $> 0.0156$ are significant with 95% confidence level. Using the tabulated $b_i$ values, the regression function y is given in final form, which describes filtration of interferences from towing vessel motion with an active depth-stable body.

Table 1. Results of complete factorial experiment.

| Experimental No. | Factors | | | | $y = 1/\sigma_\theta^2$ 1/grad$^2$ | Matrix row | $b_i$ |
|---|---|---|---|---|---|---|---|
| | $X_1(\theta)$ | $X_2(\dot{\theta})$ | $X_3(H_k)$ | $X_4(\theta_k)$ | | | |
| 1 | − | − | − | − | 0,222 | $x_1$ | 0,266 |
| 2 | + | − | − | − | 0,229 | $X_1$ | 0,0250 |
| 3 | − | + | − | − | 0,181 | $X_2$ | −0,00840 |
| 4 | + | + | − | − | 0,298 | $X_1X_2$ | −0,0436 |
| 5 | − | − | + | − | 0,115 | $X_3$ | 0,0108 |
| 6 | + | − | + | − | 0,203 | $X_1X_3$ | 0,0357 |
| 7 | − | + | + | − | 0,215 | $X_2X_3$ | 0,00525 |
| 8 | + | + | + | − | 0,279 | $X_1X_2X_3$ | −0,0112 |
| 9 | − | − | − | + | 0,272 | $X_4$ | 0,0486 |
| 10 | + | − | − | + | 0,351 | $X_1X_4$ | −0,00365 |
| 11 | − | + | − | + | 0,371 | $X_2X_4$ | −0,0340 |
| 12 | + | + | − | + | 0,121 | $X_1X_2X_4$ | −0,0515 |
| 13 | − | − | + | + | 0,216 | $X_3X_4$ | 0,0255 |
| 14 | + | − | + | + | 0,550 | $X_1X_3X_4$ | 0,0323 |
| 15 | − | + | + | + | 0,320 | $X_2X_3X_4$ | −0,0132 |
| 16 | + | + | + | + | 0,279 | $X_1X_2X_3X_4$ | 0,00550 |

Analysis of the factorial experiment data led to the following conclusions: the factors $X_1$ and $X_4$ are positive and significant, while factors $X_2$ and $X_3$ are insignificant. But $X_2$ interferes negatively and $X_3$ interferes positively with $X_1$ and $X_4$ significant factors. Thus, allowance for signals from the sensors of $\theta$ is not appropriate, but allowance for signals of $H_k$ of a twin instrument pod is advisable in formulation of the control law for an active depth-stable body.

In summary, the control function of automatic stabilization must include signals from sensors of $\theta$ of the depth-stable body and sensors of $\theta_k$ and $H_k$ of one instrument package along the towing line. This conclusion can serve as the basis for designing the control system for any given towed system with an active intermediate depth-stable body.

Lyamshev, L. M., S. A. Salosina, and A. G. Shustikov. Pressure pulsations in a turbulent boundary layer during discrete fluid suction. Akusticheskiy zhurnal, no. 3, 1974, 435-442.

An analysis was given of correlation and spectral characteristics of wall-pressure fluctuations in a turbulent boundary layer during discrete fluid suction. The fluid suction was carried out in three ways: through a system of slots, with a porous belt, and with a perforated belt. The experiments included measurements of the average flow velocity in an uncontrolled boundary layer. Results are shown graphically.

It was established that fluid suction results in a decreased longitudinal and lateral correlation as well as power spectrum of wall-pressure fluctuations in the low frequency range. The decrease is smaller in the case of fluid suction through a system of slots, and larger in the case of suction through porous or perforated belts. However, in the high frequency range the power spectrum of wall pressure fluctuations increases during fluid suction.

Trapeznikov, Yu. A. Study of two-dimensional spectral density of sea waves from records of disturbed surface at several points. Trudy GOIN, no. 122, 1974, 47-58. (RZhMekh, 10/74, #10B604). (Translation)

Problems are considered in calculating the Fourier coefficients of a two-dimensional spectrum of sea waves by the Longuet-Higgins-Sveshnikov method, using records of a disturbed sea surface at several points. It is shown that the cited method can be applied for the study of time variability in the spectral structure of sea waves. The effect of sensor spatial resolution on the calculation of spatial derivatives of a disturbed sea surface is evaluated.

Leonov, A. I., and Yu. Z. Miropol'skiy. Nonlinear internal gravity waves in a steady-state mode. Okeanologiya, no. 3, 1974, 575-576. (Translation)

This paper undertakes a study of finite-amplitude internal gravity waves in a steady-state mode, i.e., those waves for which the flux function and all other characteristics have the form $\psi(t, x, z) = \psi(\theta, z)$ where $\theta = x-vt$, $\theta$ = phase and v = phase velocity. As is generally known, complete hydrodynamic equations for two-dimensional steady-state waves in a stratified fluid account for the first two integrals, and as a result an equation containing two undetermined arbitrary functions is obtained for the flux function. The presence of two undetermined arbitrary functions complicates the problem considerably. Since the vertical profile of undisturbed Vaisalaa-Brunt frequencies N(z) can be measured, it is reasonable to use it in calculations of internal waves, both in the atmosphere and the ocean. Therefore it is of interest to express the unknown arbitrary functions through N(z). Determination of N from the solution with an arbitrary function leads to a complex or unsolvable inverse problem.

The authors of this paper show that, with certain assumptions, the undetermined arbitrary functions can be expressed through N(x). Thus they obtained the following equation describing propagation of nonlinear steady-state internal waves in a fluid at rest:

$$\Delta\Psi + \left\{\frac{\Psi}{v^2} + \frac{1}{2vg}\left[\left(\frac{\partial\Psi}{\partial\theta}\right)^2 + \left(\frac{\partial\Psi}{\partial z} - v\right)^2 - v^2\right]\right\} N^2\left(z - \frac{\Psi}{v}\right) = 0. \qquad (1)$$

here $\Delta = \left\{\frac{\partial^2}{\partial\theta^2} : \frac{\partial^2}{\partial z^2}\right\}$ and g is acceleration of gravity. This equation does not contain the unknown arbitrary functions since $N^2(z)$ and $N^2(z-\psi/v)$ are predetermined.

Asymptotic solutions of equation (1) are considered for the following cases: propagation of internal waves in a shallow-water basin in the presence of weak nonlinearity and dispersion; propagation of internal waves in a narrow pycnocline; and propagation of short internal waves (wave length L much smaller than fluid depth H).

At $\epsilon = H/L$, solution of equation (1) is obtained in the form of an asymptotic expansion in terms of $\epsilon$ by a method analogous to the Poincare method in the theory of nonlinear oscillations. It is shown that equation (1) allows solutions for both periodical and solitary waves. Frequency, wave number and amplitude of periodical waves are connected by a nonlinear dispersion relation. A calculation of wave parameters for $N(z)$ in the ocean shows that both positive and negative solitary waves can exist. In addition, the possibility of using the Boussinesque approximation was analyzed. It was established that in certain cases the use of this approximation results in some errors.

At $\epsilon = \delta/L \ll p$, where $\delta$ is pycnocline depth, the solution of equation (1) was obtained in the form of an expansion in terms of $\epsilon$, which is valid within the pycnocline. It was combined with the solution for a nonstratified fluid, which is valid outside the pycnocline. The problem was reduced to solving a nonlinear boundary-value problem for the Laplace equations. This problem also allows for solutions both for nonlinear periodical and solitary waves. However, in contrast to the case of a shallow-water basin, the dispersion relation does not exist in an ordinary sense, and wave velocity is arbitrary. A sample calculation (for $N^2 = \text{const}$) shows that both positive and negative solitary waves can exist in a narrow pycnocline.

At $\epsilon = L/H \ll 1$, solution of equation (1) was found by an asymptotic method and the problem was reduced to a system of equations in terms of the first-order partial derivatives of wave amplitude and vector slowly changing in space. This system was analyzed by the method of

characteristics. A number of conservation laws relating to the characteristics were obtained, and an amplitude increase at the resultant caustics was noticed.

In conclusion the authors discuss numerous unsolved problems, and point out the importance of studying the stability of the obtained solutions in order to understand turbulence generation in a steady-state stratified fluid.

Shelkovnikov, N. K. Techniques for studying the structure of turbulent flows. VMU, no. 2, 1974, 205-209.

A simplified method is proposed for studying the structure of turbulent flows using data on velocity or temperature pulsations measured simultaneously at several spaced points. An example is given for calculation of propagation rate and scale of turbulent inhomogeneities from measurements of velocity pulsations in the main flow direction at two points.

Assuming that velocity or temperature pulsations are stationary in time, the author analyzes the turbulence structure using the space-time correlation function

$$R_{ij}^{(AB)}(x_1, x_2, x_3, \tau) = \frac{\overline{(u_i')_A (u_j')_B}}{\sqrt{\overline{u_i'^2}}\sqrt{\overline{u_j'^2}}}, \qquad (1)$$

where $x_1$, $x_2$, $x_3$ are spacings between points in the longitudinal, lateral, and vertical directions respectively. Longitudinal integral scales of turbulence in this case are

$$L_{ij}^{(1)} = v \int_{-\infty}^{+\infty} R_{ij}(x_1, 0, 0, \tau)\, d\tau, \qquad (2)$$

where v is the variation rate of the space-time correlation function.

For the correlation function assumed, the longitudinal integral scales of turbulence are given by

$$L_{ij}^{(v)} = v \int_0^{\tau_0} R_{ij}(x_1, 0, 0, \tau)\, d\tau, \tag{3}$$

or using the mean-value theorem, by

$$L_{ij}^{(v)} = v\tau_0 h, \tag{4}$$

where h is some mean value of $R_{ij}$. The variation rate of space-time correlation function is then $v = x_1/\tau$.

The scale of turbulent inhomogeneities at the zero correlation level hence is $\ell_0 = v\tau_0$, and at the 0.5 correlation level, $\ell = v\tau_{0.5}$. Form anisotropy of turbulent inhomogeneities is given by $\ell_1 = \ell_1/\ell_2$, $\ell_2 = \ell_1/\ell_3$, $\ell_3 = \ell_2/\ell_3$, where $\ell_1$, $\ell_2$ and $\ell_3$ are turbulence scales in three mutually perpendicular directions.

The cited calculations show that the turbulence propagation rate is equal to the average flow velocity, and that the turbulence scale decreases with time.

Nozdrin, Yu. V. Effect of buoyancy force on spectra of turbulent processes in the ocean. Okeanologiya, no. 5, 1974, 797-801.

The author analyzes the behavior of the three-dimensional energy spectrum of kinetic energy of a turbulent upper ocean layer. Theory predicts that in spectra of temperature and salinity fluctuations there will be an inertial-convective interval where energy E relates to wave number k by $E(k) \sim k^{-5/3}$ and a viscous-convective interval where $E(k) \sim k^{-1}$. However, experimental results have shown some disagreement with these relationships, and it is suggested that this is attributable to buoyancy forces

on volumes of water having a local density difference.

Nozdrin accordingly analyzes small-scale turbulence with effects of buoyancy and thermal diffusion taken into account, and establishes the conditions for which one would indeed expect a deviation from the "5/3" curve.

Navrotskiy, V. V. Amplitude structure of velocity and temperature fluctuations in the upper oceanic layer. FAiO, no. 7, 1974, 771-781.

An analysis is given of probability distribution functions for medium-scale fluctuations of current velocity and temperature in the upper oceanic layer. The results were compared to theoretical probability distributions. The following model turbulence processes were considered:

$$y(t) = a \sin(\omega t + \alpha) \quad (1);$$

$$y(t) = a \sin(\omega t + \alpha) + x_N(t). \quad (2)$$

where $x_N(t)$ has a distribution close to normal; and

$$y(t) = f(t)x(t). \quad (3)$$

where f(t) is a deterministic periodical function, x(t) is a random stationary function.

The results are shown in Figs. 1-6.

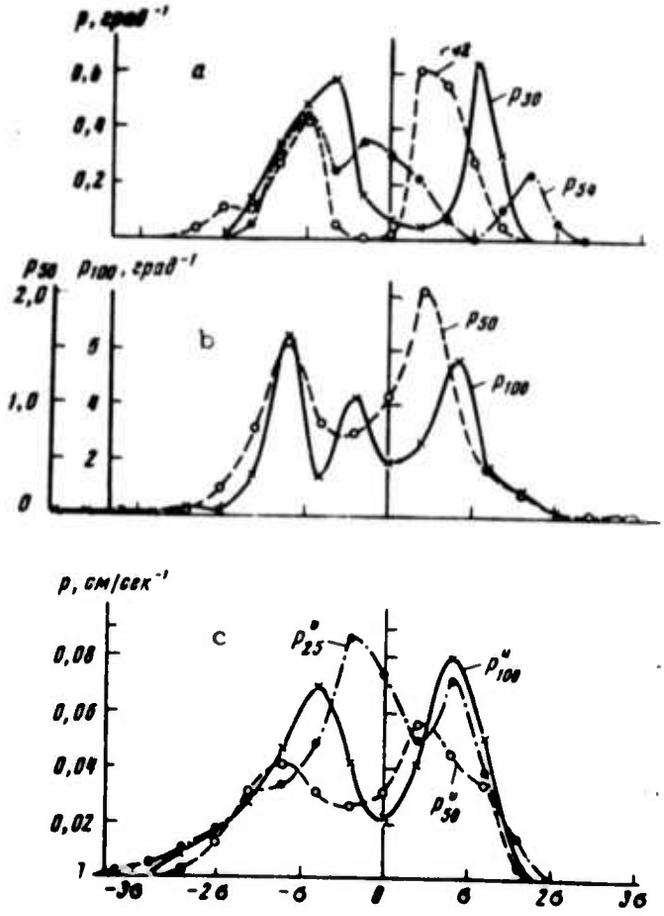


Fig. 1. Density of probability distribution for spatial (a) and time (b) temperature fluctuations, and spatial current velocity fluctuations (c) (3rd cruise of the R/V Academician Kurchatov). Mean values at different depths are:

a- $T_{30} = 25.5$, $\sigma_{30} = 0.32$; $T_{42} = 22.8$, $\sigma_{42} = 0.63$; $T_{54} = 19.8$, $\sigma_{54} = 0.52$.

b- $T_{50} = 18.2$, $\sigma_{50} = 0.27$; $T_{100} = 15.9$, $\sigma_{100} = 0.10$.

c- $\bar{v}_{25} = -9$, $\sigma_{25} = 5.2$; $\bar{v}_{50} = -15.4$, $\sigma_{50} = 7.9$; $\bar{u}_{100} = -17.8$, $\sigma_{100} = 6.1$.

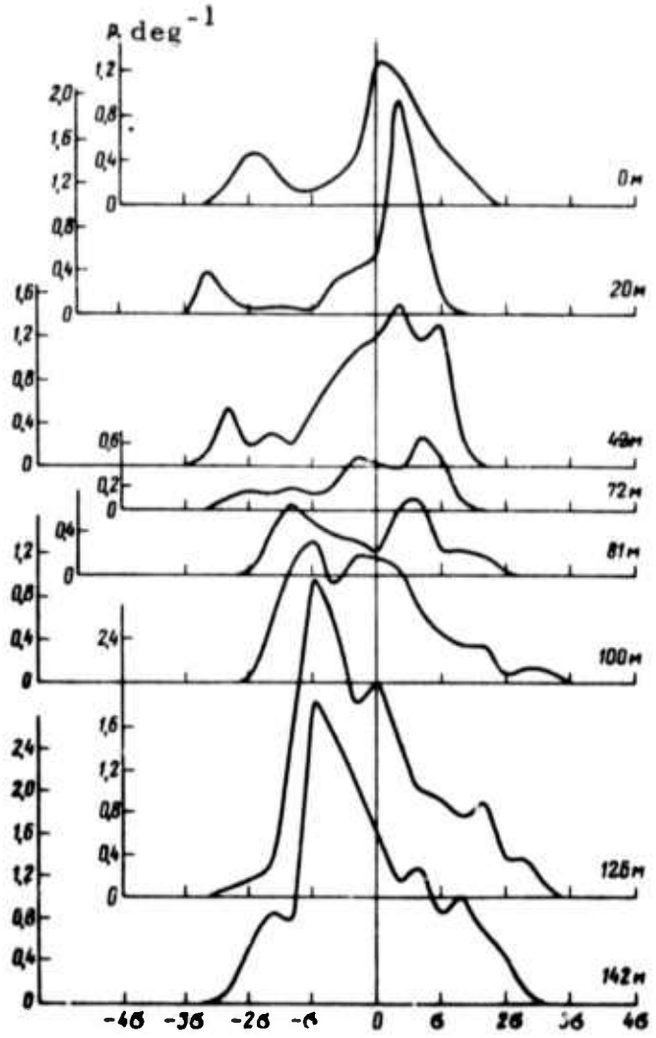


Fig. 2. Density of probability distribution for temperature fluctuations at different depths (16 May 1968, 3 rd cruise). Vertical distributions of the mean and rms values are shown in Fig. 3.

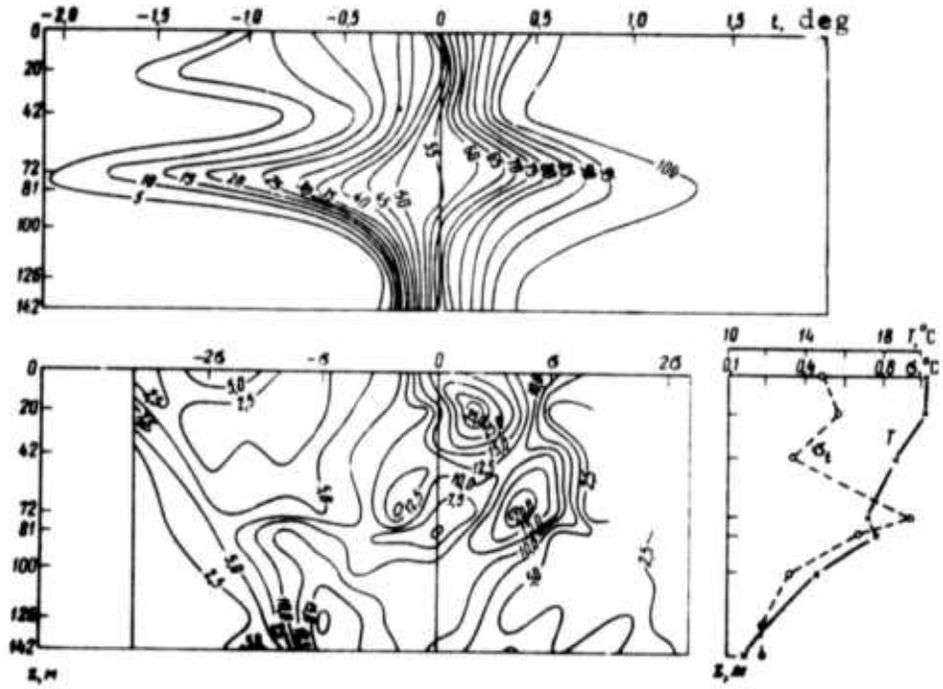

Fig. 3. Cross-section of probability distribution (above) and hit probability (below) for spatial temperature fluctuations (16 May, 1968, 3rd cruise).

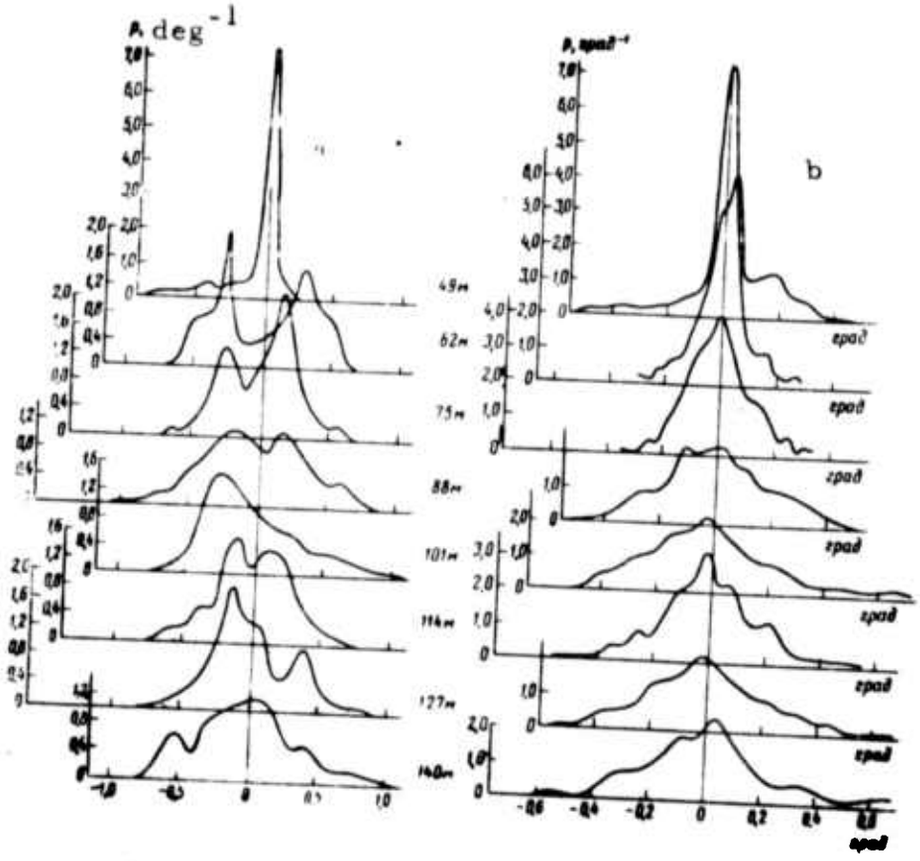

Fig. 4. Density of probability distribution for spatial temperature fluctuations before (a) and after (b) filtering (cruise 8, line 1).

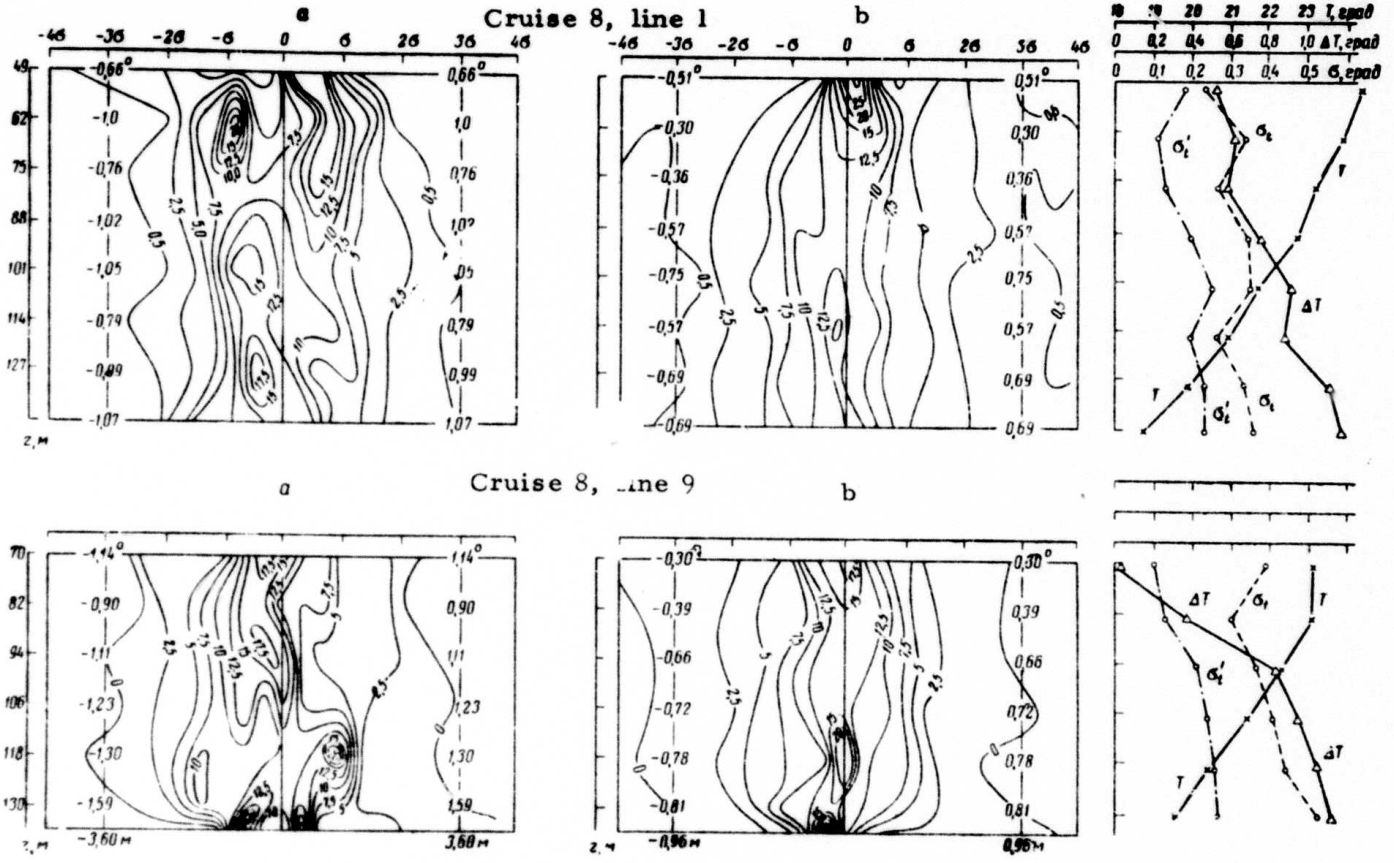


Fig. 5. Vertical distribution of probability for spatial temperature fluctuations before (a) and after (b) filtering (cruise 8, lines 1 and 9). Vertical distributions of the mean temperature T(z), the temperature difference between adjacent horizons $\Delta T(z)$, and rms fluctuations before and after filtering $\sigma_t(2)$ and $\sigma_t'(2)$ are shown on the right-hand side of the figure.

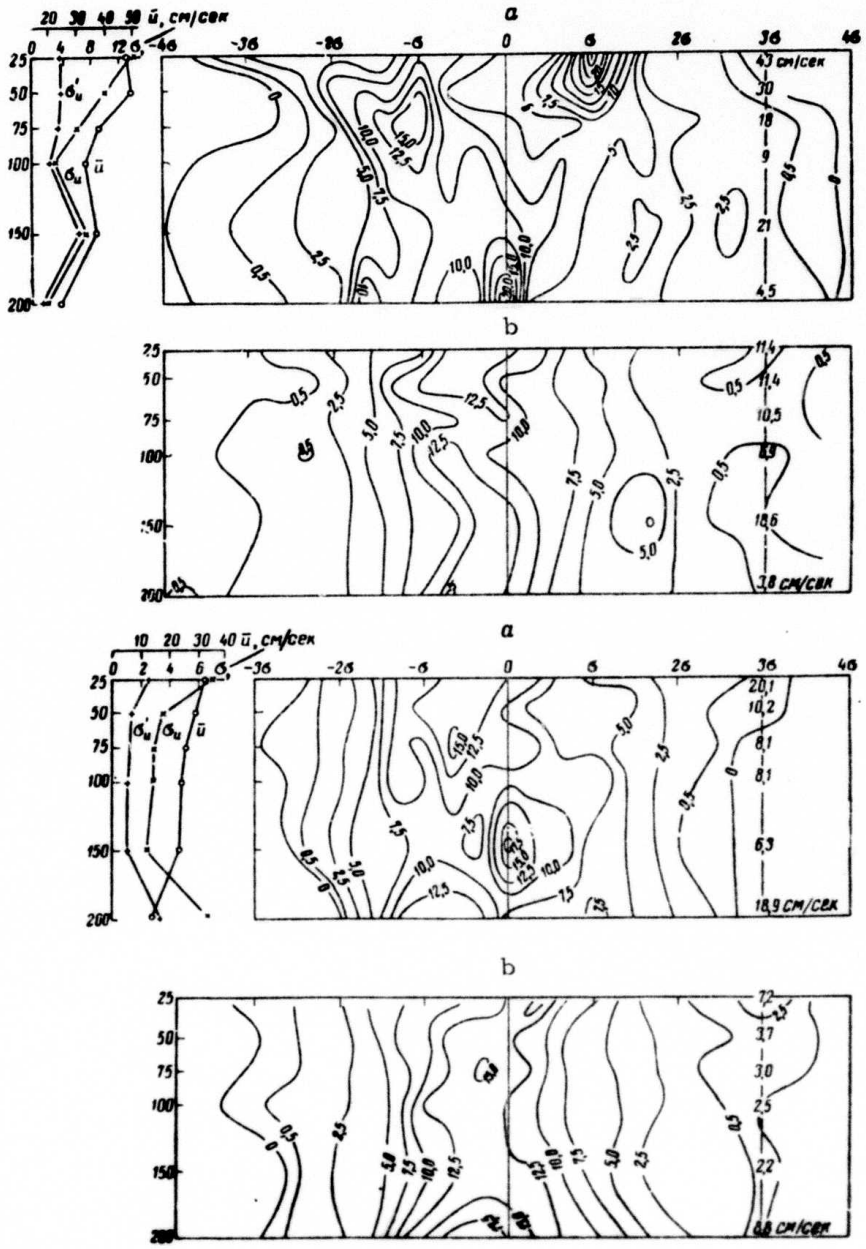


Fig. 6. Vertical distribution of probability for time velocity fluctuations before (a) and after (b) filtering (Buoy station C in upper graphs; buoy station D in lower graphs).

The probability distributions shown in Fig. 1 indicate the presence of wave oscillations in the temperature fluctuations. If side maxima are associated with internal waves, then the amplitudes of the internal waves are evaluated to be: 2 and 5m at depths of 50 and 100 m respectively in the case of time temperature fluctuations; and 3.5, 5, and 10 m at depths of 30, 42, and 54 respectively in the case of spatial temperature fluctuation. It was pointed out that instability in the phase and amplitude of the sinusoidal process can result in a quasinormal distribution. A possible distortion of probability distribution caused by deviation of wave motion from sinusoidal oscillations is illustrated in Fig. 2. The observed asymmetry of probability distribution and change of its sign with depth is explained on the basis of the theory which takes into account nonlinear effects for high-amplitude waves.

In many cases, experimental data can be approximated by model (3). As can be seen in Fig. 4, probability density peaks sharply at zero values of $\sigma$. An analysis shows that this is caused both by small-scale turbulence and by decrease of the mean temperature gradient. A comparison of experimental and theoretical data shows the following: 1. Probability distribution for velocity fluctuations, including large-scale ones, approaches a Gaussian or Rayleigh distribution only in the uppermost layer (25 m). After filtering out fluctuations exceeding 11 hours, the probability distribution approaches Gaussian or Rayleigh at greater depths. 2. The measured probability distribution of spatial and time temperature fluctuations on a medium scale do not compare favorably with theoretical values.

Rudenko, O. V., L. I. Soluyan, and R. V. Khokhlov. Problems in the theory of nonlinear acoustics. Akusticheskiy zhurnal, no. 3, 1974, 449-457.

This is a short comprehensive review of theoretical studies on nonlinear acoustics. The published data of Soviet and Western authors

are treated in an attempt to derive a unified approach to the problem, as well as to identify insufficiently covered areas and to stimulate further studies in these areas.

The unified system of phenomena classification is based on a set of three dimensionless numbers $\Gamma$, D, and N which are used to compare relative effects of dissipation, dispersion, and diffraction, respectively, on distortion of an acoustic wave profile in a nonlinear medium. This distortion is described completely by the numbers $\Gamma^{-1} = 2\epsilon\,\mathrm{Re}$, $D = m/2\epsilon M$, and $N = (\lambda/a)^2/2\pi^2\epsilon M$, where Re and M are the Reynolds and Mach numbers; $m = c_\infty^2 - c_o^2$, $C_\infty$ and $C_o$ are high and low-frequency sound velocities, $\lambda$ is the wavelength in the medium, $\epsilon = (\gamma + 1)/2$, $\gamma$ is the adiabatic exponent, and a is the acoustic beam radius.

Using the cited numbers the authors describe propagation of plane, spherical, and cylindrical acoustic waves separately in dissipative ($D = N = 0$, $\Gamma \neq 0$); relaxing ($\Gamma = N = 0$, $D \neq 0$); and diffractive ($\Gamma = D = 0$, $N \neq 0$) media. The theory of nonlinear deformation of wave spectra is reviewed in the presence of wave interaction of different types. Mathematical expressions for finite-amplitude wave propagation are presented in second and third order of approximation. A description of acoustic wind is given in terms of nonlinear acoustics and hydrodynamics.

It is emphasized that the method of approximation of a slowly-changing acoustic wave profile, which is used in most of the studies reviewed, is a powerful tool for analyzing various problems of nonlinear acoustics. All Soviet studies discussed (80% of the total number) were made at Moscow State University.

Maderich, V. S. Vertical structure of the main oceanic thermocline. Meteorologiya i gidrologiya, no. 10, 1974, 67-74.

The effect of vertical intermixing in a baroclinic ocean on formation of the main oceanic thermocline is analyzed, on the assumption that vertical diffusion is small in relation to vertical and horizontal advection. A stationary ocean model is considered, having remote horizontal boundaries, and outside the Ekman layer.

In the first approximation, vertical motion, continuity, and density transport are described by a single equation for the baroclinic correction function M(x, y, z), where x, y, and z are the coordinates oriented eastward, northward, and downward respectively. This approach treats the main thermocline as a baroclinic boundary layer at the ocean surface, with an underlying nearly barotropic abyssal region. Three particular solutions to the equation for M are obtained using the method of asymptotic expansion and assuming the parameter $\epsilon = \varkappa/W_0 H_*$ to be small; $\varkappa = 1\ cm^2/sec$ is the coefficient of vertical diffusion, and $W_0$ and $H_*$ are characteristic scales of the vertical velocity W and the depth z of the main thermocline, respectively. The solutions take into account the particular solution of Welander (Tellus, v. 11, no. 3, 1959, 309) for $M_0(x, y, z)$ in the diffusion boundary layer within the main thermocline.

Solutions for $M_0$ are thus derived and the density anomaly $\delta = \rho - \rho_0$, where $\rho_0$ is the density of a homogeneous liquid, is formulated for three cases: $\epsilon^{1/2} < \omega \leq 1$ (I), $\omega \leq \epsilon^{1/2}$ (II), and $\omega \leq \epsilon$ (III), where $\omega = W_{oe}/W_0$ is the amplitude of vertical Ekman velocity. The formulas for $\delta$ show a significant dependence of the vertical density gradient on magnitude and direction of $w_e$ and density flux q at the lower boundary of the Ekman layer.

The anomaly δ has two components: advective and diffusional. Particular solutions are discussed with respect to variations of q, magnitude and direction of $w_e$. The cases are examined when condition I exists in the center of oceanic cyclonic ($w_e < 0$) or anticyclonic circulations while conditions II or III are realized at the periphery of the oceanic circulations.

A graphical comparison between theoretical δ data and the vertical density profiles observed in the Pacific Ocean (Fig. 1) demonstrates a qualitative agreement between two sets of data, e.g., between the curves (25) and (13) or (36) and (88) of Fig. 1.

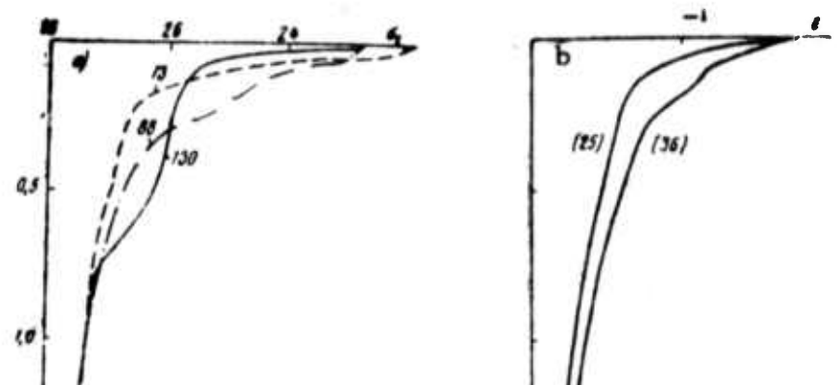


Fig. 1a. Vertical profiles of relative density in square areas 13 (in October, in the center of tropical cyclone), 88 (in September, at the periphery of anticyclone), and 130 (in July, in the center of anticyclone); b- density anomaly calculated for cases I (25) and III (36).

In summary the cited theoretical model indicates that an advective thermocline with a surface diffusion layer can exist, at least in a limited range of $w_e$ and q.

Burtsev, G. A. On a theory for the magnetic field of ocean waves. GiA, no. 2, 1974, 345-349.

Burtsev, G. A. Theory of the magnetic field of sea waves in a finite-depth sea. GiA, no. 3, 1974, 516-521.

Wave motion of seawater in the geomagnetic field generates internal currents, with associated secondary magnetic fields. A rigorous theory for the field induced by small waves in an unbounded ocean was developed by Weaver (J. Geophys. Res, 70, 1965, 1921). The present work applies this solution over a wide range of frequencies, introduces similarity criteria for wave-generated magnetic fields, and gives a comparison of rigorous and approximate solutions of the formulas.

Results show that even for a simplified model, the wave magnetic field has a very complex nature. For the more realistic case of statistically nonuniform wind waves over a rough bottom at some finite depth, the problem is further complicated. It is concluded that more rigorous solutions are needed for cases of realistic ocean parameters.

In Burtsev's second cited paper, the foregoing analysis is extended to the more practical case of a finite-depth sea. Following Weaver's theory, a set of four linear differential equations is derived from Maxwell's equations to completely define the vertical component $h_z$ of magnetic field strength in the sea, air, and sea bottom. The cited set of equations is solved for $h_z$ by known methods, taking into account the conditions at the air-sea and sea-bottom interfaces. The bottom effect as a function of magnetic field frequency is evaluated.

The solution was used to evaluate the applicability of some earlier approximate solutions to the problem. The author concludes that his method can also be used to calculate the magnetic field from sea surface turbulence with very long periods, such as swells or tides.

Savin, M. T. Oscillations at the Vaisalaa frequency in the field of a geostrophical current. Meteorologiya i gidrologiya, no. 5, 1974, 94-97.

Oscillations of a water particle in a continuously stratified ocean in the presence of a geostrophical current are analyzed theoretically, on the assumption of horizontal gradients of density and pressure and oscillations normal to an isobaric surface. Such an assumption is reasonable for a real ocean; presumably the isobaric surfaces P = const are randomly oriented.

An elemental volume dxdydz in a static equilibrium is subjected to the force of gravity $g\rho\,dxdydz$ and the resulting pressure $g\rho\,dxdydz\,1/n$, where $\rho$ is density and $n = \cos\theta$, where $\theta$ is the angle between the normal to an isobaric surface and the Z axis. The resultant of these two forces must be in equilibrium with the Coriolis force. Thus a particle in a state of static equilibrium moves horizontally at a constant geostrophic speed which is defined by its projections $u_o$ and $v_o$ on the x and y axes, respectively. In an intermediate position (x, y, z), the elemental volume is subjected to the same force of gravity and the resulting pressure $g\left(\rho + \frac{\partial \rho}{\partial x}x + \frac{\partial \rho}{\partial y}y + \frac{\partial \rho}{\partial z}z\right)$

Motion of the elemental volume subjected to the cited forces is described by a set of three second-order partial differential equations, taking into account static equilibrium conditions. This set of equations is reduced to a known equation which describes the motion of a particle in a calm stratified ocean in which $\rho$ and pressure horizontal gradients are absent. In the particular case of isobars inclined in the x-z plane only, at an angle $\theta$ with the horizontal plane, the set of three equations of motion is reduced to

$$\frac{d^2x}{dt^2} + N^2lx = -N^2lz,$$
$$\frac{d^2z}{dt^2} + N^2nz = -M^2nx, \qquad (1)$$

where $N^2 = \frac{g}{\rho}\frac{\partial \rho}{\partial z}$, N is the Vaisalaa frequency, $M^2 = \frac{g}{\rho}\frac{\partial \rho}{\partial x}$, $n = \cos\theta$, $l = \sin\theta$. Equations (1) are solved for the coordinates x and z of an oscillating particle, allowing for the fact that $tg\theta = \lambda/gV_o$, where $\lambda$ is the Coriolis parameter. The author concludes that in a real ocean, where isobaric surfaces are not horizontal and geostrophic currents are present, particle oscillations have a horizontal component whose amplitude is $10^{-5}$ to $10^{-6}$ that of the vertical component. The oscillation frequency with allowance for isobars inclination is given by the approximate formula

$$\Pi = \sqrt{N^2 + \frac{\lambda}{\rho} v_0 \frac{\partial \rho}{\partial x}}, \qquad (2)$$

different from the known formula of N insofar as $\Pi$ is a function of geostrophic current speed and the horizontal $\rho$ gradient in addition to the vertical $\rho$ gradient. In most cases, the addend with $v_o$ is small ($\sim 10^{-12}$)

In the case of the fine structure of internal waves e.g., their stability, it may hence be necessary to take into account the frequency variations due to horizontal components of particle oscillations in the fields of a geostrophic current.

Trofimov, I. L. Effect of spatial inhomogeneities of the magnetotelluric field on its vertical distribution in the sea. GiA, no. 3, 1974, 560-563.

A theoretical solution to the title problem is obtained, using a horizontal layer model of geoelectric cross-section and an arbitrary electromagnetic field source. Horizontal ($e_2$, $e_1$, $h_2$, $h_1$) and vertical $h_{z2}$, $h_{z1}$) components of the complex electric $\underline{e}$ and magnetic $\underline{h}$ vectors at the levels $z_2$ and $z_1 < z_2$ within the nth layer are intercorrelated, assuming that e and h in each layer obey the Helmholz equation for electromagnetic waves. Then approximate correlations between the components $E_2$, $E_1$, $H_2$, $H_1$ and $H_{z2}$, $H_{z1}$ of the integral complex vectors E(x, y, z) and H (x, y, z) are derived for variations of magnetotelluric fields with periods of up to 30 min. or more.

It follows from analysis of the approximate correlations and evaluation of the spectral impedance $Z^* = e_x/hy = e_y/h_x$ of the sea geoelectric cross-section, that vertical distribution of the horizontal components of the magnetotelluric field in a seawater layer is nearly independent of the field spatial inhomogeneity, and practically coincides with their distribution in the case of a plane wave. Also it follows that variations of the vertical component of magnetic field are identical with the variations of electric field in a vertical direction. Consequently, at e-m wavelengths $\lambda > 10$ d, where d is the depth of the first layer, the vertical component of magnetic field practically does not vary. Measurement of the $(E_2-E_1)$ and $(H_2-H_1)$ differences between the horizontal components of E and H may be used as an indirect method of measuring E and H, respectively. In practice, a magnetometer which measures the modulus of the integral magnetic field vector T can be used for a gradient magnetic sounding. The T variations are given by

$$\delta T(t) = \cos I \delta T_H(t) + \sin I \delta T_z(t), \qquad (1)$$

where $\delta T_H(t)$ and $\delta T_z(t)$ are the variations of horizontal and vertical components of T and I is the magnetic inclination. Limitations of the proposed sounding method result from its theoretical base, i. e., the horizontally homogeneous geoelectric cross-section model. This model, however, is applicable to significant surface areas of the global ocean. Advantages of sounding with a component magnetometer are listed as follows: 1) the same apparatus measures E and H, 2) the absence of spatially oriented parts, and 3) potential for a very precise determination of impedance since present magnetometers have resolutions down to a fraction of a $\gamma$.

Anuchin, V. N., A. M. Gusev, and Yu. G. Pyrkin. The turbulent structure of bottom density currents. Meteorolog. i gidr., no. 2, 1974, 85-88.

A theoretical interpretation is given of the flow characteristics of stable bottom currents in the ocean. This interpretation is based on the fact, confirmed by numerous experimental studies, that there is an inflection in the vertical profiles of current velocity and fluid density $\rho$ at the fluid interface in the mixing zone. It follows that $d\rho/dz$, hence stability E of a water mass, attain their maximum values in that zone, while the turbulence transfer coefficient

$$k = \frac{k_0}{1 + cE} \qquad (1)$$

where c is the impurity concentration, is at its minimum.

The vertical diffusion profile is evaluated from the equation

$$\lambda \frac{\partial \bar{c}}{\partial z} - \overline{w'c'} = A, \qquad (2)$$

where $\lambda$ is the coefficient of molecular diffusion, $w'$ is the current velocity component, and A is an integration constant. Equation (2) is derived for a stationary two-dimensional current, on the assumption that $\partial c/\partial x$ is negligible. The effects of molecular viscosity and $\lambda$ can be neglected in the central zone with a developed turbulent flow, but not in the mixing zone, where the coefficient of eddy diffusion is minimum.

The current velocity gradient and turbulent stress exhibit maxima in the region of the profile inflection, as confirmed by several experimental studies. The presence of the maximum turbulent stress in the mixing zone allows us to draw an analogy between the processes at the interface of two fluids of different density and fluids at a wall.

Published experimental data on turbulent stresses at the fluid interface and near the bottom lead to the conclusion that viscosity exerts a strong influence at the interface of two fluids of different density. The experimental data of Barr plus those of the authors are cited to support the conclusion that the bottom density currents can be considered as nearly plane-parallel, with different turbulent stresses at the boundaries. The strong effect of viscosity must be taken into account at the bottom boundary and at the fluid interface. Propagation of bottom currents over great distances from their origin is explained by the minimum turbulent diffusion across the interface.

All the cited data point to the dual nature of the bottom density currents; i. e. laminar or turbulent, depending on whether analysis is made on a large or a small scale.

Kuznetsov, O. A., and G. N. Panin. Effect of a surface oil film on turbulence in the near-water atmospheric layer. Meteorologiya i gidrologiya, no. 5, 1974, 97-99.

An experimental study of sea-atmosphere interaction was carried out in 1971 in the Caspian Sea from an offshore platform over a sea surface area partly covered with an oil film. The urgency of the study is emphasized in view of increasing oil exploration in sea shelf regions, the colossal volume of oil transported in big tankers and the inevitable risk of oil pollution.

During the cited study fluctuations of vertical wind velocity component and atmospheric moisture content were measured, and integral moisture flow was determined. The measuring instruments were an acoustic anemometer and a spectrally selective hygrometer operating in the u-v range.

The data are compared with the measurements under similar wind and sea conditions in the absence of oil film.

The comparative wind velocity data (Fig. 1) show the wave

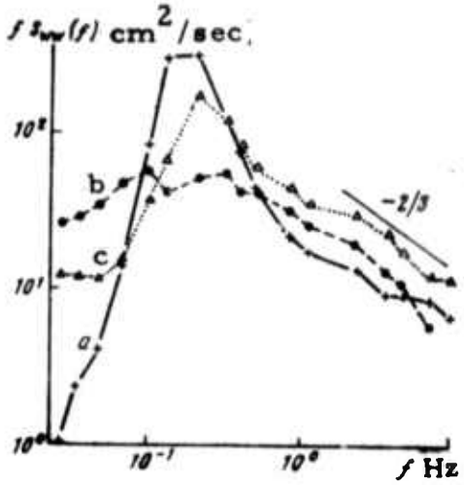


Fig. 1. Wind velocity vertical component spectra $fS_{ww}(f)$ measured above the surface covered by oil film at 2.45 m (a) and 11.0 m (b) altitudes, and above oil free surface at 2.45 m (c) altitude during decaying sea roughness (swell).

peak of $fS_{ww}(f)$ to be more pronounced over the oil film (Fig. 1a) than above an oil-free surface (Fig. 1c). This fact is due to the structural similarity of an oil-covered surface with ocean swell. The $fS_{ww}(f)$ spectrum measured at 11 m. altitude does not reflect any wave turbulence. The spectral energy decay at $f > 1$ cps closely conforms to the -2/3 law. In the spectral range, the calculated average wind dynamic velocities $U_* = 9$ and 15 cm/sec in the cases of Fig. 1a and 1b, respectively, do not differ from $U_*$ data usually observed over a sea surface at average wind velocities $\bar{U}_{10} = 2.5$ and 3.5 m/sec. at 10 m. altitude. This finding confirms the conclusion of the 1968 U. S. experiment (Barger et al, J. Appl. Meteorol, v. 9, no. 3, 1970) that an oil film does not significantly affect momentum flow between atmosphere and ocean. However, measurements of moisture flow indicated a tremendous effect of oil film on evaporation. The integral moisture flow E over the oil-covered surface was found to be $4 \times 10^{-3}$ g/m$^2$ sec versus

$E = 1.1 \times 10^{-2}$ g/m$^2$ sec in the absence of film. The moisture gradient was hardly detectable, because of a very small evaporation. Under the given conditions, even a very substantial increase in wind velocity cannot cause a corresponding increase in evaporation in the presence of an uninterrupted surface film. This fact points to the need for a thorough study both of film behavior and atmospheric turbulence over a film under a variety of conditions.

Shifrin, K. S. Effect of wind on effective sea radiation. FAiO, no. 7, 1974, 803-805.

A theoretical evaluation is made of the effects of wind-generated sea surface roughness, increase in sea surface area, spray, and foam on thermal radiation of the sea.

The effect of sea surface slope $\mathrm{tg}\,\theta_n$, where $\theta_n$ is the zenith angle of the normal to the surface, on the water emission coefficient $\epsilon$ is evaluated approximately by averaging, over different wind directions, the probability P of steep surface slopes, as determined from the formula of Cox and Munk (Bull. Scripps Inst. Oceanogr, v. 6, 1956, 401). At a typical 10 m/sec wind velocity, dispersion $\sigma$ in the cited formula is = 0.164, i.e., 95% of the slopes are confined within $2\sigma$ limits, or in the region of $\theta_n \leq$ 18 degrees. The calculated $\epsilon$ values (Table 1) are constant within a fraction of a percent, hence a more accurate evaluation of $\epsilon$ is unnecessary.

Table 1. Water emission coefficient at different $\theta_n$.

| $\lambda, \mu$ | $\theta_n$, degree | | |
|---|---|---|---|
| | 0 | 10 | 20 |
| 8,0 | 0,9834 | 0,9833 | 0,9832 |
| 9,0 | 0,9856 | 0,9856 | 0,9854 |
| 10,0 | 0,9901 | 0,9901 | 0,9900 |
| 11,0 | 0,9927 | 0,9927 | 0,9927 |
| 12,0 | 0,9853 | 0,9853 | 0,9851 |

The effect of an increased radiating surface area is evaluted by means of the Cox-Munk formula. The increase is given by

$$S/S_0 = 1 + \frac{1}{2}\sigma^2 - \ldots = 1 + \frac{1}{2}10^{-4}(15+25{,}4v) - \ldots \qquad (1)$$

where v is wind velocity and $\sigma^2 = 0.03$. The increase in $S/S_0$ is correlated with the change in effective radiation temperature by

$$T_{\text{эф}} = T\left(1 + \frac{1}{4}\frac{\Delta S}{S_0}\right) \quad \text{or} \quad \Delta T = T_{\text{эф}} - T = \frac{1}{4}\frac{\Delta S}{S_0}T. \qquad (2)$$

The $\Delta S/S_0$ and $\Delta T$ values calculated from (1) and (2) for $T = 300^\circ$ K (Table 2)

Table 2

| v, m/sec | σ | ΔS/S₀, % | ΔT, °C |
|---|---|---|---|
| 5 | 0,119 | 0,7 | 0,5 |
| 10 | 0,164 | 1,4 | 1 |
| 15 | 0,200 | 2,0 | 1,5 |
| 20 | 0,230 | 2,6 | 2 |

show that in moderate winds, a sea roughness-caused increase in thermal radiation is equivalent to 1 degree rise in T. This is considered to be a significant effect, which must be taken into account in calculations. The $\Delta S/S_0 = 2\%$ value in Table 2 coincides with the four $\Delta S/S_0$ values calculated by Monin (FAiO, no. 6, 1967) for four different models of sea roughness and the mean square wave slope $k = 0.2$ ($k \sim \sigma$).

The negative sea radiation balance R during the night is decreased by fog from water spray. In the absence of large water drops in the fog, the decrease $\Delta R$ can be evaluated from

$$\Delta R/R = -(8w)\%. \qquad (3)$$

where w is the amount of water in the fog layer over the sea. Assuming the

fog water content to be 0.2 g/m$^3$ and fog layer thickness to be 1 m, Eq. (3) gives $\Delta R/R = -1\%$. This value of the effective sea radiation change is balanced by the equal radiation loss from the fog cover into the atmosphere, so that R of the sea-fog system remains unaffected by fog.

A detailed calculation of the IR emission coefficient of sea foam indicates that the presence of foam for any $v \geq 10$ m/sec. should not change $\epsilon$ of the sea in the spectral region of the atmospheric window.

Volkov, Yu. A., L. G. Yelagina, and B. M. Koprov. Spectral characteristics of turbulent exchange between the ocean and atmosphere in the tropical Atlantic. FAiO, no. 6, 1974, 619-627.

Spectral treatment is described of a tape recorded set of experimental data on wind velocity components, atmospheric temperature T and humidity e at 10 m. altitude above the sea surface. Systematic simultaneous measurements of the vertical turbulent fluxes of heat, moisture, and momentum were carried out during the TROPEKS-72 Atlantic expedition in the summer of 1972 from the R/V Akademik Kurchatov. (The methods used and the results obtained in this field experiment are described in Sb. Tr. "TROPEKS-72". Gidrometeoizdat, 1974).

Fig. 1 shows a general view of the instrument boom extended from the ship's bow. During measurements, the ship was either moving to windward or drifting. The angle of roll $\psi$ was of the order of 1 deg; the vertical displacement amplitude, about 1 m, and the vertical velocity amplitude, 1 m/sec.

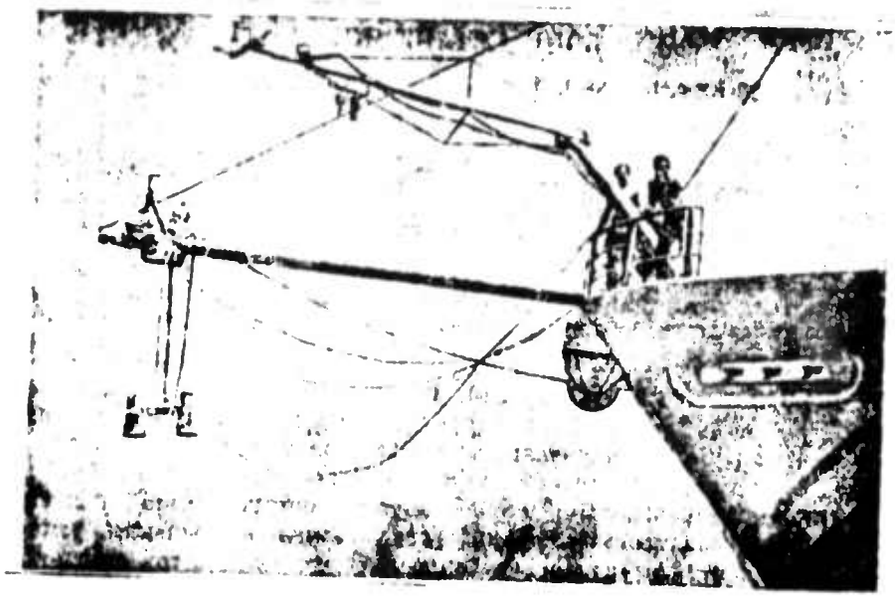



Fig. 1. Instrument boom.

The formulas of the real component (cospectrum) $\Phi_{\alpha\beta}(f)$ and imaginary component (quadratic law spectrum) $\psi_{\alpha\beta}(f)$ of the reciprocal spectrum $F_{\alpha\beta}(f)$ of measured quantities $\alpha$, $\beta$ are derived from the expressions

$$w_i' = w' + \bar{u}\varphi + \dot{z}, \tag{1}$$

and

$$\gamma_i^{\prime(i)} = \gamma^{(i)} + z\partial\gamma^{(i)}/\partial z, \quad i = 1, 2, 3, \tag{2},$$

where $w_\chi'$ and $\gamma_\chi^{(i)}$ are the measured fluctuations of the vertical velocity component w; $\gamma^{(1)} = T$, $\gamma^{(2)} = e$; $\gamma^{(3)} = u$, the horizontal velocity component; z is deviation from mean value of the vertical coordinate of sensor suspension point, and $\dot{z}$ is the time differential of z. The vessel's reaction to fluctuations w' and u' in the suspension point, and $\varphi$, z, and $\dot{z}$ correlation with the wave induced fluctuations of u, w, T, and e, are neglected.

A method of compensation for the ship's pitching effect on the measured fluxes, or the corresponding cospectra, was used. The method consisted of measuring u and $\varphi$, hence $u\varphi$ and correcting the measured $w_\chi'$ signal by the value of $u\varphi$. Such compensation may not be sufficiently

accurate, as illustrated by the spike on the $fF_{ww}(f)$ plot at f near the predominant pitch frequencies. The true of $\Phi_{ww}(f)$ and $f\Phi_{w_\chi w_\chi}(f)$ values, however, can be reconstructed with sufficient accuracy in a narrow frequency range, using an interpolation method. Numerical results from 12 data series are tabulated and the functions

$$S_{\alpha\beta}(\Omega) = \Omega\tilde{\Phi}_{\alpha\beta}(\Omega) \Big/ \int_{\Omega_1}^{\Omega_2} \tilde{\Phi}_{\alpha\beta}(\Omega)\, d\Omega, \tag{3}$$

where $\Phi_{\alpha\beta}(\Omega) = f\Phi_{\alpha\beta}(f)/\Omega$, are plotted (Fig. 2 and 3) against the wave

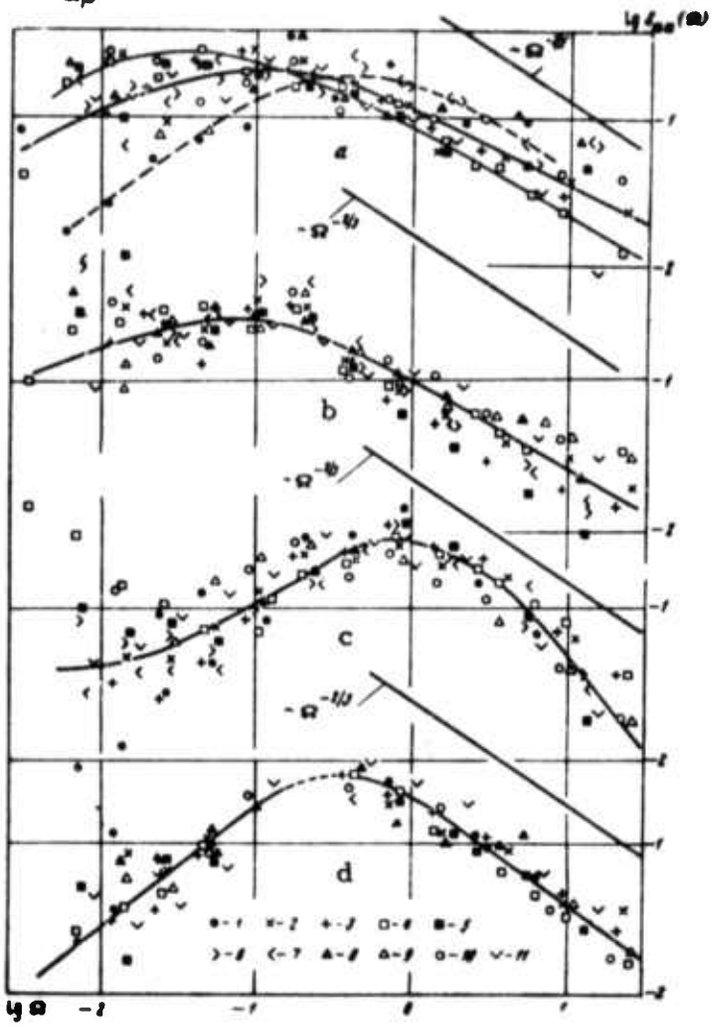


Fig. 2. $S_{\alpha\alpha}$ $\Omega$ functions of fluctuation spectra in log coordinates. Heavy continuous lines correspond to averaged values of the functions $S_{ee}(\Omega)$ (a), $S_{uu}(\Omega)$ (b), $S_{TT}(\Omega)$ (c), and $S_{ww}(\Omega)$ (d). Dashed and fine continuous lines of $S_{ee}(\Omega)$ plot represent two different data series, 1 and 4.

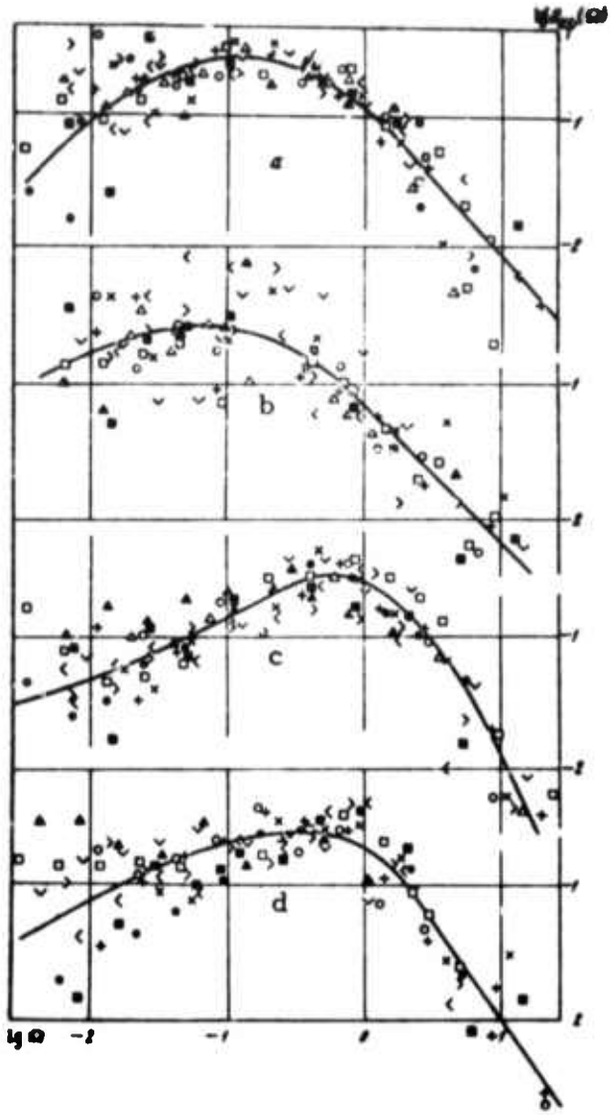


Fig. 3. $S_{\alpha\beta}(\Omega)$ functions of turbulent flux spectra in log coordinates: $S_{we}(\Omega)$- a, $S_{wu}(\Omega)$ (with inverse sign) -b, $S_{wT}(\Omega)$- c, and $S_{eT}(\Omega)$- d curve. Same notations as in Fig. 1.

numbers $\Omega = fz/u$ in the $10^{-2}$ to 20 range, where u is the total (vessel plus wind) velocity of the incoming flow.

A detailed analysis of the $S_{TT}(\Omega)$ and $S_{ee}(\Omega)$ plots (Fig. 2c and 2a) revealed a significant difference between these functions in the $\Omega < 1$ range. This difference is interpreted as the result of different T(z) and e(z) vertical profiles. The low-frequency fluctuations more significantly contribute to e fluctuations than to T fluctuations, because significant T inhomogeneity arises

only near the surface, while e inhomogeneity occurs at any altitude owing to unstable stratification by density.

At the surface T and e profiles must be similar. This conclusion is confirmed by the fact that the $S_{TT}(\Omega)$ function shows a maximum at the same $\Omega$ as the $S_{eT}(\Omega)$ function (Fig. 3d) and the spectral correlation coefficient $r_{eT}(\Omega) = \Phi_{eT}(\Omega)/\Phi_{ee}(\Omega)\,\Phi_{TT}(\Omega)$ (Fig. 4).

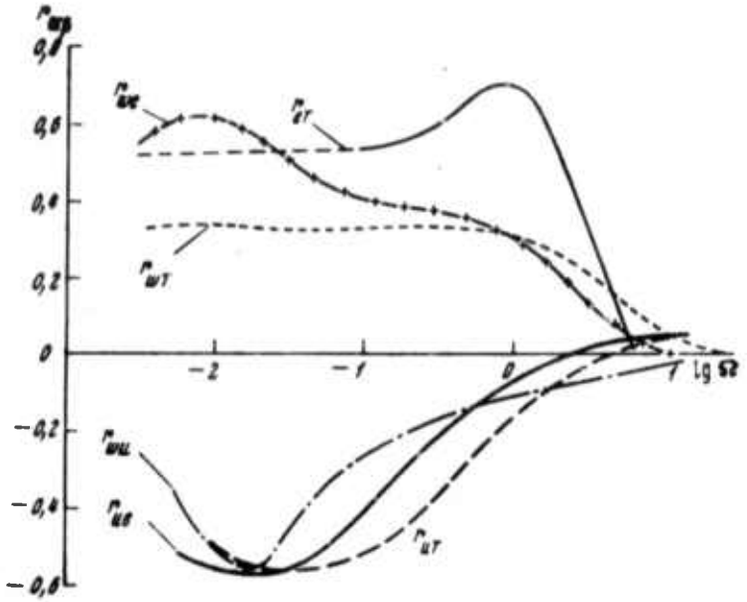


Fig. 4. Spectral correlation coefficients $r_{\alpha\beta}(\Omega)$.

A decrease of $S_{eT}(\Omega)$ at $\Omega < 1$ is correlated with the appearance of large inhomogeneity at high altitudes, simultaneously with lesser T inhomogeneity. Similar considerations may explain the difference between the $S_{wT}(\Omega)$ and $S_{we}(\Omega)$ functions (Fig. 3c and a).

The underlying cause of peculiar T spectra is a small difference between water and air temperature, which was also observed during the BOMEX expedition. The turbulence parameter $\lambda = \rho w'T;/0.61\ Tw'e'$, analogous to the Bowen number, is introduced and found to be about two, as in the BOMEX expedition.

The $r_{wT}(\Omega)$ data (Fig. 3) and other turbulence spectral characteristics are in good agreement with data of the BOMEX expedition. This agreement is considered to be an additional confirmation of the possibility of studying turbulence characteristics on shipboard using the cited method.

Kuchumova, L. S., V. V. Khlopov, and O. I. Sheremetevskaya. Heat balance and its role in the change of temperature of the surface oceanic layer. IN: Trudy AANII, no. 315, Leningrad, 1974, 41-52.

Components of the oceanic surface heat balance are calculated, using meteorological data obtained during the fourteenth and fifteenth cruises of the R/V Professor Vize in the test areas off the Azores and in an equatorial region of the Atlantic, respectively.

A formula for calculating total solar radiation flux

$$Q_{\odot} = Q_{max}(0{,}80 - 0{,}60N^2_*)(1 - A), \quad (1)$$

where $Q_{max}$ is the maximum solar radiation in the absence of atmosphere, N* is the half-sum of the total, and lower cloudiness, and A is the sea albedo, was derived by unifying the actinometric observation data in the seas and oceans. The radiation balance was calculated from

$$B = Q_{\odot} - Q_{rad} \quad (2)$$

where $Q_{rad}$ is the effective heat loss due to backscatter. Comparison of the $Q_o$ and B data calculated from Eqs. (1) and (2) with direct measurement data shows that this method can be used to calculate $Q_o$ and B within 8 to 12% in both test areas.

Other heat balance components were calculated using known formulas from the literature. The vertical gradients of wind velocity, air temperature and moisture were the logarithmically approximated observation data. The calculated heat balance data plotted in Figs. 1 and 2 show significant fluctuations in the solar heat flux and sharp differences in heat

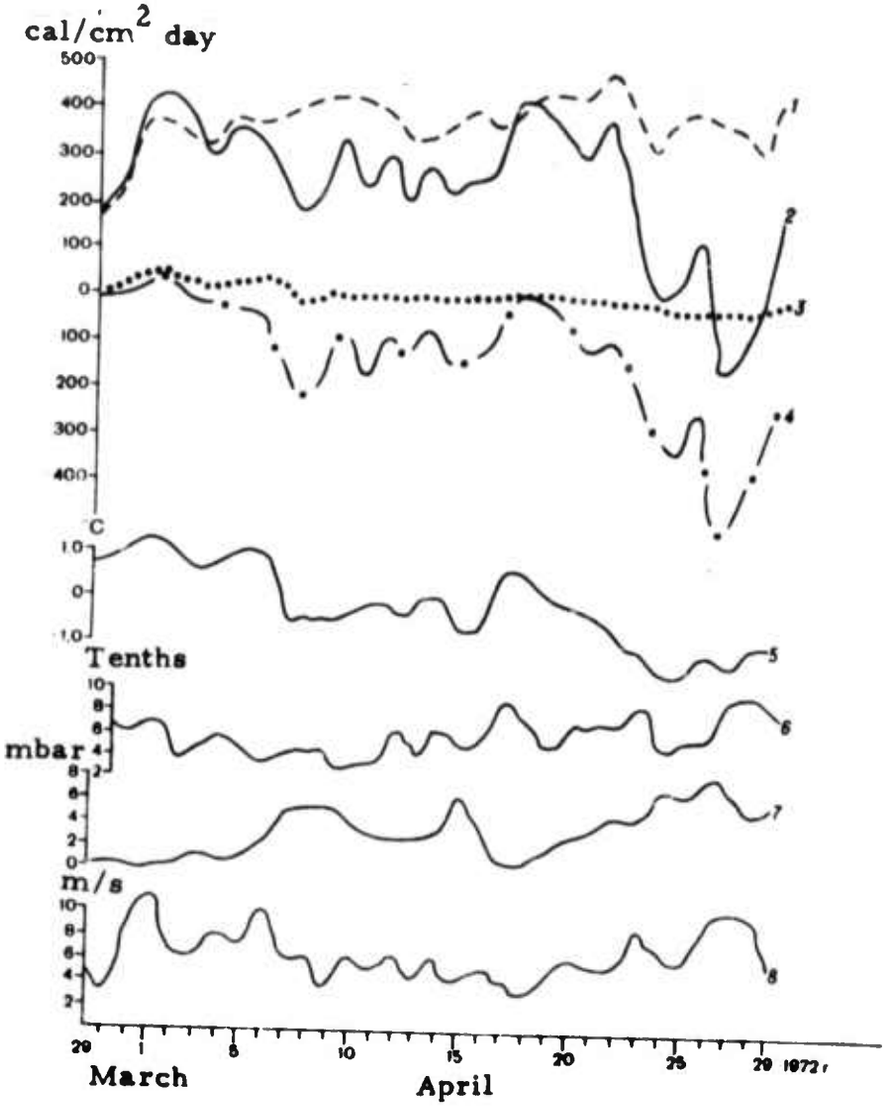


Fig. 1. Heat balance components (1, 2, 3 and 4) and their calculation base data (5, 6, 7 and 8) from observations made during the 14th cruise of the R/V "Professor Vize": 1- radiation balance, 2- total heat balance, 3- turbulent heat transfer, 4- heat loss by evaporation, 5- temperature difference between air and water, 6- half sum of total and lower cloudiness, 7- moisture deficit, 8- wind velocity.

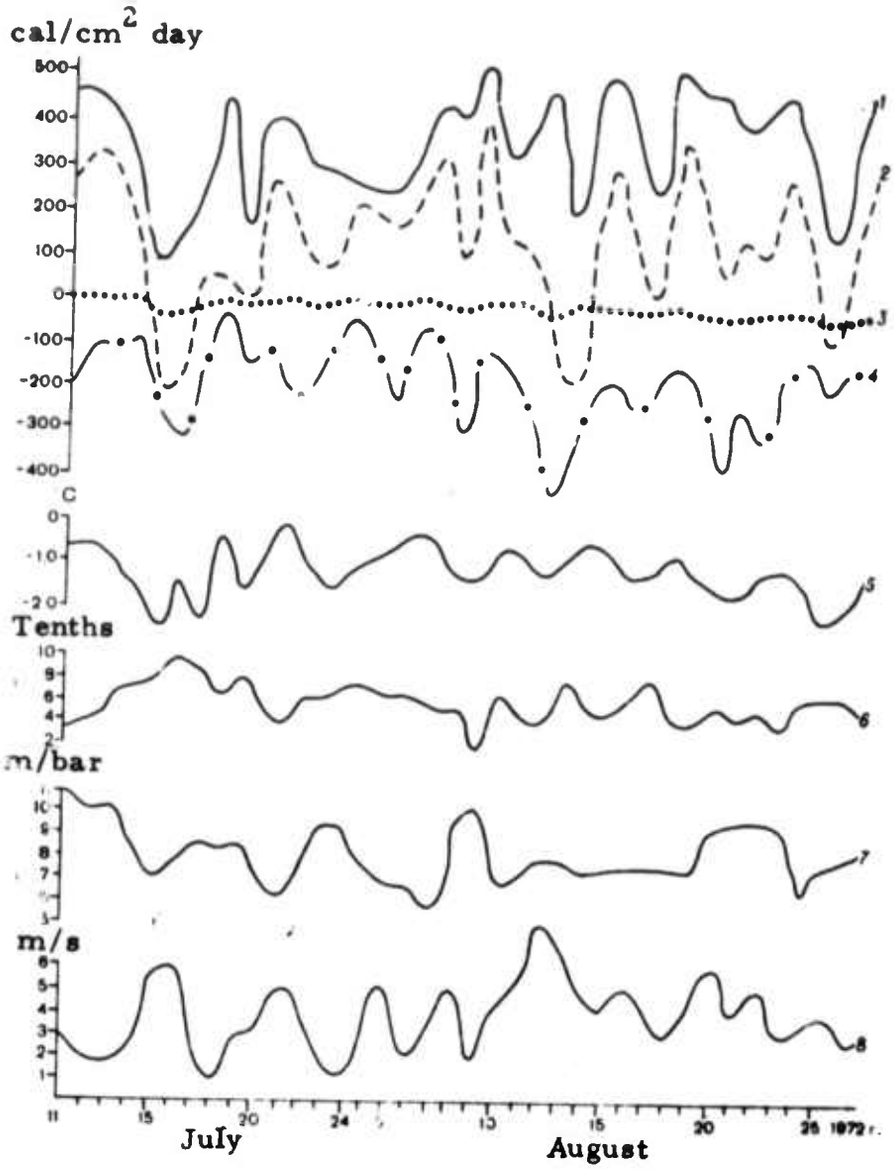


Fig. 2. Heat balance components (1, 2, 3, and 4) and their calculation-base data (5, 6, 7 and 8) from observations made during the 15th cruise of the R/V "Professor Vize". Conventional indicators are the same as in Fig. 1.

loss by evaporation. Evidently, B and $Q_{ev}$ are the principal factors in total heat balance.

Analysis of the calculated heat balance indicates the fluctuations of the basic heat balance components are dependent on hydrometeorological factors. Fluctuations in the subtropical region near the Azores are explained

by activity of the Azorian anticyclone; those in the equatorial region are interpreted as the result of an increased activity of the intertropical convergence zone during the July-August test period. Statistical treatment of the data confirm that evaporation and total solar radiation are subjected to greater fluctuations in the subtropical region.

The authors conclude that heat transfer fluctuations were significant during the observation period in the test area and did co relate with changes in weather conditions. Heat losses due to evaporation and turbulent heat exchange were relatively stable. Advective and local variations in temperature of the oceanic upper layer were calculated using the observed temperature and current velocity data and the calculated heat balance data, respectively. Local temperature variations in the upper oceanic layer during the observation periods were calculated to be $1.9^{\circ}$ and $1.6^{\circ}$, respectively, in the Azores region and in the Atlantic equatorial region. Heat balance fluctuations are estimated to cause about 85% of temperature variations, with the remainder attributable to advective heat transfer.

Zykov, I. D., and K. S. Pomeranets. Results of calculating statistical characteristics of currents. IN: Trudy Arktich. i antarktich. n.-i. inst., Leningrad, vol. 312, 1974, 192-196.

The statistical treatment is described of current velocity data, collected in the northeastern Atlantic at 400 m depth over a thirty day period at half-hour intervals. Variable mathematical expectation $M_i$ and spectral density function $S_k$ of the meridional vector component of the current are calculated by the method described by Ozmidov (Horizontal turbulence and turbulent exchange in the ocean, Moskva, 1968). Also a procedure of separating out long-period fluctuations of sea waves was used. $M_i$ was thus calculated using preassigned values of the smoothing interval $\delta$ of long period fluctuations (Fig. 1). This reveals irregular background fluctuations with a

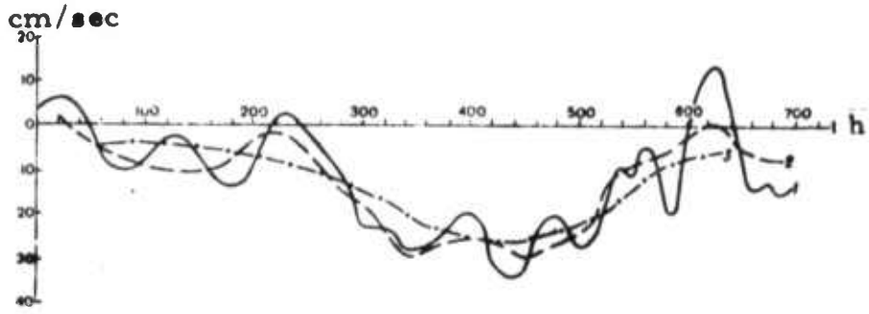


Fig. 1. Variable mathematical expectation at different smoothing intervals: $\delta_1$ = 12.5 h, $\delta_2$ = 25 h., and $\delta_3$ = 87.5 h.

period twice the observational interval.

The effects of duration of the observation series, the discrete interval $\Delta$ of time series, and the degree of freedom $\gamma = 2N/m$, where N is the number of observations and m is the shift of correlation function, are then evaluated from comparison of the $S_k$ maxima for different periods. A comparison between $S_k$ values in Table 1 shows that

Table 1. Spectral characteristics for different durations of observation series.

| Ordinate | Quantity of ordinates | Spectral density $cm^2/s^{-2}$, h | | |
|---|---|---|---|---|
| | | $T_1$=75 h | $T_2$=24 h | $T_3$=12.5 h |
| 1—1440 | 1440 | 470 | 1620 | 290 |
| 1—720 | 720 | 50 | 1400 | 100 |
| 721—1440 | 720 | 550 | 1170 | 150 |
| 1—480 | 480 | — | 830 | 75 |
| 481—960 | 480 | — | 910 | 110 |
| 961—1440 | 480 | 500 | 350 | 145 |
| 1—960 | 960 | 65 | 1560 | 195 |
| 481—1440 | 960 | 390 | 1075 | 200 |

$S_k$ calculated for a part of the observation series equal to 1/2, 1/3, or 2/3 of the series is always smaller than $S_k$ for the whole series. Fundamental fluctuations with 12.5, 24, and 75 hour periods arise in each part of the

whole series. At a 75 h period, the $S_k$ value always increases toward the end of a series. Fluctuations of the diurnal tidal period are predominant. At different $\Delta$ = 0.5 to 2 h and a constant $\nu$ = 10, the tabulated $S_k$ maxima for long-period (75 h) and diurnal (24 h) fluctuations are the same (470 and 1600 $cm^2$ $sec^{-2}$ h, respectively), but $S_k$ values for semi-diurnal (12.5 h) fluctuations decrease by 7 and 11% at $\Delta$ = 1 and 2 hr, respectively. For a given N and $\Delta$, the absolute $S_k$ values decrease with increase in $\nu$ from 10 to 19. At both $\nu$ values, three main periods of current fluctuations are evident. This finding reveals a satisfactory ratio of accuracy to detail of spectra evaluation.

In summary, the results show that selection of the governing parameters is of prime methodological importance in any statistical analysis of long-term series of current observations.

## 2. Surface Effects

Zagorodnikov, A. A. Using artificial earth satellites to measure waves. FAiO, no. 7, 1974, 791-798.

The possibility is investigated of using artificial earth satellites for measurements of spatial two-dimensional spectra of sea waves.

In satellite-borne measurements of sea state, a radar with high longitudinal and low lateral resolution should be used ($\Delta W_x < \bar{\Lambda}$, $\Delta W_y >> \bar{\Lambda}$, $S_w(v) = \delta(v)$. In such a case the spatial spectra of one-dimensional realizations of full-viewing or side-looking radars are given in the form

$$S_{0z}(K, \alpha) \approx \int_{-\pi}^{\pi} \frac{K^3}{|\cos(\theta-\alpha)|^3} S_z\left[\frac{K}{|\cos(\theta-\alpha)|}; \theta\right] \times$$

$$\times S_{wz}\left[\frac{K}{|\cos(\theta-\alpha)|}\right] \delta(\theta-\alpha)\, d\theta = K^3 S_{wz}(K) S_z(K; \alpha), \qquad (1)$$

$$S_{0u}(u) \approx \int_{-\infty}^{\infty} u^2 S_z(u, v) S_{wu}(u) \delta(v)\, dv = u^2 S_{wu}(u) S_z(u, 0). \qquad (2)$$

In the case of sea waves with $\bar{\Lambda} \geq 5\, \Delta W_x$, the filtering affect of the radar can be neglected and eqns. (1) and (2) become

$$S_{0z}(K, \alpha) \approx K^3 S_z(K, \alpha), \quad S_{0u}(u) \approx u^2 S_z(u, 0), \qquad (3)$$

where $S_z(k, \alpha)$ and $S_z(u, 0)$ are cross-sections of two-dimensional spectra of waves in $\alpha$ and $v = 0$ directions. The structure of eq. (3) shows that the spatial spectrum of a one-dimensional realization at antenna direction $\alpha$ is uniquely related to the cross-section of the two-dimensional spectra of waves in the same direction.

Scanning of sea surface from a polar orbiting satellite at a height of 62.5-630 km is illustrated in Fig. 1. Geometrical considerations

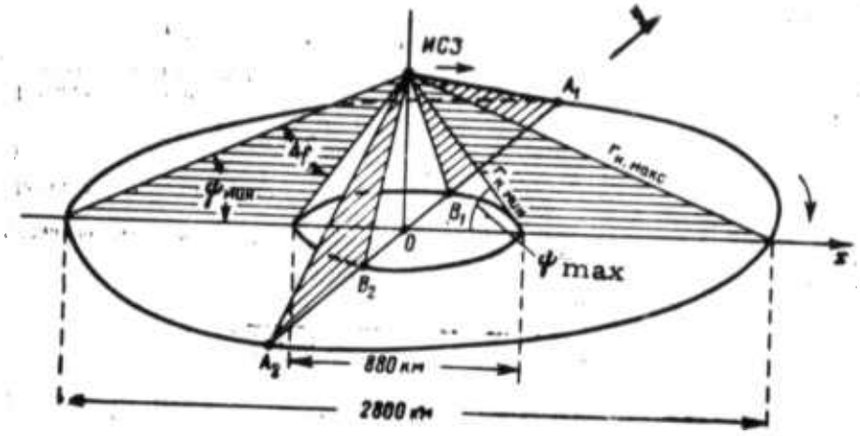


Fig. 1. Model for satellite scanning of a sea surface.

show that at $\Delta\alpha = 2^{\circ}$, $T \geq 10^{-2}$ sec and satellite rotation period of $\sim$100 min, each point of the target zone is irradiated numerous times. In order to reproduce spectral function of sea waves, cross-sections in an angular sector $\theta = 0 - \pi$ are needed, which can be achieved by a system of three satellites: one polar orbiter and two orbiting at angles of $+53^{\circ}$ and $-53^{\circ}$ with the equatorial plane.

The author concludes that spatial two-dimensional spectra of sea waves can be measured from satellites, and that the use of aerial photography is also promising for these measurements. Some sample aerial photos of sea states are included.

Belousov, P. S., Ye. O. Zhilko, A. A. Zagorodnikov, V. I. Korniyenko, V. S. Loshilov, and K. B. Chelyshev. Results of studying sea turbulence using SLAR. IN: Sb. Predvarit. rezul'taty ekspeditsii "Bering", Leningrad, 1973, 84-94. (RZhGeofiz, 4/74, no. 4V66). (Translation)

Results are reported of radar ocean mapping in the Bering Sea during February-March 1973. The following was observed: (1) radar image characteristics remain unchanged when radar illumination direction is changed; also the spectral component series do not shift from their position on the wave number plane, but images and spectra of the wave systems with beam direction close to the illumination direction become more prominent; (2) the two-dimensional spectrum of radar images reflects foam bands, and (3) analysis of a two-dimensional spectrum makes it possible to determine the number of wave systems, the positions of the spectral density peaks on the wave number plane, beam and average wave length of each move system, and the integral angular spectrum of all wave systems and of each system (if the spectra do not overlap too much). Also, it is possible to evaluate the narrow frequency band in the angular spectrum of each wave system, the three-dimensional frequency spectrum, and the spectrum of a wave series. Wind direction at the time of mapping can be determined from the foam bands.

Troilin, V. N. Determining the structure of the scattering matrix in the case of perpendicular irradiation of a surface. Trudy Taganrog r-t in-ta, no. 39, 1973, 32-35. (RZhF, 6/74, #6Zh151). (Translation)

It is shown that in the case of perpendicular irradiation of a perfectly reflecting surface, the scattering matrix is diagonal, while flux density of the energy carried by the reflected signal does not change in time,

regardless of polarization. In the case of perpendicular irradiation of a rough surface with a finite conductivity, the scattering matrix contains all elements, while the energy flux density has a maximum which depends on the selection of transmitter polarization.

Sosunov, A. S., and V. T. Lobach. Distribution moments of a radio signal reflected from a statistically uneven surface. IN: Trudy Taganrog r-t in-ta, no. 39, 1973, 3-7. (RZhF, 6/74, #6Zh147). (Translation)

The average value and dispersion are considered of the quadrature components of a field reflected from a statistically rough surface.

Timokhin, A. A. Possibility for height measurement of sea waves using phase fluctuations of reflected radio signal. IN: Trudy Taganrog r-t in-ta, no. 39, 1973, 12-15. (RZhF, 6/74, #6Zh149) (Translation)

The possibility is considered of height measurement of sea waves using phase fluctuations of a radar signal reflected from the sea surface. Expressions are obtained for the standard deviation of the phase of reflected signal at different ratios of coherent and incoherent components. It is shown that $\sigma_\varphi$ is a function of the relative heights of sea waves when $H_{3\%}/\lambda \leq 0.5$, where $H_{3\%}$ is wave height at 3% tolerable error.

Timonov, V. V., and I. T. Zamkov. Problem of increasing the accuracy of Doppler true air speed indicators while flying over the sea. IN: Trudy Taganrog r-t in-ta, no. 39, 1973, 44-49. (RZhF, 6/74, no. 6Zh153). (Translation)

The possibility is considered of using current information on the state of a disturbed sea surface and a priori data on the relative shift of the spectral peak of a Doppler echo-signal. The purpose is to reduce the error of true air speed measurements while flying over the sea.

Timokhin, A. A. Profiling of a statistically nonuniform suface. IN: Trudy Taganrog r-t in-ta, no. 39, 1973, 23-26 (RZhF, 6/74, no. 6Zh150). (Translation)

The possibility is considered of designing equipment for height determination of irregularities of a statistically uneven surface (e.g. a sea surface) from an aircraft by a noncontact method. A functional diagram of the equipment is discussed.

Okishev, V. B., S. V. Polozhentsev, and I. A. Podval'nyy. Depth dependence of the accuracy of measurement of sea wave height by a radio method. Trudy Taganrog r-t in-ta, no. 39, 1973, 36-38. (RZhF, 6/74, #6Zh152). (Translation)

Accuracy in measuring the height of sea waves from an aircraft is analyzed as a function of water depth for the cases of a deep and a shallow sea.

Molebnyy, V. V. Remote device for measuring the orientation of sea surface facets. Otkr. izobr., no. 23, #433339, 1974, 100. (Translation)

A remote device for measuring the orientation of sea surface facets contains a highly directional light source, a unit for polarization control, a generator of signals for polarization control, photodetector, and a unit for analysis. The device features a linear-circular polarizer and a phase difference meter which is connected to the polarization control signal generator and to an amplitude modulation meter for echo signals. Both additions were introduced for the purpose of automation.

Lobach, V. T. Possibility of determining the average length and principal propagation direction of sea waves by radar. Trudy Taganrog r-t inta, no. 39, 1973, 16-22. (RZhF, 6/74, #6Zh418) (Translation)

The possibility was investigated of determining the average length of sea waves, from data on scattering of radiowaves in the meter range by the sea surface. The transmitter/receiver device is assumed to move uniformly over the surface. The problem was considered in an approximation of the method of perturbations, for the case in which the fluctuating component of the field is small relative to the regular one. It is shown that the average length of sea waves in a given direction correlates in a simple fashion with the mean number of zero crossings per unit time of the envelope of the reflected signal. The principal direction of propagation is determined from the average wave lengths in various directions. The results of experiments with a radar at a transmitted frequency of 30 MHz and pulse duration of 1 microsec are given, which corroborate theoretical conclusions.

Matveyev, D. T., Yu. A. Volkov, A. P. Kestner, and S. O. Lomadze. Measurement of slope characteristics of a disturbed sea surface by remote microwave sounding. IN: Sb. TROPEKS-72. Leningrad, Gidrometeoizdat 1974, 540-547. (RZhGeofiz. 8/74, #8B73). (Translation)

The results are given of microwave measurements of slope characteristics of a disturbed sea surface, using a 2.5 cm wavelength. Measurements were conducted from an elevation-stabilized platform at an angle of 20° to the horizon, aboard the R/V Akademik Kurchatov. Measurements with a wire-type wave gage were conducted simultaneously. Data were recorded on magnetic tape and computer processed. Spectra were obtained of slope projections onto the main and orthogonal directions of sea wave propagation. Analysis shows that the spectra obtained have rather steep slopes at high frequencies, which is caused by the limited spatial resolution of the radiometer. In other respects the results of microwave measurements agree well with the results of wave-gage measurements as well as with theoretical considerations.

Lande, B. Sh. On a theory for determining parameters of sea surface profile from radar reflections. IN: Tr. Sev. -Zap. zaoch. politekhn. in-ta, no. 25, 1974, 8-10. (RZhF, 11/74, #11Zh141). (Translation)

An explanation is given for polarization and spectral characteristics of a scattered field, based on a two-dimensional model of scattering of microwaves at a sea surface and using the method of small perturbations. This was accomplished by modeling spectra of capillary waves using finite functions in a frequency-time domain. Recommendations are given for determining the volume of data required for reconstruction of the main parameters of the sea surface.

Garnaker'yan, A. A., A. S. Sosunov, and V. T. Lobach. Coherent and incoherent components of a radio signal reflected from an isotropic sea surface with a quasiharmonic correlation function. Trudy Taganrog r-t in-ta, no. 39, 1973, 3-7. (RZhF, 6/74, #6Zh148). (Translation)

Expressions are obtained for the power of fluctuating and regular components of a field scattered by an isotropic sea surface. The effect of the length of sea waves upon the power of the scattered signal is analyzed.

Bol'shakov, E. A., and V. I. Saplin. Determining the phasor of a radio signal reflected from a statistically rough surface. Trudy Taganrog radiot. in-ta., no. 39, 1973, 27-31. (RZhF, 8/74, #8Zh212) (Translation)

Expressions were derived for modulus and phase of the polarization ratio (phasor) of a radio signal reflected from a statistically rough surface, having large gently-sloping irregularities whose heights have a normal distribution. Analysis of these expressions shows that polarization characteristics of the reflected signal depend on angle of incidence, as well as on the statistical parameters and electrical properties of the rough surface.

Bespalov, A. A., N. Ye. Kuznetsov, V. V. Naumova, and V. D. Rusin. Recording system for space-time characteristics of surface wave disturbances. VMU, no. 4, 1974, 406-410.

A description is given of a system for simultaneous measurements of height and period of wind waves at eight points, and spatial correlation

at any two of these points. Block diagrams of the measuring system, recording gage channel and correlator are given in Figs. 1-3, respectively.

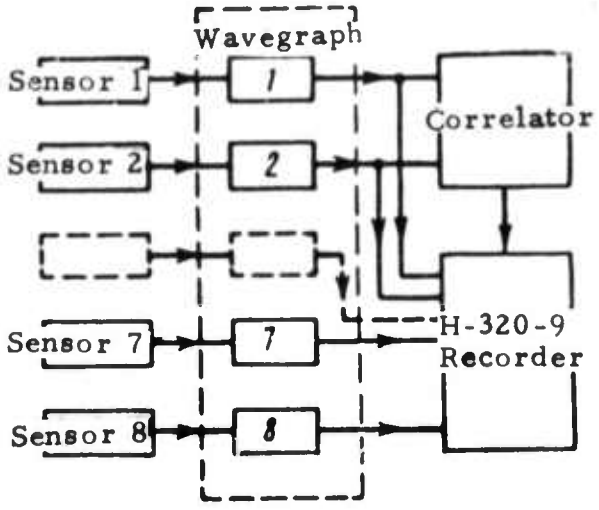


Fig. 1. Measuring system.

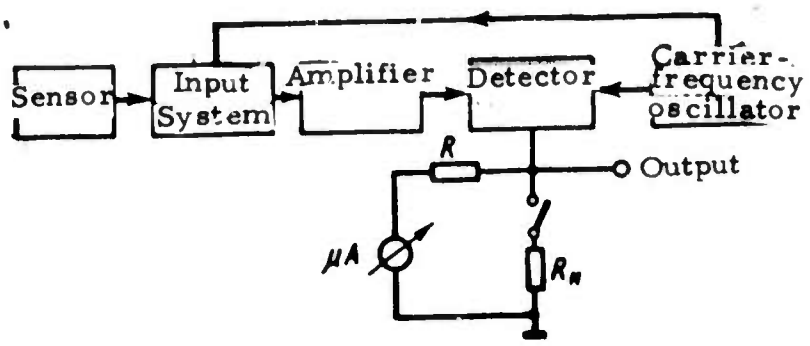


Fig. 2. Wavegraph channel

The sensor arrangement of the system is as follows: seven sensors are set along a 2.8 m-long base line with various spacing between them; one sensor is placed to form an equilateral triangle 20 cm distant from either of two sensors set on the base line. The system can be used for dip measurements at $\bar{\lambda}$ = 1.2-1.6 m. The accuracy of height measurements is $\pm$ 5%.

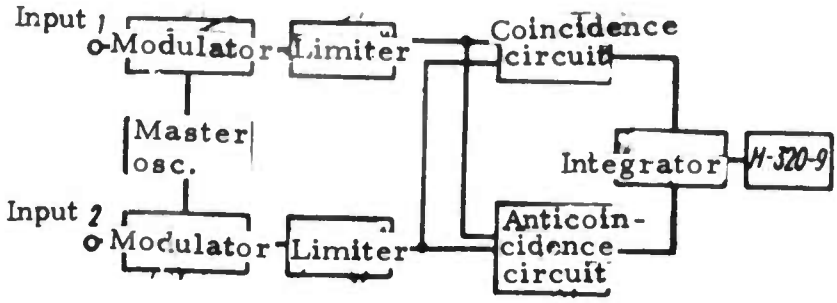


Fig. 3. Correlator

Schematics of the modulator and one stage of the limiter in the correlator are included. This system has been used in the study of surface waves in the near-shore zone of a reservoir.

Vinogradov, V. V., L. V. Mironov, Yu. I. Popov, and V. V. Ukrainskiy. Results of measuring water surface temperature by infrared radiometer in the tropical Atlantic. IN: Sb. TROPEKS-72, Leningrad, Gidrometeoizdat, 1974, 609-619. (RZhGeofiz, 8/74, no. 8B32). (Translation)

Technical specifications are given for a new shipboard IR radiometer, and its accuracy in measuring surface water temperature is evaluated. Systematic errors in the shipboard measurements are discussed. Preliminary results are given of measuring the daily variation in sea surface temperature and of computational methods for mapping it. Questions are treated on using radiation temperature to calculate the heat balance of the sea surface.

Fuks, I. M. Spectral widths of signals scattered by a wavy sea surface. Akusticheskiy zhurnal, no. 3, 1974, 458-468.

Reasons are analyzed for the spectral broadening of sonic signals, reflected from a wavy sea surface. Formulas are obtained for scattered field spectra, and the effect is evaluated of attenuation on spectral broadening of a signal scattered by small ripples. Criteria are stated for the applicability of the "two-scale" model of a scattering surface for the case of developed sea waves. The contribution is considered of Doppler broadening, caused by ripple motion on large-scale wave components, on the instantaneous frequency fluctuation and energy spectrum of the scattered signal. Spectral width is correlated with wave parameters, namely wind velocity, wave height, and frequency of energy-carrying components.

Korzun, V. A. Technical possibilities of remote (space) imaging of the ocean. Ekspress informatsiya, ser. 9, no. 1, 1974, Promyslovaya okeanologiya, 1-28.

This is a review of the modern technical means for oceanographic and surface meteorological studies, with emphasis on possibilities of remote imaging from space in selected areas of research. The review is based on ocean data collections published from 1967 through 1973. Technical means of remote imaging of the ocean include space carriers, on-board instrumentation, reception, and processing of data.

Selection of technical means is correlated with the purpose, i.e. forecast or research, of the experiment. The requirements of observation frequency, accuracy, and volume are summarized for meteorological and oceanographic purposes. Characteristics of different types of U. S. spacecraft used for the cited purposes are tabulated. Selection of the optimum system of data collection by means of satellites is discussed. The advantage is indicated of using manned space stations, such as Salyut or Skylab, for certain

experiments. Technical potentialities of photographic and TV cameras, IR and microwave radiation meters including side-looking radar, are examined in relation to oceanography and surface meteorology.

The spatial resolution of various cited instruments is discussed as the main problem in data collection. Technical possibilities of remote sensors with respect to their resolution power are illustrated by tabulated data from a Western source. The relatively low detection capability of IR sensors is indicated to be the main cause of the lower resolution power of IR instruments, in relation to TV instruments. The use of scanning and point-locked radiation meters in observation of cloud-free regions is outlined. Potential resolving power of present on-board thermal radiation instruments can be very high, e.g., 5-10 km on board geosynchronous satellites.

Active radar systems and passive microwave radiometers used for ocean imaging are reviewed with respect to their resolving power, weight, and power requirements. It is concluded that only active systems can be used on orbiting space stations. The fundamental deficiency of photographic, TV, IR, and microwave imaging is considered to be ambiguity in interpretation of the collected data. Analysis of the Earth spectral imaging data collected during orbiting of the Soyuz-6, 7, and 8 spacecrafts showed that the spectral brightness coefficient data at a few wavelengths is sufficient to identify a surface from its reflection spectrum.

Methodological problems of data reception, processing, and interpretation are also discussed. A comparison is made between direct transmission of data and transmission from the satellite to Earth via buoy with data recording on magnetic tape or drum. Potentialities are examined of photo-interpretation and digital processing of the data. Specifications of marine meteorological and oceanographic parameters collected from buoys are summarized and discussed; a communications flow chart is given for the satellite-buoy and satellite-ground station systems.

In the near future the author sees data being collected by buoy from geostationary or heliosynchronous observation satellites. Advantages and deficiencies of these two satellite-buoy systems are compared in a table. Examples are cited of the operational and projected U. S. geostationary and heliosynchronous satellites. The author's further views and recommendations are given on future developments of the ocean imaging from space. There are 52 references, of which some 20% are Soviet.

Timofeyev, N. A., and Ye. N. Shutova. Angular structure of the emitted shortwave radiation field over the ocean. IN: Sb. Mor. gidrofiz. issled., Sevastopol', no. 2(61), 1973, 132-141. (RZhGeofiz, 12/73, no. 12B234). (Translation)

The angular structure of the brightness field of the ocean-atmosphere system is investigated, on the basis of actinometric measurements and cloud observations made in October 1969 by the Meteor-1 and Meteor-2 meteorological satellites. A method is introduced for converting the satellite-measured intensity of 0.3-3.0 $\mu$ radiations reflected to space into radiation flux into a hemisphere at a nominal upper boundary of the atmosphere.

Kondrat'yev, K. Ya., V. V. Melent'yev, and Yu. I. Rabinovich. The Soviet-American Bering experiment. IN: Sb. Predvarit. rezul'taty ekspeditsii "Bering", Leningrad, 1973, 3-29. (RZhGeofiz, 4/74, no. 4B36). (Translation)

The chief purposes of the joint American-Soviet expedition in the Bering Sea from February 15 to March 7, 1973 were: (1) Airborne measurements

of microwave radiation from an open sea surface and from an area of rainfall; (2) shipboard measurements of ice parameters, surface temperature, surface waves, and liquid water content of the atmosphere, and (3) exchange of comparable microwave and direct measurement data on characteristics of atmosphere, ice cover, and sea surface.

Martsinkevich, L. M. Preliminary analysis of results of wave measurements in the Bering experiment (Bering Sea, Feb.-Mar. 1973). IN: Sb. Predvarit. rezultaty ekspeditsii "Bering", Leningrad, 1973, 95-111. (RZhGeofiz, 4/74, no. 4V69). (Translation)

The aggregate wave heights and periods measured on radar maps obey known distribution laws. Ripple components and secondary energy peaks, which probably are related to nonlinear effects of wave decay, were revealed by spectral analysis of one sea roughness state. An approximate correlation was obtained between a foam-covered sea surface area (in %) and wind velocity. In the absence of an experimental cyclone distribution over a turbulent sea surface, theoretical studies are required for interpretation of a mixed sea roughness from radar mapping data. Also, solution of such a problem requires synchronized measurements of r-f thermal radiation from a rough sea surface, surface slope, and characteristics of the foam cover.

Bykova, V. Ye., I. V. Kireyev, L. F. Monakhov, and A. V. Svechnikov. [Radar] measurement of the true gradients and synchronous measurements of wave heights, periods, and velocities. IN: Tr. Gos. okeanograf. inst., no. 117, 1973, 17-24.

Measurement procedures and data are reported and discussed on the interaction of radar waves with a wavy sea surface. The true instantaneous

wave slope tan $\alpha$ was measured in directions of wave propagation and normal to it. A nine-channel wire-type wave gage synchronously recorded oscilloscope traces of signals from five wire sensors spaced at 50 or 100 cm distances from each other. The oscilloscope data were read out, converted to digital form, and recorded on punched tape by means of an analog-digital converter-recorder. The wave slope values were computed on a Minsk-22 computer.

The plotted tan $\alpha$ data (Fig. 1 and 2) show that under given

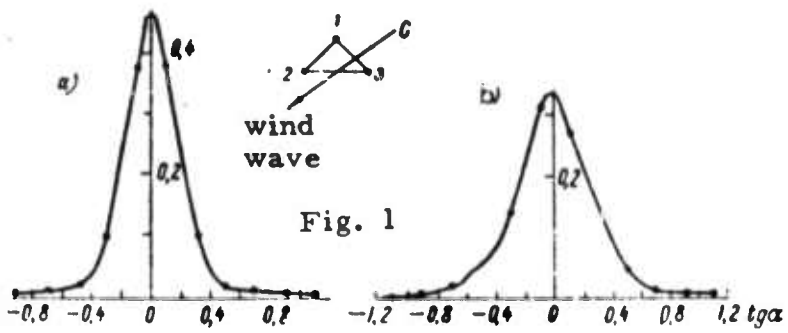


Fig. 1

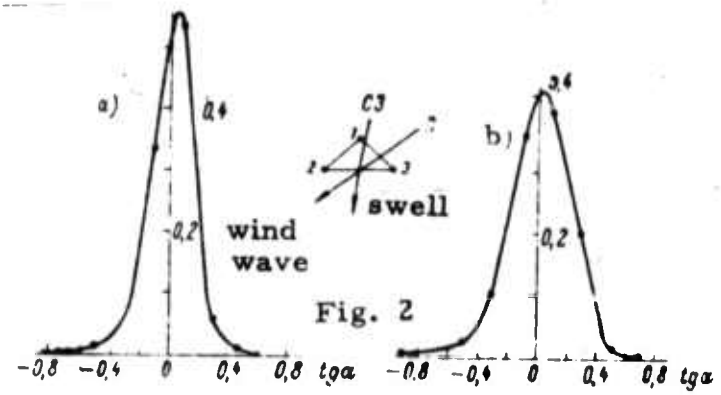


Fig. 2

Fig. 1 and 2. Slope distribution density for a simple wave system and a hybrid system:

a- normal to direction of wind wave propagation,
b- in the same direction; 1, 2, and 3- sensor numbers.

hydrometeorological conditions, true wave steepness increases with an increase in wave amplitude, and that tan $\alpha$ distribution is nearly symmetrical for developed wind waves but asymmetric with respect to the ordinate axis for a hybrid wave system. Statistical analysis of the true tan $\alpha$ data was made

using the Kolmogorov test for normality and the chi-square compatibility test. Both tests verified applicability of the normal distribution hypothesis to the slopes normal to wave propagation direction, but only for developed wind waves.

The tabulated tan $\alpha$ data measured at 0.5 and 1 m. separation intervals in the direction of wave propagation are found to be in fairly good agreement, a fact which indicates that statistical distribution of slope data is practically the same for measurements at the cited intervals. Comparison of the charts in Fig. 3 shows that the highest tan $\alpha$ values correspond to ripples, while the low tan $\alpha$ values are more characteristic of large waves.

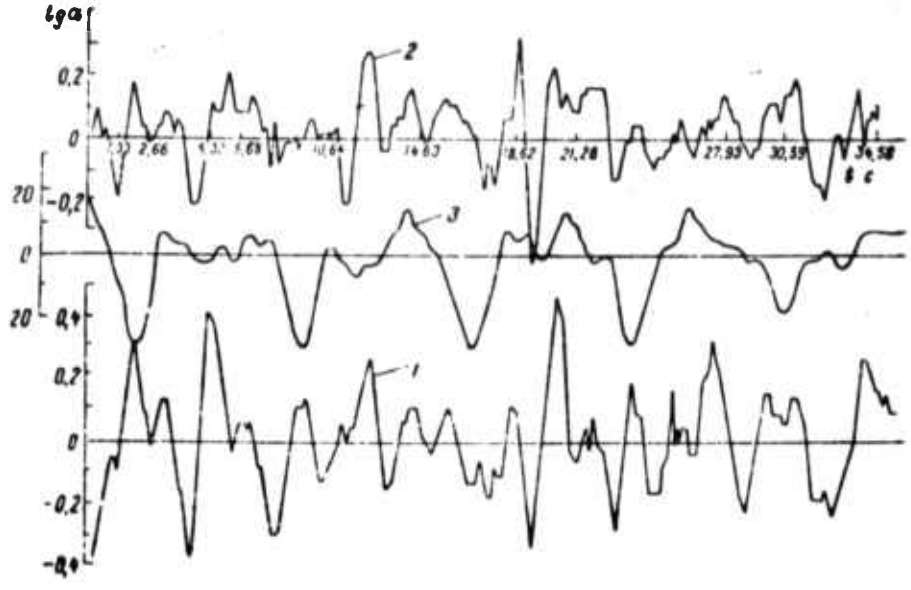


Fig. 3. Wave slope vs. time charts:

1 - in direction of wave propagation, 2 - in normal direction, 3 - wave oscilloscope trace.

Synchronous measurements of wave height, period T, and sum velocity $V_\epsilon$ are also described. A wire type wave recorder with vertical and horizontal wire sensors was used in the measurements. A series of the $V_\epsilon$ and T data from one oscilloscope trace are tabulated. Analysis of the data from a horizontal sensor led to the conclusion that time intervals between adjacent peaks or an adjacent minimum and inflection

point of a wave profile have to be considered as the wave oscillation period, when correlating sea wave parameters with radar signals. Analysis of the vertical velocity spectrum revealed that the frequency spectrum is asymmetric with respect to the frequency of maximum energy, and the corresponding random processes are concentrated in a narrow band.

## 3. SOURCE ABBREVIATIONS

| | | |
|---|---|---|
| AiT | - | Avtomatika i telemekhanika |
| APP | - | Acta physica polonica |
| DAN ArmSSR | - | Akademiya nauk Armyanskoy SSR. Doklady |
| DAN AzSSR | - | Akademiya nauk Azerbaydzhanskoy SSR. Doklady |
| DAN BSSR | - | Akademiya nauk Belorusskoy SSR. Doklady |
| DAN SSSR | - | Akademiya nauk SSSR. Doklady |
| DAN TadSSR | - | Akademiya nauk Tadzhikskoy SSR. Doklady |
| DAN UkrSSR | - | Akademiya nauk Ukrainskoy SSR. Dopovidi |
| DAN UzbSSR | - | Akademiya nauk Uzbekskoy SSR. Doklady |
| DBAN | - | Bulgarska akademiya na naukite. Doklady |
| EOM | - | Elektronnaya obrabotka materialov |
| FAiO | - | Akademiya nauk SSSR. Izvestiya. Fizika atmosfery i okeana |
| FGiV | - | Fizika goreniya i vzryva |
| FiKhOM | - | Fizika i khimiya obrabotka materialov |
| F-KhMM | - | Fiziko-khimicheskaya mekhanika materialov |
| FMiM | - | Fizika metallov i metallovedeniye |
| FTP | - | Fizika i tekhnika poluprovodnikov |
| FTT | - | Fizika tverdogo tela |
| FZh | - | Fiziologicheskiy zhurnal |
| GiA | - | Geomagnetizm i aeronomiya |
| GiK | - | Geodeziya i kartografiya |
| IAN Arm | - | Akademiya nauk Armyanskoy SSR. Izvestiya. Fizika |
| IAN Az | - | Akademiya nauk Azerbaydzhanskoy SSR. Izvestiya. Seriya fiziko-tekhnicheskikh i matematicheskikh nauk |

| | | |
|---|---|---|
| IAN B | - | Akademiya nauk Belorusskoy SSR. Izvestiya. Seriya fiziko-matematicheskikh nauk |
| IAN Biol | - | Akademiya nauk SSSR. Izvestiya. Seriya biologicheskaya |
| IAN Energ | - | Akademiya nauk SSSR. Izvestiya. Energetika i transport |
| IAN Est | - | Akademiya nauk Estonskoy SSR. Izvestiya. Fizika matematika |
| IAN Fiz | - | Akademiya nauk SSSR. Izvestiya. Seriya fizicheskaya |
| IAN Fizika zemli | - | Akademiya nauk SSSR. Izvestiya. Fizika zemli |
| IAN Kh | - | Akademiya nauk SSSR. Izvestiya. Seriya khimicheskaya |
| IAN Lat | - | Akademiya nauk Latviyskoy SSR. Izvestiya |
| IAN Met | - | Akademiya nauk SSSR. Izvestiya. Metally |
| IAN Mold | - | Akademiya nauk Moldavskoy SSR. Izvestiya. Seriya fiziko-tekhnicheskikh i matematicheskikh nauk |
| IAN SO SSSR | - | Akademiya nauk SSSR. Sibirskoye otdeleniye. Izvestiya |
| IAN Tadzh | - | Akademiya nauk Tadzhikskoy SSR. Izvestiya. Otdeleniye fiziko-matematicheskikh i geologo-khimicheskikh nauk |
| IAN TK | - | Akademiya nauk SSSR. Izvestiya. Tekhnicheskaya kibernetika |
| IAN Turk | - | Akademiya nauk Turkmenskoy SSR. Izvestiya. Seriya fiziko-tekhnicheskikh, khimicheskikh, i geologicheskikh nauk |
| IAN Uzb | - | Akademiya nauk Uzbekskoy SSR. Izvestiya. Seriya fiziko-matematicheskikh nauk |
| IBAN | - | Bulgarska akademiya na naukite. Fizicheski institut. Izvestiya na fizicheskaya institut s ANEB |
| I-FZh | - | Inzhenerno-fizicheskiy zhurnal |

| | | |
|---|---|---|
| IiR | - | Izobretatel' i ratsionalizator |
| ILEI | - | Leningradskiy elektrotekhnicheskiy institut. Izvestiya |
| IT | - | Izmeritel'naya tekhnika |
| IVUZ Avia | - | Izvestiya vysshikh uchebnykh zavedeniy. Aviatsionnaya tekhnika |
| IVUZ Cher | - | Izvestiya vysshikh uchebnykh zavedeniy. Chernaya metallurgiya |
| IVUZ Energ | - | Izvestiya vysshikh uchebnykh zavedeniy. Energetika |
| IVUZ Fiz | - | Izvestiya vysshikh uchebnykh zavedeniy. Fizika |
| IVUZ Geod | - | Izvestiya vysshikh uchebnykh zavedeniy. Geodeziya i aerofotos"yemka |
| IVUZ Geol | - | Izvestiya vysshikh uchebnykh zavedeniy. Geologiya i razvedka |
| IVUZ Gorn | - | Izvestiya vysshikh uchebnykh zavedeniy. Gornyy zhurnal |
| IVUZ Mash | - | Izvestiya vysshikh uchebnykh zavedeniy. Mashinostroyeniye |
| IVUZ Priboro | - | Izvestiya vysshikh uchebnykh zavedeniy. Priborostroyeniye |
| IVUZ Radioelektr | - | Izvestiya vysshikh uchebnykh zavedeniy. Radioelektronika |
| IVUZ Radiofiz | - | Izvestiya vysshikh uchebnykh zavedeniy. Radiofizika |
| IVUZ Stroi | - | Izvestiya vysshikh uchebnykh zavedeniy. Stroitel'stvo i arkhitektura |
| KhVE | - | Khimiya vysokikh energiy |
| KiK | - | Kinetika i kataliz |
| KL | - | Knizhnaya letopis' |
| Kristall | - | Kristallografiya |
| KSpF | - | Kratkiye soobshcheniya po fizike |

| | | |
|---|---|---|
| LZhS | - | Letopis' zhurnal'nykh statey |
| MiTOM | - | Metallovedeniye i termicheskaya obrabotka materialov |
| MP | - | Mekhanika polimerov |
| MTT | - | Akademiya nauk SSSR. Izvestiya. Mekhanika tverdogo tela |
| MZhiG | - | Akademiya nauk SSSR. Izvestiya. Mekhanika zhidkosti i gaza |
| NK | - | Novyye knigi |
| NM | - | Akademiya nauk SSSR. Izvestiya. Neorganicheskiye materialy |
| NTO SSSR | - | Nauchno-tekhnicheskiye obshchestva SSSR |
| OiS | - | Optika i spektroskopiya |
| OMP | - | Optiko-mekhanicheskaya promyshlennost' |
| Otkr izobr | - | Otkrytiya, izobreteniya, promyshlennyye obraztsy, tovarnyye znaki |
| PF | - | Postepy fizyki |
| Phys abs | - | Physics abstracts |
| PM | - | Prikladnaya mekhanika |
| PMM | - | Prikladnaya matematika i mekhanika |
| PSS | - | Physica status solidi |
| PSU | - | Pribory i sistemy upravleniya |
| PTE | - | Pribory i tekhnika eksperimenta |
| Radiotekh | - | Radiotekhnika |
| RiE | - | Radiotekhnika i elektronika |
| RZhAvtom | - | Referativnyy zhurnal. Avtomatika, telemekhanika i vychislitel'naya tekhnika |
| RZhElektr | - | Referativnyy zhurnal. Elektronika i yeye primeneniye |

| | | |
|---|---|---|
| RZhF | - | Referativnyy zhurnal. Fizika |
| RZhFoto | - | Referativnyy zhurnal. Fotokinotekhnika |
| RZhGeod | - | Referativnyy zhurnal. Geodeziya i aeros"-yemka |
| RZhGeofiz | - | Referativnyy zhurnal. Geofizika |
| RZhInf | - | Referativnyy zhurnal. Informatics |
| RZhKh | - | Referativnyy zhurnal. Khimiya |
| RZhMekh | - | Referativnyy zhurnal. Mekhanika |
| RZhMetrolog | - | Referativnyy zhurnal. Metrologiya i izmeritel'naya tekhnika |
| RZhRadiot | - | Referativnyy zhurnal. Radiotekhnika |
| SovSciRev | - | Soviet science review |
| TiEKh | - | Teoreticheskaya i eksperimental'naya khimiya |
| TKiT | - | Tekhnika kino i televideniya |
| TMF | - | Teoreticheskaya i matematicheskaya fizika |
| TVT | - | Teplofizika vysokikh temperatur |
| UFN | - | Uspekhi fizicheskikh nauk |
| UFZh | - | Ukrainskiy fizicheskiy zhurnal |
| UMS | - | Ustalost' metallov i splavov |
| UNF | - | Uspekhi nauchnoy fotografii |
| VAN | - | Akademiya nauk SSSR. Vestnik |
| VAN BSSR | - | Akademiya nauk Belorusskoy SSR. Vestnik |
| VAN KazSSR | - | Akademiya nauk Kazakhskoy SSR. Vestnik |
| VBU | - | Belorusskiy universitet. Vestnik |
| VNDKh SSSR | - | VNDKh SSSR. Informatsionnyy byulleten' |
| VLU | - | Leningradskiy universitet. Vestnik. Fizika, khimiya |
| VMU | - | Moskovskiy universitet. Vestnik. Seriya fizika, astronomiya |

| | | |
|---|---|---|
| ZhETF | - | Zhurnal eksperimental'noy i teoreticheskoy fiziki |
| ZhETF P | - | Pis'ma v Zhurnal eksperimental'noy i teoreticheskoy fiziki |
| ZhFKh | - | Zhurnal fizicheskoy khimii |
| ZhNiPFiK | - | Zhurnal nauchnoy i prikladnoy fotografii i kinematografii |
| ZhNKh | - | Zhurnal neorganicheskoy khimii |
| ZhPK | - | Zhurnal prikladnoy khimii |
| ZhPMTF | - | Zhurnal prikladnoy mekhaniki i tekhnicheskoy fiziki |
| ZhPS | - | Zhurnal prikladnoy spektroskopii |
| ZhTF | - | Zhurnal tekhnicheskoy fiziki |
| ZhVMMF | - | Zhurnal vychislitel'noy matematiki i matematicheskoy fiziki |
| ZL | - | Zavodskaya laboratoriya |

## 4. AUTHOR INDEX